

DESIGN AND MANUFACTURE OF AN OIL COOLER BY ADDITIVE
MANUFACTURING

A THESIS

SUBMITTED TO THE FACULTY OF
UNIVERSITY OF MINNESOTA

BY

KUNAL SUDAM GARDE

IN PARTIAL FULFILLMENT OF THE REQUIREMENTS
FOR THE DEGREE OF
MASTER OF SCIENCE

JANE H. DAVIDSON, ADVISER
SUSAN C. MANTELL, CO-ADVISER

May 2017

Acknowledgements

I would like to thank my parents and my sister for their continued love and support throughout my life. For their pivotal role in shaping my life and for making me who I am.

I would like to thank Dr. Jane Davidson and Dr. Susan Mantell for giving me the opportunity to work on this exciting project and also for the guidance, support and suggestions that have helped me improve in countless number of ways.

My sincere thanks Dr. Brandon J. Hathaway for his contribution to this project. His invaluable advice has guided me throughout the course of this project. I would like to thank my colleague Lauren Kolstadt for her contributions during the early stages of the project.

I would also like to thank Dr. Kim Stelson, Mike Gust and all the members of the Center for Compact and Efficient Fluid Power at the University of Minnesota for overlooking such a wonderful project.

I would like to thank the members of the Solar Energy Laboratory at the University of Minnesota for their ideas and inputs during the entire duration of the project and for creating a great work environment.

I am truly grateful to National Science Foundation and Department of Energy for the financial support during the project.

Dedication

This thesis is dedicated to my family

Abstract

The objective of this study is to design and fabricate an oil cooler (oil to air heat exchanger) by metal additive manufacturing as a swap-in replacement for an existing aluminum oil cooler in a Case New Holland model CX55B excavator. The oil cooler must provide a heat duty of 15 kW with pressure drops less than 343 Pa and 170 kPa on the air and oil side respectively. The dimensions of the designed heat exchanger are limited to those of the existing heat exchanger (430 mm x 530 mm x 50 mm) for interchangeability. The heat exchanger must be fabricated by selective laser melting using the Concept Laser Xline 1000R machine and the design must satisfy the design constraints specific to this process. The design must sustain a burst pressure of 2 MPa and meet standard test requirements specified by Case New Holland.

To produce a design that satisfies these specifications and meets the performance requirements, a finned lenticular tube bank concept with internal heat transfer enhancement techniques (such as offset strip fins) is selected from numerous ideas presented during a brainstorming session. Lenticular tube shape offers more internal space to accommodate enhancement features and results in lower pressure drop on air side as compared to circular tubes. Due to unavailability of heat transfer and pressure drop correlations, the finned lenticular tube bank is approximated as a finned circular tube bank and analyzed over a range of tube diameters (5 mm to 10 mm) and transverse pitch to diameter ratios (1.7 to 2.5). The heat transfer and pressure drop is assumed to be equivalent for same tube diameter and transverse pitch to diameter ratio as long as the number of tubes accommodated in the constrained volume are the same. Finite element analysis of the tubes and headers is done

using SolidWorks to produce a design which withstands the specified burst pressure of 2 MPa. Manufacturability of the parts with desired dimensions and features based on results of the thermal and mechanical analysis is verified based on the limitations of the Concept Laser machine. Two test prints are fabricated to test the combinations of various feature geometries and sizes.

The final design is based on the analysis and test prints and consists of 8 mm diameter lenticular tubes with a thickness of 1mm and a slenderness ratio of 0.77. Plain external fins with a thickness of 0.5 mm and an optimum fin spacing of 4.5 mm are employed on the air side while internal offset strip fins with a fin length of 10 mm are fabricated on the oil side. The external fins and internal offset strip fins are angled at 45 degrees with the tube axis for printability in selected print orientation. The design is predicted to produce a heat duty of 16.9 kW with pressure drops of 92 Pa and 26.6 kPa on air and oil side respectively. The design conforms to all the requirements from the product design specification.

Additive manufacturing enables fabrication of intricate shapes and unconventional geometries which can be optimized for heat transfer or pressure drop (such as shaped tubes or fin shapes) without being limited by the constraints imposed by conventional manufacturing. The study utilizes the design freedom offered by additive manufacturing advantageously to successfully fabricate an oil cooler consisting of small diameter shaped tubes with internal features which would be difficult to manufacture by conventional manufacturing. The successful fabrication of the oil cooler bolsters the suitability of additive manufacturing to fabricate oil coolers, however extensive testing is necessary to put these heat exchangers to practical use.

Table of Contents

Acknowledgements.....	i
Dedication.....	ii
Abstract.....	iii
Table of Contents.....	v
List of Tables.....	viii
List of Figures.....	ix
Nomenclature.....	xiv
Chapter 1. Introduction.....	1
1.1 Motivation.....	1
1.2 Problem Definition.....	3
1.3 Geometry of stock heat exchanger.....	5
Chapter 2. Product Design Specification.....	7
Chapter 3. Idea generation.....	16
3.1 Ideas Generated.....	16
3.2 Categorization.....	20
3.3 Down-selection.....	20
Chapter 4. Methods.....	27
4.1 Stock heat exchanger.....	27

4.1.1	Thermal analysis	27
4.1.2	Numerical method.....	37
4.1.3	Mechanical analysis	39
4.2	Finned tube bank heat exchanger	40
4.2.1	Geometry.....	41
4.2.2	Thermal analysis	43
4.2.3	Numerical method.....	49
4.2.4	Mechanical analysis	52
4.3	Lenticular design selection.....	53
Chapter 5.	Results.....	57
5.1	Modelling results.....	57
5.1.1	Thermal analysis of stock heat exchanger	57
5.1.2	Mechanical analysis of stock heat exchanger	59
5.1.3	Thermal analysis of finned tube bank heat exchanger	61
5.1.4	Mechanical analysis of finned tube banks	66
5.2	Test prints.....	67
5.3	Final design selection.....	75
Chapter 6.	Conclusion	83
References	85

Appendix A: Air flow measurement.....	88
Appendix B: Ideas from brainstorming	92

List of Tables

Table 1.1. Dimensions of stock heat exchanger.....	6
Table 2.1. Inlet design conditions for heat exchanger	8
Table 2.2. Primary customer needs and deduced corresponding secondary needs.....	9
Table 2.3. Metal AM processes available at ORNL with respective build volumes	10
Table 2.4. Table of metrics corresponding to the secondary needs	15
Table 4.1. Interpolating polynomials for thermophysical properties.....	30
Table 5.1. Performance estimate of the stock heat exchanger	59
Table 5.2. Details of parts printed in first test print	68
Table 5.3. Details of parts printed in the second test print.....	71
Table 5.4. Results of visual and flow tests for second test print.....	72
Table 5.5. Dimensions of the final printed heat exchanger design	77
Table 5.6. Thermal performance estimate for the final heat exchanger.....	81
Table 5.7. Product specification of printed heat exchanger	82

List of Figures

Figure 1.1. Layout of heat exchangers under the hood of the excavator	4
Figure 1.2. Schematic of the stock heat exchanger.....	5
Figure 2.1. Selective laser melting (SLM) process.....	11
Figure 2.2. Illustration of overhanging geometries.....	12
Figure 2.3. Overhang limitations for selective laser melting process	13
Figure 2.4. Fan curve for approximation of existing fan [20].....	14
Figure 3.1. Grouping of ideas from brainstorming	19
Figure 3.2. Relative magnitude of convective resistances for stock heat exchanger. The conductive resistance across the wall is $3.8e-6$ K/W (not visible on plot).....	21
Figure 3.3. Euler number for different tube shapes as a function of Reynolds number[25]	22
Figure 3.4. Internal space in tubes for offset strip fins	23
Figure 3.5. Orientations of heat exchanger relative to the build volume	24
Figure 3.6. External fin overhang modification (changing fin angle) for printability	25
Figure 3.7. Offset strip fin modification (changing fin angle) for printability.....	25
Figure 3.8. Header cross-section modification for printability	26
Figure 4.1. Thermal resistance network for the heat exchanger	29
Figure 4.2. Approximation of air side flow channel	32
Figure 4.3. Offset strip fin layout for stock heat exchanger.....	35
Figure 4.4. Flowchart of program implementation for stock heat exchanger	38

Figure 4.5. Tube geometry, loads and constraints used for mechanical analysis of flat tubes in stock heat exchanger	39
Figure 4.6. Geometry, loads and constraints used for analysis of the existing circular header of stock heat exchanger	40
Figure 4.7. Equal flow gap layout for circular tubes	41
Figure 4.8. Equilateral layout for circular tubes	41
Figure 4.9. End view of circular tube with offset strip fins and the minimum spacing constraint based on test prints.....	43
Figure 4.10. Illustration of circular finned tube bank with air flow going into the page	46
Figure 4.11. Division of fin area into hexagonal elements for evaluation of fin efficiency	47
Figure 4.12. Flowchart of program implementation for circular finned tube banks	51
Figure 4.13. Geometry, loads and constraints used for the analysis of the rotated square header .	52
Figure 4.14. Definition of slenderness ratio for lenticular tube shape	53
Figure 4.15. Effect of varying slenderness ratio on lenticular tube shape	53
Figure 4.16. Tube thickness comparison for constant thickness and constant slenderness options for same tube diameter and minimum thickness.....	54
Figure 4.17. Minimum tube thickness for constant slenderness and constant thickness options for lenticular tubes	54
Figure 4.18. Transformation of circular tube bank into lenticular tube bank in equal flow gap configuration.....	56

Figure 5.1. von Mises stress plot for the flat tube with offset strip fins with a 2 MPa internal pressure load	60
Figure 5.2. von Mises stress plot for the existing circular header with a 2 MPa internal pressure load.....	60
Figure 5.3. Contour plot of heat transfer rate (W) for finned tube bank heat exchanger assuming circular tubes.....	61
Figure 5.4. Contour plot of air and oil side convective heat transfer coefficients for finned tube banks heat exchanger assuming circular tubes	62
Figure 5.5. Contour plot for air side pressure drop (Pa) for finned tube bank heat exchanger assuming circular tubes.....	63
Figure 5.6. Contour plot for oil side pressure drop (Pa) for finned tube bank heat exchanger assuming circular tubes.....	64
Figure 5.7. Decrease in slenderness ratio made possible by decreasing tube diameter	65
Figure 5.8. von Mises stress plot for rotated square header for AM heat exchanger for a 2MPa internal pressure load	66
Figure 5.9. Parts fabricated in the first test print.....	69
Figure 5.10. Parts fabricated in the second test print.....	74
Figure 5.11. Depiction of final configuration with a slenderness ratio of 0.77	75
Figure 5.12. Von Mises stress plot for tube with slenderness ratio of 0.77 and tube wall thickness of 1 mm with a 2 MPa internal pressure load	76
Figure 5.13. Overall dimensions of the heat exchanger core and header.....	78

Figure 5.14. Dimensions of lenticular tubes with corresponding tube pitches	78
Figure 5.15. Dimension of external plain fins	79
Figure 5.16. Dimensions of internal offset strip fins	79
Figure 5.17. Final printed heat exchanger.....	80
Figure A.1. Symbols used for locations of air velocity measurements in the excavator	88
Figure B.1. Teardrop shaped fins.....	92
Figure B.2. Vortex generators[42]	92
Figure B.3. Metal foams[43].....	92
Figure B.4. Optimized pin fins[44].....	92
Figure B.5. Sinusoidal cross section tubes.....	92
Figure B.6. Modification to used bypassed cooler air	92
Figure B.7. Zig zag oil tubes.....	93
Figure B.8. Tube with corrugations	93
Figure B.9. Offset strip fins[24].....	93
Figure B.10. Twisted ribbon insert[45].....	93
Figure B.11. Utilizing engine vibrations.....	93
Figure B.12. Connected double spiral tubes	93
Figure B.13. Honeycomb tubes	94
Figure B.14. Hollow strut metal foams.....	94
Figure B.15. Header redesign	94

Figure B.16. Tree like oil passages[22] 94

Nomenclature

A_{air}	Air side heat transfer area (m ²)
$A_{cs,fc}$	Flow cross sectional area (m ²)
C	Heat capacity rate (W/K)
c_p	Specific heat capacity (J/kg-K)
C_r	Heat capacity ratio
D_h	Hydraulic diameter (m)
D_c	Fin collar diameter (m)
D_o	Tube outer diameter (m)
f	Friction factor
F_h	Fin height (m)
F_p	Fin pitch (m)
F_s	Fin spacing (m)
G_c	Mass flux of air based on minimum flow area (kg/s)
Gz	Graetz number
h_{osf}	Height of offset strip fin (m)
h_{tube}	Height of flat tube (m)
h	Convective heat transfer coefficient (W/m ² -K)
j	j-factor
k	Thermal conductivity (W/m-K)
K_c	Coefficient of entry pressure loss

K_e	Coefficient of exit pressure loss
L^+	Dimensionless duct length
l_o	Half-length of tube (m)
l_{osf}	Length of offset strip fins (m)
l_{tube}	Length of tube (m)
\dot{m}	Mass flow rate (kg/s)
$N_{columns}$	Number of tube columns
N_{fins}	Number of fins
N_{osf}	Number of offset strip fins per row
N_{rows}	Number of tube rows
N_{tubes}	Number of tubes
NTU	Number of transfer units
Nu	Nusselt number
$P_{internal}$	Internal pressure (Pa)
Pr	Prandtl number
Q_{actual}	Actual heat transfer rate (W)
Q_{max}	Maximum heat transfer rate (W)
R	Thermal resistance (K/W)
r	Tube radius (m)
$r_{f,eq}$	Equivalent fin radius (m)
Re	Reynolds number

S_1, S_2	Flow gaps (m)
S_L	Longitudinal tube pitch (m)
s_{osf}	Transverse spacing between offset strip fins (m)
S_T	Transverse tube pitch (m)
S_{UT}	Ultimate tensile strength (MPa)
S_{YT}	Tensile yield strength (MPa)
T	Temperature (K)
t_f	Fin thickness (m)
t_{osf}	Thickness of offset strip fin (m)
t_{tube}	Wall thickness of flat tube (m)
$(UA)_{overall}$	Overall heat transfer coefficient (W/K)
V	Flow velocity (m/s)
\dot{V}	Volume flow rate (kg/s)
V_{∞}	Approach velocity of air (m/s)
w_{tube}	Width of flat tube (m)
$x_{fd,h}$	Hydraulic entrance length (m)
$x_{fd,t}$	Thermal entrance length (m)

Greek symbols

Φ_f	Optimum fin density
δ_f	Fin spacing (m)
η_{fin}	Fin efficiency

$\eta_{surface}$	Overall surface efficiency
$\sigma_{Hoop,allowable}$	Allowable Hoops stress (MPa)
σ_{Hoop}	Induced Hoops stress (MPa)
ΔT_{lm}	Logarithmic mean temperature difference (K)
Δp	Pressure drop (Pa)
μ	Dynamic viscosity (m ² -s)
\mathcal{L}	Modified length scale (m)
ε	Effectiveness of heat exchanger
λ	Tube slenderness ratio
ν	Kinematic viscosity (m ² -s)
ρ	Density (kg/m ³)
σ	Area contraction ratio
ϵ	Duct aspect ratio

Subscripts

air	value related to air flow
D_h	value based on hydraulic diameter
D_c	value based on fin collar diameter
entry	value at entry
exit	value at exit
fin	value related to fin
in	value at inlet
\mathcal{L}	value based on modified length scale

max	maximum value of property
mean	mean value of property
min	minimum value of property
oil	value related to oil flow
osf	value related offset strip fin
out	value at outlet
tube	value related to tube

Chapter 1. Introduction

1.1 Motivation

At inception, additive manufacturing (AM) was a tool used explicitly for rapid production of prototypes. However, the advancement of additive manufacturing over the years provides the possibility to produce parts which would be difficult to manufacture with conventional manufacturing processes.

One application where additive manufacturing has been demonstrated as a replacement of traditional manufacturing is in the production of automobiles and construction equipment. Local Motors manufactured the world's first additively manufactured car in collaboration with the Department of Energy's Manufacturing Demonstration Facility (MDF) at the Oak Ridge National Laboratory (ORNL) in 2014[1]. Another passenger vehicle, Shelby Cobra, was manufactured later in 2015[2]. The parts for these cars were produced from carbon fiber reinforced ABS using Big Area Additive Manufacturing (BAAM) with a material deposition rate of 18 kg/hour, resulting in a total printing time of less than 24 hours.

Building on this experience, the work in this thesis is a part of an effort to fabricate an excavator using additive manufacturing. The project goal is to design and manufacture the boom, cab and oil cooler for a 37 horsepower excavator donated by Case New Holland for the project (model CX55B) by additive manufacturing. This thesis addresses the design of the oil cooler.

Being a relatively new manufacturing approach, very few attempts have been made to use metals in additive manufacturing of heat exchangers. Processes such as direct metal laser sintering, direct metal laser melting (or selective laser melting), and electron beam melting allow the use of metal alloy powders for additive manufacturing of heat exchangers possible. Saltzman et al. at the Penn State University manufactured and compared the performance of an additively manufactured aircraft oil cooler with a conventional one. The heat exchanger was created using a laser based powder bed fusion process with the conventional design as a baseline, and reflects the design changes (such as orienting the air and liquid side extended features and the header walls at an angle) that must be incorporated for compatibility with additive manufacturing [3]. Kirsch and Thole studied the heat transfer and pressure losses in additively manufactured wavy micro channels for applications in gas turbine engines. The wavy shapes and the small sizes of these channels are examples of the design freedom that additive manufacturing offers [4]. The University of Maryland fabricated an unfinned shaped tube bank for refrigerant to air heat exchanger applications utilizing the design freedom offered by AM to produce teardrop shaped tubes optimized for heat transfer and air side pressure drop[5]. Norfolk and Johnson manufactured and tested a microchannel heat exchanger using the ultrasonic sheet lamination (USL) approach[6]. USL is a hybrid manufacturing approach (a combination of additive and subtractive manufacturing approaches) in which thin sheets of metal are laid layer by layer and welded together ultrasonically. As a new sheet is laid, the part geometry for that specific layer is machined out using a CNC mill.

A team at Bremen University made a nature inspired heat exchanger which harvested heat from a central processing unit (CPU) of a computer[7]. This bioinspired idea has leaf like structures which would be extremely difficult to fabricate by conventional manufacturing. Assad et al. produced a wire mesh compact heat exchanger using cold spray additive manufacturing wherein they used pulsed gas dynamic spraying to deposit metal powder on a wire mesh [8]. Another application of the same process was tapered pin fins for applications such as heat sinks[9].

While there have been separate efforts to produce heat exchangers with small diameter shaped tubes for air side enhancement (without internal features) and flat tubes with internal features for oil side enhancement, the design in this thesis combines these features to produce small diameter shaped tubes with internal features to enhance heat transfer performance on both air and oil side.

1.2 Problem Definition

The problem presented is to replace the stock oil cooler on an excavator, Case New Holland model CX55B, by an additively manufactured counterpart. The problem is imposed with constraints including overall dimensions, operating parameters, flow rates, performance (heat duty and pressure drop), and compatibility with additive manufacturing. The layout of components under the hood of the excavator is such that the oil cooler is sandwiched between the condenser of the air conditioning circuit and the engine radiator with a single fan drawing air across all three heat exchangers. The arrangement is illustrated in Figure 1.1.

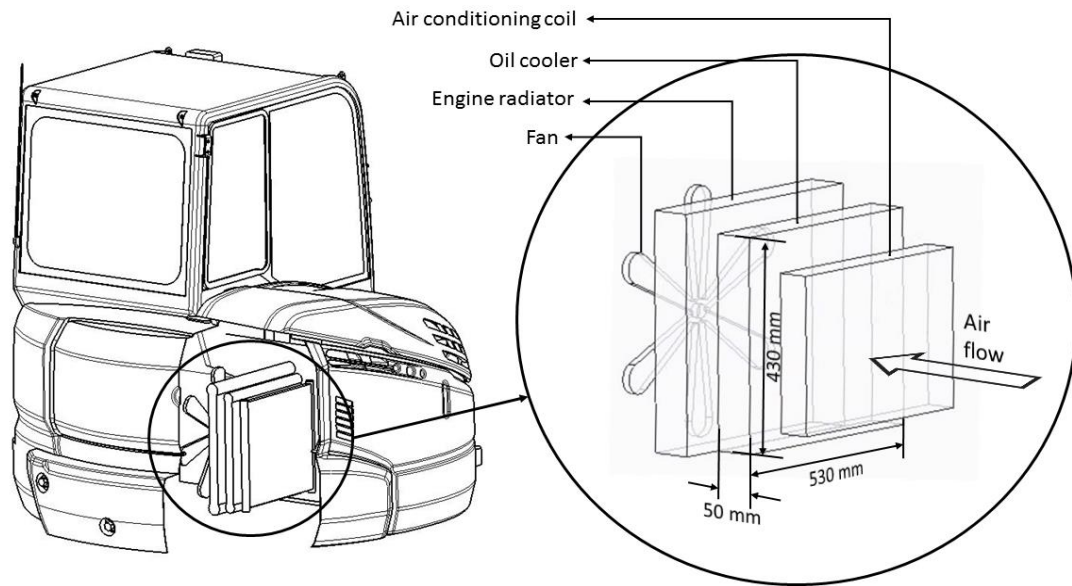


Figure 1.1. Layout of heat exchangers under the hood of the excavator

The four basic needs that the heat exchanger design must satisfy are called the primary needs. These primary needs are generic and are broken down into several secondary needs which are specific, and are detailed in chapter 2 along with their quantification into the product design specifications. To develop heat exchanger concepts, a brainstorming process was conducted and is detailed in chapter 3 along with the down selection of a final concept for analysis. Chapter 4 explains the methods used for analysis of the stock heat exchanger and down selected designs with all the relevant equations and correlations. Chapter 5 presents the results of the analysis and the test prints fabricated to evaluate the printability of promising options based on these results. This chapter concludes with the selection of the final printed design and its performance prediction. Chapter 6 summarizes the work done and presents suggestions for future work.

1.3 Geometry of stock heat exchanger

The stock oil cooler illustrated in Figure 1.2. is a microchannel brazed aluminum heat exchanger. The ISO VG 46 oil (a commonly employed oil grade in hydraulic circuits[10][11]) flows through the flat tubes while the air flows over them through the channels formed between the tubes and the herringbone wavy fins. The flat tubes include offset strip fins which enhance the heat transfer coefficient by periodic redevelopment of the thermal boundary layer. The heat exchanger is made entirely of aluminum to make it lighter and lead-free for easier maintenance[12].

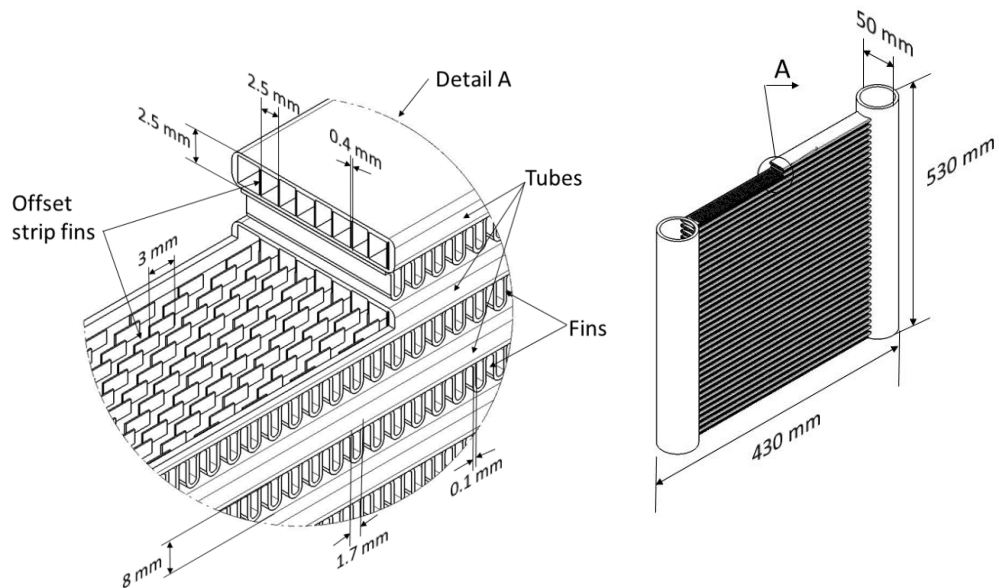


Figure 1.2. Schematic of the stock heat exchanger

The stock heat exchanger consists of 38 flat with an offset strip fin spacing of 2.5 mm (in transverse direction) and a fin length of 3 mm (in oil flow direction). This small fin length helps in keeping the flow in the hydraulic entrance region where the heat transfer

coefficients are high [13]. Each of this flat tubes has arrays of 9 fins in each row of the offset strip fins. These flat tubes are attached to the headers and form the core of the heat exchanger along with the fins. The small fin thickness of 0.1 mm allows a high fin density of 555 fins/m resulting in ~200 fins per row.

The dimensions of the heat exchanger and its various features are listed in Table 1.1.

Table 1.1. Dimensions of stock heat exchanger

Feature	Dimension	Value
Overall Heat exchanger	Length	50 mm
	Width	430 mm
	Height	530mm
Flat tubes	Length	360 mm
	Width	30 mm
	Height	2.5 mm
	Thickness	0.75 mm
	Spacing	8 mm
	Number of flat tubes	38
Fin	Length	30 mm
	Height	8 mm
	Thickness	0.1 mm
	Spacing	1.7 mm
Offset strip fin	Length	3 mm
	Width	2.5 mm
	Height	2.5 mm
	Thickness	0.4 mm
	Number of offset strip fins per row in a flat tube	9

Chapter 2. Product Design Specification

The primary needs mentioned in the previous section are unaltered statements of the stakeholders' viz., Case New Holland (CNH), Center for Compact and Efficient Fluid Power (CCEFP) and Oak Ridge National Laboratory (ORNL). These needs are compatibility with additive manufacturing, interchangeability with the stock heat exchanger, provision of adequate heat transfer performance and a design that conforms to the test requirements specified by CNH [14]. The breakdown of these needs into corresponding secondary needs is explained in the following paragraphs.

The secondary needs associated with the compatibility with additive manufacturing (AM) are related to the constraints that accompany the design freedom that AM offers. These constraints include the minimum feature size, geometry limitations and print volume. The equipment for the metal AM process must be available at Oak Ridge National Laboratory (ORNL), which is the manufacturing facility for this project. Based on build volumes, a selective laser melting (SLM) machine is selected which is compatible with metals such as aluminum alloy (AlSi10Mg), nickel based alloy (Inconel 718) and titanium alloy (TiAl6V4 ELI) [15].

The need of interchangeability with the stock heat exchanger translates into multiple needs such as fitting in the existing volume envelope of the stock heat exchanger on the excavator, use of standard threaded connections at the inlet and outlet of oil, retaining the existing fan for drawing air, maintaining the existing mounting points on the excavator and performing adequately without affecting performance of the other two heat exchangers.

The performance requirement is to achieve an oil outlet temperature of 365 K at design operating conditions which are specified as an oil inlet temperature of 373 K, an air inlet temperature of 318 K and an oil flow rate of 65 liters per minute. The air flow rate is calculated using air velocity measurements taken on a working excavator and are detailed later in this section. At the aforementioned inlet conditions, the heat duty is calculated using eq. (2-1). Based on the thermophysical properties of the oil and the oil outlet temperature requirement of 365 K, the heat duty is ~15 kW.

$$Q_{actual} = m_{oil}c_{p,oil}(T_{oil,in} - T_{oil,out}) \quad (2-1)$$

Table 2.1. Inlet design conditions for heat exchanger

Parameter	Value
Air inlet temperature (K)	318
Air flow rate (m ³ /s)	0.6
Oil inlet temperature (K)	373
Oil flow rate (lpm)	65

Oil coolers must pass standard tests before being subjected to regular operation. The heat exchanger must withstand a pressure of 2 MPa and withstand a fatigue testing of cycling from 0 to 125 kPa for 50,000 cycles at a frequency of 30 cycles per minute. It must also be able to withstand a maximum operating temperature of 398 K and a minimum temperature of 233 K [14].

All the primary and corresponding secondary needs are compiled in Table 2.2. The derived secondary needs act as design constraints.

Table 2.2. Primary customer needs and deduced corresponding secondary needs

Primary Needs	Need #	Secondary Needs
Heat exchanger is fabricated by additive manufacturing	1.	Manufactured using existing equipment at Oak Ridge National Laboratory
	2.	Fabricated using materials compatible with available equipment
	3.	Minimum feature size is not less than that of the selected equipment
	4.	Heat exchanger geometry satisfies geometry related design rules based on the selected AM process
	5.	Fits within limits of build volume of the selected manufacturing equipment
	6.	Uses design features that demonstrate advantages of additive manufacturing over conventional manufacturing
Heat exchanger is interchangeable with stock heat exchanger	7.	Has the same overall dimensions as the stock heat exchanger
	8.	Uses standard hydraulic fluid threaded connections at inlet and outlet of oil cooler
	9.	Retains the mounting points of the stock heat exchanger
	10.	Uses the existing fan without affecting performance of the other two heat exchangers; has maximum air side pressure drop of 343 Pa
Heat exchanger keeps oil outlet temperature below 365 K	11.	Uses the existing hydraulic flow circuit for oil; has maximum oil side pressure drop of 170 kPa
	12.	Provides sufficient heat transfer to get an oil outlet temperature of 365 K at inlet design conditions specified in Table 2.1. This results in a heat duty of 15 kW.
Heat exchanger meets standard test requirements	13.	Withstands internal pressure of 2 MPa
	14.	Passes fatigue test cycling of 0 to 125 kPa for 50000 cycles at 30 cycles per minute
	15.	Withstands a maximum temperature of 393 K
	16.	Withstands a minimum temperature of 233 K

For this project, the manufacturing options were limited to metal AM processes due to their higher conductivities and tensile strengths. To select a specific metal AM process, the build envelope of the machine must be large enough to accommodate the dimensions of the stock heat exchanger (530mm, 430mm, and 50mm) so that the designed heat

exchanger can retain the same overall dimensions of the stock heat exchanger. The processes available at ORNL with the build volumes for respective machines are listed in Table 2.3.

Table 2.3. Metal AM processes available at ORNL with respective build volumes

Additive manufacturing process	Build Volume (x,y,z)
Selective laser melting (SLM)	630mm, 400mm, 500mm
Selective laser sintering (SLS)	250mm, 250mm, 350mm
Electron beam melting (EBM)	350mm, 350mm, 380mm
Binder jetting (BJ)	40mm, 60mm, 35mm
Laser blown powder deposition/direct metal deposition (DMD)	305mm, 305mm, 305mm

The SLM process is selected because it is the only machine offering a build volume required by the dimensions of the stock heat exchanger. Experts at ORNL recommended leaving a clearance of 20 mm (~0.75 inches) from every edge in the x-y plane (see Figure 2.1.). This results in a usable build volume of 590 mm x 360 mm x 500 mm which is large enough to accommodate the heat exchanger dimensions.

The machine available at ORNL for SLM is Concept Laser Xline 1000R [16]. The selective laser melting process is illustrated in Figure 2.1. The equipment consists of robotically controlled laser, a feed powder chamber and a build chamber with movable platforms and a powder roller. The powder feed piston moves up hence raising a layer of powder above the feed chamber. The roller moves and rolls this layer of powder uniformly onto the build chamber piston. The robotically controlled laser shines over this rolled bed/layer of powder and traces the desired geometry, melting the powder selectively as it moves. Once the geometry on this layer is traced entirely by the laser, the build piston moves down by a decrement equal to the layer thickness of the part and the feed piston

moves up by a proportionate amount, and a new layer of powder is rolled onto the previous layer of powder by the roller. The laser shines again and traces the geometry for the next layer. This process is repeated until the final layer of the part is printed. The printed part resides within the bed of un-melted powder and may contain residual powder inside it depending on the geometry. The part is then removed and shaken to get rid of the un-melted powder. If the geometry consists of internal passageways, the minimum internal passageway dimension is limited to facilitate removal of powder. In present case, this dimension is limited to 3 mm.

The materials compatible with the Concept laser Xline 1000R are aluminum alloy (AlSi10Mg), nickel based alloy (Inconel 718) and titanium alloy (TiAl6V4 ELI) with thermal conductivities of 110 W/m-K [17], 11.2 W/m-K [18] and 6.6 W/m-K [19] respectively. AlSi10Mg is selected due to its higher thermal conductivity.

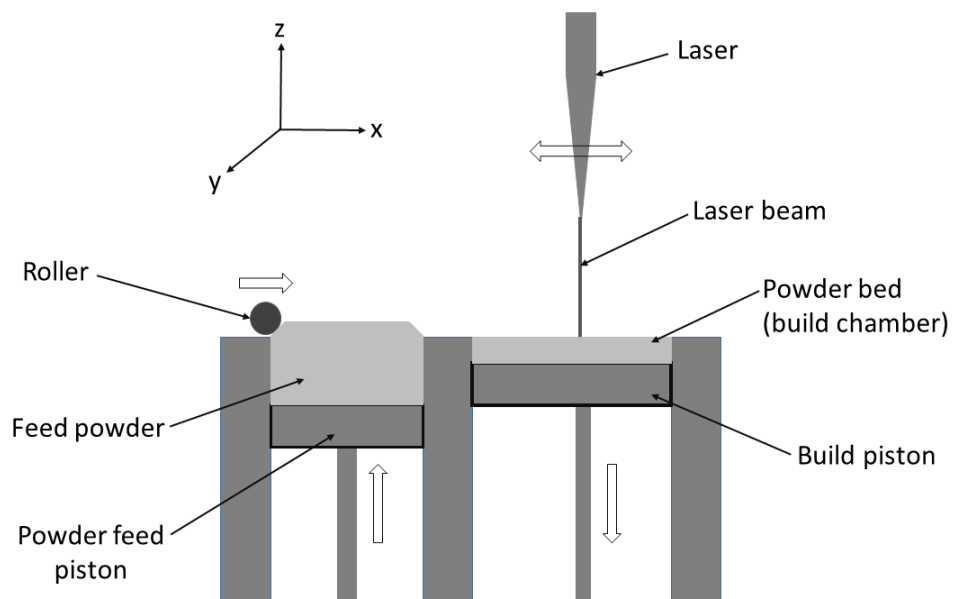


Figure 2.1. Selective laser melting (SLM) process

The SLM process has a set of design constraints. The minimum feature size that can be printed in the xy plane is limited by the laser diameter which varies from 0.1 mm to 0.5 mm for Concept Laser Xline 1000R. Based on feedback from experts at ORNL, the minimum feature size is limited to 0.5 mm [20]. Due to the variation of the laser diameter, a tolerance of ± 0.2 mm is assumed in the parts printed by this machine [15].

Due to the inherent nature of the process in which the part is built up layer by layer by melting metal powder, there is a limitation on the unsupported overhangs that can be fabricated. An overhang is an unsupported part of a geometry that protrudes out the main geometry as shown in Figure 2.2.

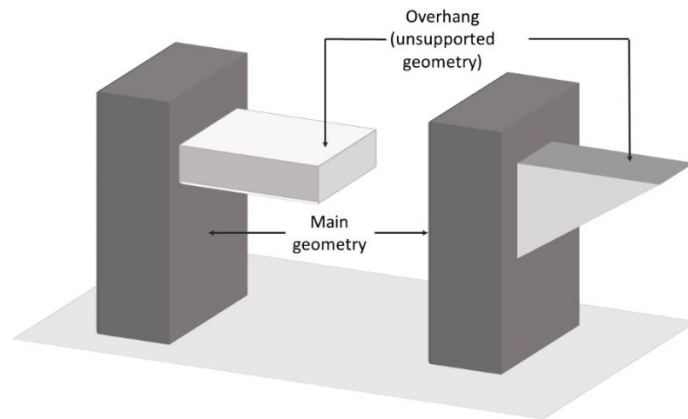


Figure 2.2. Illustration of overhanging geometries

If the amount of overhang exceeds a certain threshold, the overhang will droop before the melted layer has solidified. This threshold is defined by the angle that the overhang makes with the horizontal and is explained in Figure 2.3. The dotted lines indicate the sliced computer aided design (CAD) model geometry for printing while the solid lines represent the actual designed geometry. For SLM processes, this threshold angle is 45 degrees.

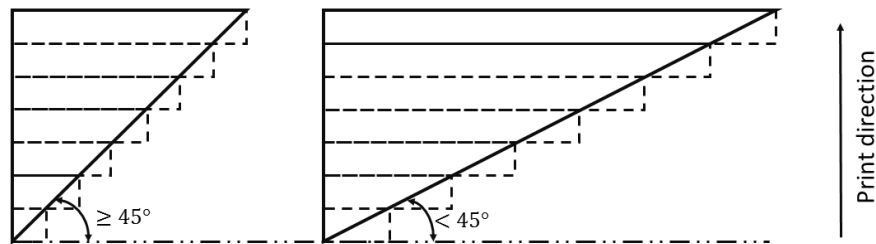


Figure 2.3. Overhang limitations for selective laser melting process

The overall dimensions of the AM heat exchanger are restricted to equal or smaller than those of the stock heat exchanger (430 mm x 530 mm x 50 mm). To use the hoses present in the existing hydraulic circuit, the heat exchanger must have threaded connections which can be adapted to the Japanese International Standard (JIS) B 2351 threads with a thread size of $\frac{3}{4}$ inch, which are used on the hydraulic hoses of the circuit [21].

The three heat exchangers in the excavator are arranged in series with a single fan pulling air across them (Figure 1.1). To avoid disturbances in the air flow pattern under the hood across the heat exchangers, the mounting points for the new design are kept unaltered. To retain the existing fan (a 7 blade axial fan with a blade diameter of 480 mm), a maximum allowable air side pressure drop across the designed heat exchanger is calculated from the fan curve of a fan similar to the existing fan and is shown in Figure 2.4. [22] (because the fan curve for the existing fan is unavailable). The air flow rates are plotted on the x-axis (in cfm) while the corresponding static pressure is indicated on the y-axis (in inches of water).

Measurement of air flow across the face of the stock heat exchanger installed on a running excavator using a hot wire anemometer resulted in an air velocity ranging between 3.5 m/s to 7 m/s. Details of the air flow measurement are presented in Appendix A.

The measured velocities correspond to air flow rates of 0.6 m³/s (1280 cfm) and 1.2 m³/s (2560 cfm) respectively based on the frontal area of the heat exchanger. The static pressure produced by the fan at these flow rates is 1030 Pa (4.15 inches of water) and 810 Pa (3.25 inches of water) respectively. The air flow rate for all design calculations is conservatively assumed to be 0.6 m³/s (1280 cfm). The allowable pressure drop across the designed heat exchanger at this flow rate is ~343 Pa (assuming that pressure drop across all three heat exchangers is the equal).

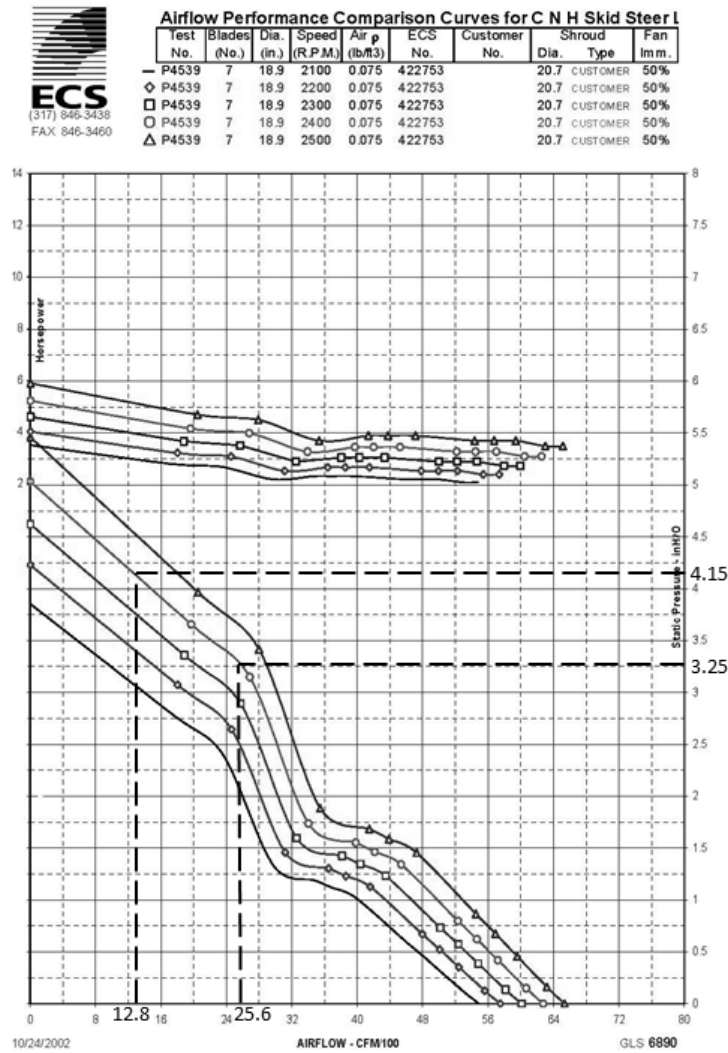


Figure 2.4. Fan curve for approximation of existing fan [22]

To retain the existing hydraulic circuit, the oil side pressure drop must be maintained below a threshold that does not affect the hydraulic circuit performance. Based on feedback from hydraulic experts at the CCEFP, the pressure drop on the oil side is limited to 170 kPa (~25 psi) [23].

All these needs are summarized in terms of quantified metrics in Table 2.4.

Table 2.4. Table of metrics corresponding to the secondary needs

Metric #	Need #	Metric	Ideal Value
1.	1	Additive manufacturing equipment	Concept Laser Xline 1000R
2.	2	Material used	AlSi10Mg
3.	2	Thermal conductivity of AlSi10Mg (W/m-K)	110
4.	3	Minimum feature size (mm)	≥ 0.5
5.	4	Maximum overhang angle (degrees)	≥ 45
6.	4	Minimum internal passageway dimension (mm)	≥ 3
7.	5	Maximum build volume (mm ³)	590 x 360 x 500
8.	6	Showcase additive manufacturing	Yes
9.	7	Maximum height (mm)	430
10.	7	Maximum width (mm)	530
11.	7	Maximum depth (mm)	50
12.	8	Threaded connections	JIS B 2351
13.	9	Use existing mounting points	Yes
14.	10	Air side pressure drop (Pa)	<343
15.	11	Oil side pressure drop (Pa)	<170000
16.	12	Heat transfer rate (W)	15000
17.	13	Design pressure (Pa)	2e6
18.	14	Fatigue testing from 0 to 125000 Pa at 30 cycles/min for 50,000 cycles	Pass
19.	15	Maximum design temperature (K)	398
20.	16	Minimum design temperature (K)	233

Chapter 3. Idea generation

This chapter presents the ideas generated during a brainstorming session and their categorization based on the type of enhancement they offered. A final concept is selected following the process explained in section 3.3.

3.1 Ideas Generated

A brainstorming session was conducted with members of Solar Energy Laboratory and Polymer Materials and Mechanics Laboratory at the University of Minnesota to generate ideas for the heat exchanger. The desired outcome from this exercise was to develop a design which is different than the stock heat exchanger rather than modifying the stock heat exchanger for compatibility with additive manufacturing. The participants were provided with the problem definition. As a result of this exercise, more than 30 ideas were generated and are categorized as mentioned in section 3.2. Images and sketches of these ideas are included in Appendix B.

Many of the ideas are different embodiments of similar concepts and are hence grouped as follows to eliminate redundancy.

- a. External flow – ideas in this category enhance performance on the air side of the heat exchanger.
 - i. Fin designs to reduce pressure drop or increase heat transfer. An example in this category is a teardrop shaped fin. (see Figure B.1)
 - ii. Boundary layer control to enhance heat transfer. Examples are vortex generators, metal foams and pin fins. (see Figure B.2, Figure B.3 and Figure

B.4)

iii. Modification to the air flow path to enhance heat transfer. One idea is to employ tubes with a sinusoidal cross section so that the air has to flow through a serpentine channel formed between two tubes. (see Figure B.5)

iv. Modifications to use the cooler air that bypasses the relatively smaller air conditioning coil. (see Figure B.6)

b. Internal flow – ideas in this category enhance performance on the oil side of the heat exchanger.

i. Change the tube shape so that the oil flow encounters a tortuous path. An example is a zig zag shaped tube along the oil flow direction. (see Figure B.7)

ii. Flow disruptors on the oil side to enhance the heat transfer coefficient. Examples are corrugated tubes (see Figure B.8), offset strip fins (which are also employed in the stock heat exchanger) (see Figure B.9) and a twisted ribbon insert. (see Figure B.10)

c. Internal and external flow – ideas under this category enhance performance on both the air and oil sides.

i. Mount the heat exchanger on the excavator such that the vibrations from the engine are transferred directly to the oil cooler. (see Figure B.11)

ii. Network of tubes such that the flow on the oil side is disrupted and the heat transfer area is increased. Examples are tubes shaped like fish veins, leaf

veins and connected double spiral tubes etc. (see Figure B.12)

iii. Lattice geometries to get a large surface area. Examples are honeycombs and hollow strut metal foams. (see Figure B.13 and Figure B.14)

d. Headers to ensure uniform distribution of oil in the flow passages (see Figure B.15).

Preliminary calculations however revealed insignificant variation in flow through the tubes, and hence header modifications are deemed to be unnecessary.

e. Nature inspired ideas mimic nature to enhance heat transfer performance. One example is the work by Bejan et al.[24] (see Figure B.16)

The grouping of all these ideas is represented in the form of a tree diagram in Figure 3.1.

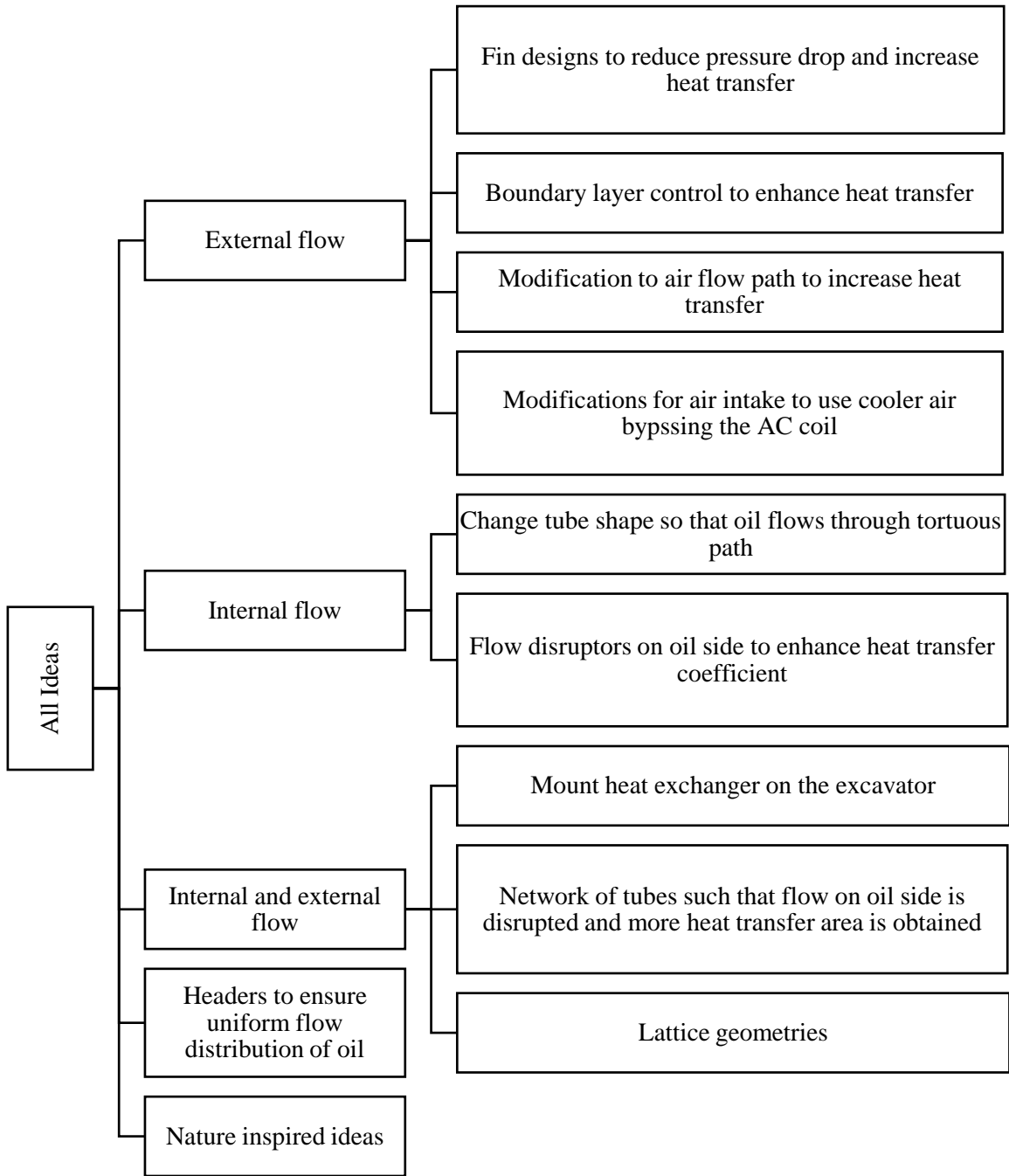


Figure 3.1. Grouping of ideas from brainstorming

3.2 Categorization

To simplify the down-selection, these ideas are categorized based on the fundamental enhancement technique that they employ into the following categories:

1. Air side area increase without fins – This category consists of ideas such as the zig zag tubes, connected double spiral tubes, sinusoidal tubes etc.
2. Air side area increase with fins – This category consists of ideas such as finned tube banks, optimized pin fins, spine fins etc.
3. Oil side heat transfer enhancement – This category consists of ideas such as twisted ribbon inserts, offset strip fins, internal corrugations etc.
4. Ideas saved for future consideration – All the remaining ideas are grouped into this category and are not investigated. Some ideas are categorized under this category because they do not satisfy one or more of the requirements from the product design specifications (for example shape modifications to utilize cooler air bypassing the AC coil would not comply with the need to retain the dimensions of the stock heat exchanger), while some were eliminated based on a preliminary analysis of their applicability for this problem specification (such as elimination of header modification based on calculations of flow variation in tubes). Some ideas are removed from consideration as they require complex analysis methods for performance evaluation (for example nature inspired ideas and lattice geometries).

3.3 Down-selection

The analysis of the stock heat exchanger (using method explained in section 4.1) revealed that the thermal convective resistance on the air side is an order of magnitude

higher than the convective resistance on oil side and three orders of magnitude higher than the conductive resistance. This observation is typical for heat exchangers employed in liquid to air applications due to the thermophysical properties of air compared to oil[25]. Hence, ideas contributing to the enhancement of air side performance are prioritized. A plot of convective resistances is shown in Figure 3.2. for the range of measure air flow velocities measured on the excavator (see Appendix A). The oil side enhancement ideas are combined with these ideas to maintain the low oil side thermal resistance. Oil side enhancement methods such as offset strip fins and twisted ribbon inserts are widely employed in viscous flows with high Prandtl number due to their higher thermal entrance lengths and low thermal diffusivities. These methods not only enhance the heat transfer coefficient by reducing the thermal boundary layer length, but also increase the heat transfer area on the viscous fluid side [26].

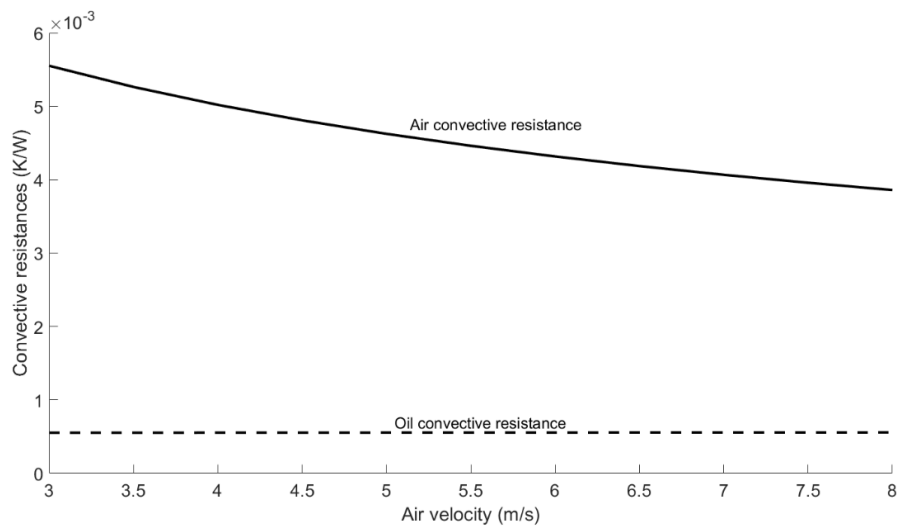


Figure 3.2. Relative magnitude of convective resistances for stock heat exchanger. The conductive resistance across the wall is 3.8×10^{-6} K/W (not visible on plot)

$$T_{\text{air,in}} = 318\text{K}; T_{\text{oil,in}} = 373\text{K}; \dot{V}_{\text{oil}} = 65 \text{ lpm}$$

The air side thermal resistance can be decreased by increasing the heat transfer area and/or the convective heat transfer coefficient. To bring about this increase, finned tube banks are considered as they are compatible with AM. The finned tube banks can consist of either circular tubes or shaped tubes. To evaluate the advantage of shaped tubes over circular tubes in terms of the reduction of air side pressure drop, unfinned tube banks of circular and shaped tubes are considered. Figure 3.3 shows the Euler number as a function of Reynolds number for different tube shapes. Euler number is a non-dimensional quantification of the air side pressure drop [27]. As lenticular tubes have the least pressure drop on air side, shaped tube analysis is limited to lenticular shape.

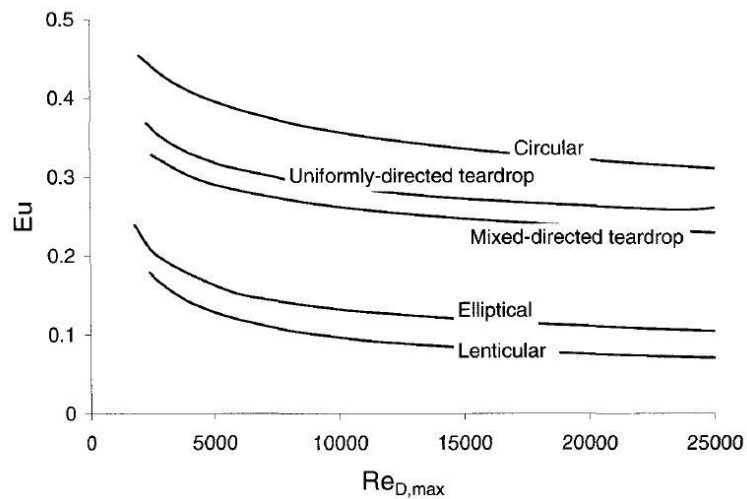


Figure 3.3. Euler number for different tube shapes as a function of Reynolds number[27]

A major advantage that the lenticular tubes offer is more cross sectional area inside the tube as compared to circular tubes (for the same tube diameter), which enables better additive manufacturing of internal features such as offset strip fins (which are considered for oil side heat transfer enhancement). Considering a tube diameter of 8 mm with slenderness ratios of 1 (circular tube) and 0.5 and 1 mm tube thickness, the internal space

for 0.5 mm thick offset strip fins is shown in Figure 3.4. The minimum spacing between these fins for clearance of residual powder is 1.41 mm based on test prints detailed in section 5.2. The circular tube does not offer sufficient space to maintain this spacing, but making the tubes more slender increases the internal space. The shaped tubes are also a good example of the design freedom that AM can offer as illustrated by the University of Maryland team [5].

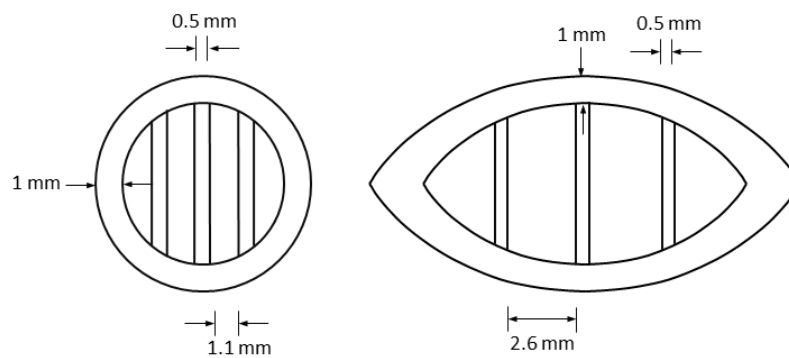


Figure 3.4. Internal space in tubes for offset strip fins

To match the heat transfer performance of the stock heat exchanger on the oil side, employment of enhancement features such as offset strip fins or twisted ribbon inserts is necessary for the AM heat exchanger. Based on test prints (detailed in section 5.2), the twisted ribbon insert is found to clog the tubes in many cases. Hence, finned tube banks with internal offset strip fins are selected as a final choice for analysis. The method used for analysis of parametric designs of this configuration is explained in section 4.2.

For finned tube banks with internal features to be compatible with additive manufacturing, certain modifications are necessary based on the orientation of the part relative to the print direction. The dimensions of the heat exchanger are restricted to 430 mm x 530 mm x 50 mm and the build volume dimensions are annotated in Figure 3.5(a).

The various orientations in which the heat exchanger can be oriented are shown in Figure 3.5. The heat exchanger fits inside the build volume only in orientation (c).

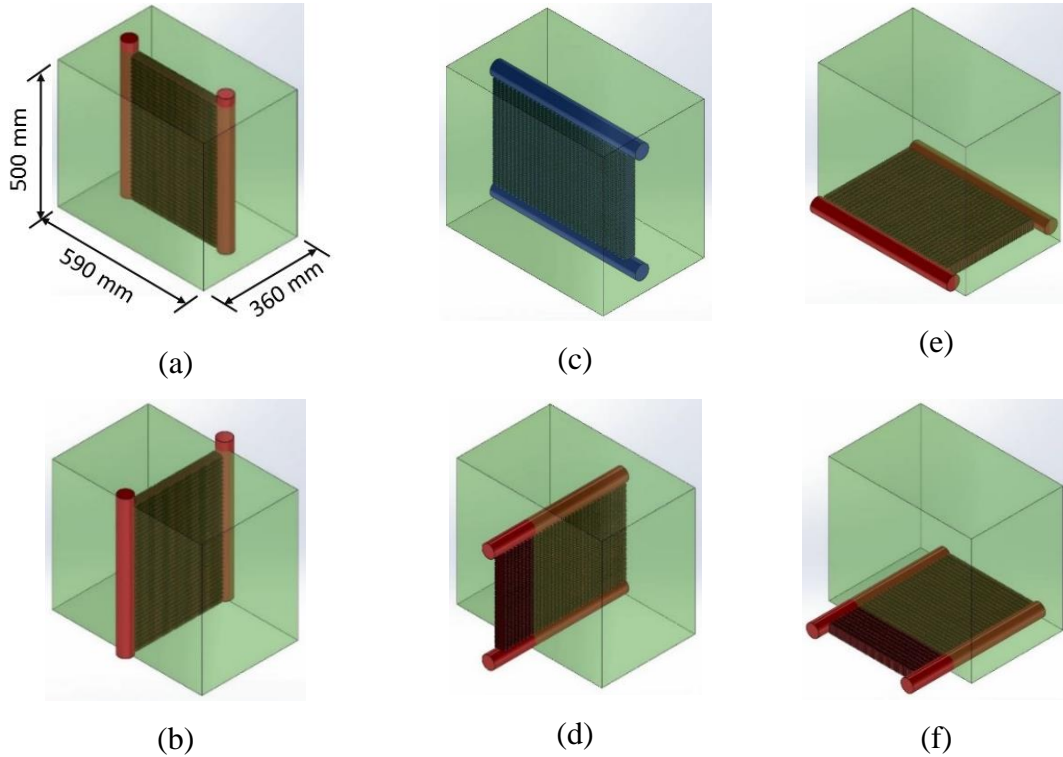


Figure 3.5. Orientations of heat exchanger relative to the build volume

Figures 3.6 to 3.8 show the modifications done for printability in orientation (c), with the idealized versions on the left hand side and the modified versions on the right. The modifications and their justifications are as follows.

First, the external fins must be angled relative to the print direction to avoid unprintable unsupported overhangs. Two ways to avoid this overhang are to either provide external support structures during printing or orient the fins at an angle that is acceptable for printing. The former solution would require complex post-processing and could lead to rougher surface finish. Hence the latter solution is implemented as shown in Figure 3.6.

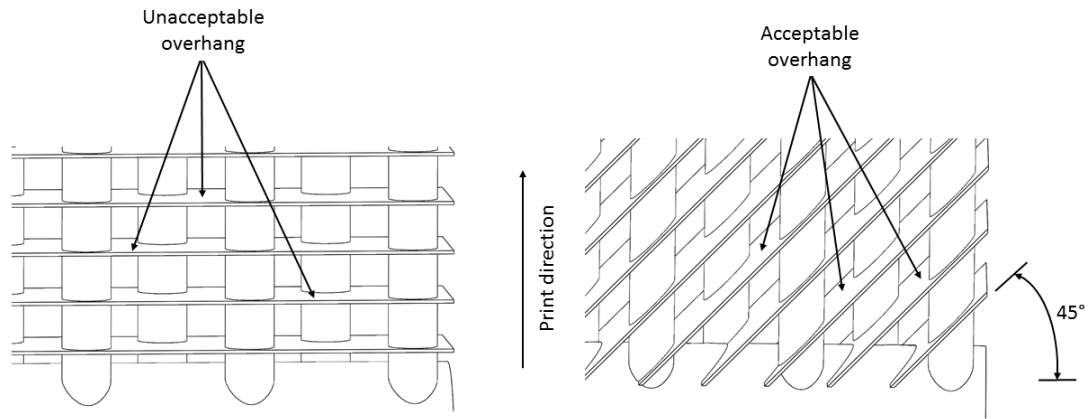


Figure 3.6. External fin overhang modification (changing fin angle) for printability

Second, the internal offset strip fins also result in an unsupported overhang as shown in Figure 3.7. The two solutions for these fins are identical those for the external fins, either add support structures to make the offset strip fins printable or modify the overhang angle such that it is printable without supports. Clearing the internal support structures is even more difficult in closed geometries such as tubes. Hence the offset strip fins are angled similar to the external fins as shown in Figure 3.7.

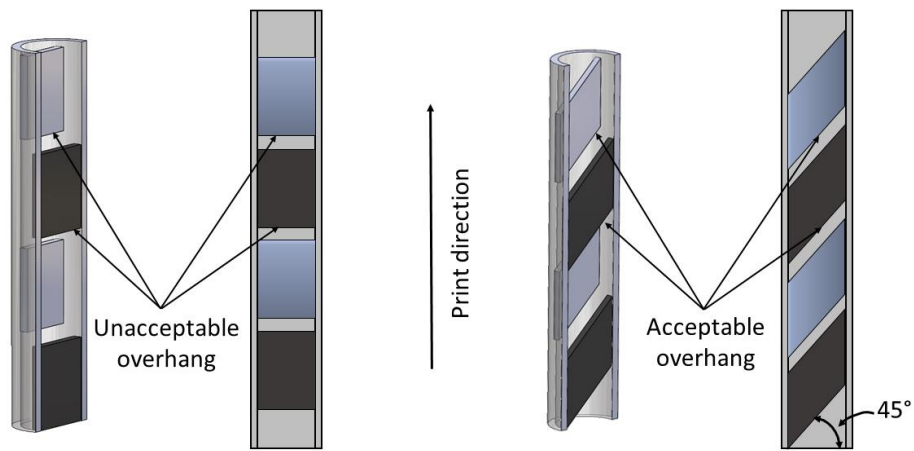


Figure 3.7. Offset strip fin modification (changing fin angle) for printability

Lastly, the circular header violates the overhang rule for printing by making an angle less than 45 degrees for a considerable portion of the print. Hence it is modified to form a rotated square shape as shown in Figure 3.8 to avoid the unsupported overhang.

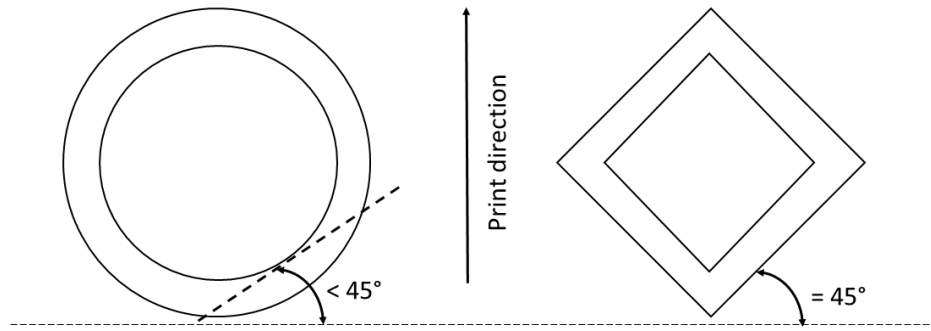


Figure 3.8. Header cross-section modification for printability

Chapter 4. Methods

In this chapter the methods implemented to predict thermal and mechanical performance of the stock heat exchanger and to finalize the design of the AM heat exchanger are presented. The geometry for the stock heat exchanger is explained in section 1.2 while that of the AM heat exchangers is specified in section 4.2.1.

4.1 Stock heat exchanger

This section presents the thermal analysis method and mechanical analysis methods for the stock heat exchanger.

4.1.1 Thermal analysis

The aim of the thermal analysis is to evaluate the heat transfer from the stock heat exchanger and the pressure drop on the air and oil side. To evaluate the heat transfer, the effectiveness – number of transfer units ($\varepsilon - NTU$) method mentioned in standard texts is used [13].

Effectiveness of a heat exchanger is the ratio of the actual heat transfer and the maximum possible heat transfer given in equation (4-1).

$$\varepsilon \equiv \frac{Q_{actual}}{Q_{max}} \quad (4-1)$$

The maximum possible heat transfer is the product of the difference of the fluid inlet temperatures and the minimum heat capacity rate given by eq. (4-2).

$$Q_{max} = C_{min}(T_{oil,in} - T_{air,in}) \quad (4-2)$$

The heat capacity rate is the product of its specific heat and the mass flow rate (eq. (4-3)).

$$C_{fluid} = \dot{m}_{fluid} c_{p,fluid} \quad (4-3)$$

In the present case, the minimum heat capacity rate out of the two fluids is always on the air side ($C_{air} = 654 \text{ kJ/K}$ and $C_{oil} = 1902 \text{ kJ/K}$).

For a single pass cross flow heat exchanger with both fluids unmixed, the effectiveness is a function of the number of transfer units (NTU) and is given by eq. (4-4)[28].

$$\varepsilon = 1 - \exp \left[\frac{NTU^{0.22}}{C_r} \{ \exp(-C_r NTU^{0.78}) - 1 \} \right] \quad (4-4)$$

The ratio of the minimum to the maximum heat capacity rate is termed the heat capacity ratio (C_r) and is given by (4-5).

$$C_r = \frac{C_{min}}{C_{max}} = \frac{C_{air}}{C_{oil}} = \frac{\dot{m}_{air} c_{p,air}}{\dot{m}_{oil} c_{p,oil}} \quad (4-5)$$

The NTU is the ratio of the overall heat transfer coefficient-area product to the minimum heat capacity rate[13].

$$NTU \equiv \frac{(UA)_{overall}}{C_{min}} \quad (4-6)$$

The overall heat transfer coefficient-area product (UA) is inversely proportional to the sum of thermal resistances of the system and is defined in eq. (4-7) [13].

$$\begin{aligned} (UA)_{overall} &= \frac{N_{tubes}}{R_{oil} + R_{tube} + R_{air}} \quad (4-7) \\ &= \frac{N_{tubes}}{\frac{1}{h_{oil} A_{oil}} + \frac{1}{2 \left(\frac{k_{Al} l_{tube} (w_{tube} + h_{tube})}{t_{tube}} \right)} + \frac{1}{h_{air} A_{air}}} \end{aligned}$$

To calculate the thermal resistances, the heat exchanger is modelled as 38 flat tubes acting in a parallel thermal resistance network. The thermal resistances for a single flat tube act in series and are shown in Figure 4.1. The convective coefficients are calculated using published correlations as detailed in the following paragraphs. The thermal conductivity of aluminum is temperature dependent and is evaluated using a function obtained regression analysis for six data points between 300 K and 800 K [29].

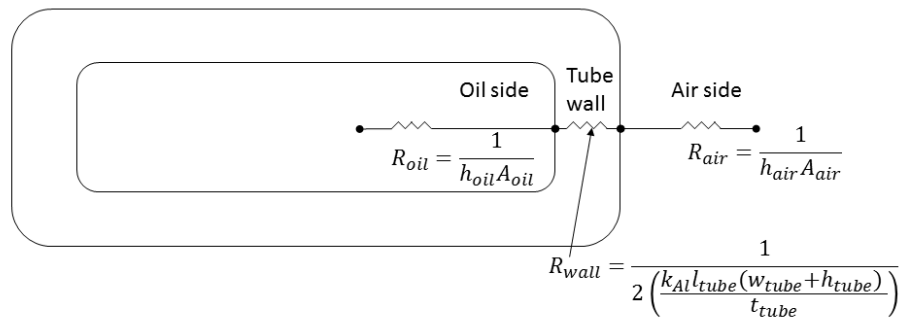


Figure 4.1. Thermal resistance network for the heat exchanger

The temperature dependent thermophysical properties for ISO VG 46 oil [30] and dry air[31] are available online. Interpolating polynomials are defined using a regression analysis based on the available data from 273 K to 673 K for oil and 175 K to 1900K for air. Eight data points are used to generate the interpolating functions for the oil and 35 data points are used to develop the functions for the air. The minimum goodness of fit factor for these functions is 0.999. The derived polynomials are listed in Table 4.1. with all temperatures in Kelvin.

Table 4.1. Interpolating polynomials for thermophysical properties

	Air	Oil
Density (kg/m ³)	$\rho_{air} = \frac{101325}{(286.98T)}$	$\rho_{oil} = -0.6907T + 1066$
Kinematic viscosity (m ² -s)	$\nu_{air} = (-1e^{-9}T^3 + 9e^{-6}T^2$ $+ 0.0046T$ $- 0.5434)10^{-5}$	ν_{oil} $= (-0.5797T$ $+ 222.54)10^{-6}$
Specific heat (kJ/kg-K)	$c_{p,air} = (-5e^{-17}T^5 + 3e^{-13}T^4$ $- 1e^{-9}T^3 + 1e^{-6}T^2$ $- 0.0004T$ $+ 1.0481)10^3$	$c_{p,oil} = 3.6286T + 821.9$
Thermal conductivity (kW/m-K)	$k_{air} = (7e^{-10}T^3 - 3e^{-6}T^2$ $+ 0.0094T$ $+ 0.0751)10^{-2}$	$k_{oil} = -7e^{-5}T + 0.1553$

To obtain the mean temperatures for evaluation of these properties, the outlet temperatures for both the fluids and the mean flat tube wall temperature must be determined. These temperatures can be determined using eq. (4-9), (4-10) and (4-11)[13] respectively. The heat transfer rate used in these equations is evaluated using eq. (4-8). This system of four equations with four unknown variables viz., heat transfer, air outlet temperature, oil outlet temperature and wall mean temperature are solved using the iterative procedure explained in section 4.1.2.

$$Q_{actual} = \varepsilon Q_{max} = \varepsilon \dot{m}_{air} c_{p,air} (T_{oil,in} - T_{air,in}) \quad (4-8)$$

$$Q_{actual} = \dot{m}_{air} c_{p,air} (T_{air,out} - T_{air,in}) \quad (4-9)$$

$$Q_{actual} = \dot{m}_{oil} c_{p,oil} (T_{oil,out} - T_{oil,in}) \quad (4-10)$$

$$Q_{actual} = h_{oil} A_{oil} (T_{wall,mean} - T_{oil,mean}) \quad (4-11)$$

Equation (4-12) is used to evaluate a mean temperature on the oil side by accounting for the logarithmic variation of temperature with the flow while the mean temperature for air is calculated using eq. (4-13). Using arithmetic mean approach for air side temperatures is suggested in standard texts [32].

$$T_{oil,mean} = \frac{T_{oil,in} - T_{oil,out}}{\log_e \left(\frac{T_{oil,in}}{T_{oil,out}} \right)} \quad (4-12)$$

$$T_{air,mean} = \frac{T_{air,in} + T_{air,out}}{2} \quad (4-13)$$

Calculation of the hydraulic and thermal entrance lengths (eq. (4-14)[33] and eq. (4-15)[34] respectively) revealed that the flow is developing for both hydraulic and thermal regimes with entrance lengths of 120 mm and 85.5 mm respectively compared to the flow length of 27 mm.

$$x_{fd,h} = 0.05 D_h Re_{D_h} \quad (4-14)$$

$$x_{fd,t} = 0.05 Re_{D_h} Pr \quad (4-15)$$

The convective heat transfer coefficient for air is evaluated from the Nusselt number correlation for developing flow in a circular duct given by eq. (4-16) for Prandtl numbers greater than 0.1 [35]. This equation is used for the rectangular duct based on the hydraulic diameter defined in eq. (4-19). The Prandtl number for air is 0.71 while the Graetz number is 60.

$$Nu_{air} \equiv \frac{h_{air} D_{h,air}}{k_{air}}$$

$$= \frac{\left(\frac{3.66}{\tanh(2.264 Gz_{air}^{-\frac{1}{3}} + 1.7 Gz_{air}^{-\frac{2}{3}})} \right) + 0.0499 Gz_{air} \tanh(Gz_{air}^{-1})}{\tanh(2.432 Pr_{air}^{\frac{1}{6}} Gz_{air}^{-\frac{1}{6}})} \quad (4-16)$$

$$Pr_{air} = \frac{\mu_{air} c_{p,air}}{k_{air}} \quad (4-17)$$

$$Gz_{air} = \frac{D_{h,air}}{F_l} Re_{air} Pr_{air} \quad (4-18)$$

$$D_{h,air} = \frac{4F_h F_s}{2(F_h + F_s)} \quad (4-19)$$

$$Re_{air} = \frac{V_{air} D_{h,air}}{\nu_{air}} \quad (4-20)$$

Flow on the air side is approximated to be through a straight duct with a rectangular cross section as shown in Figure 4.2. The air flow velocity is assumed to be uniform across the face of the heat exchanger. The arrangement results in a thin slender channel with a cross section of 1.7 mm x 8 mm and a flow length of 27 mm.

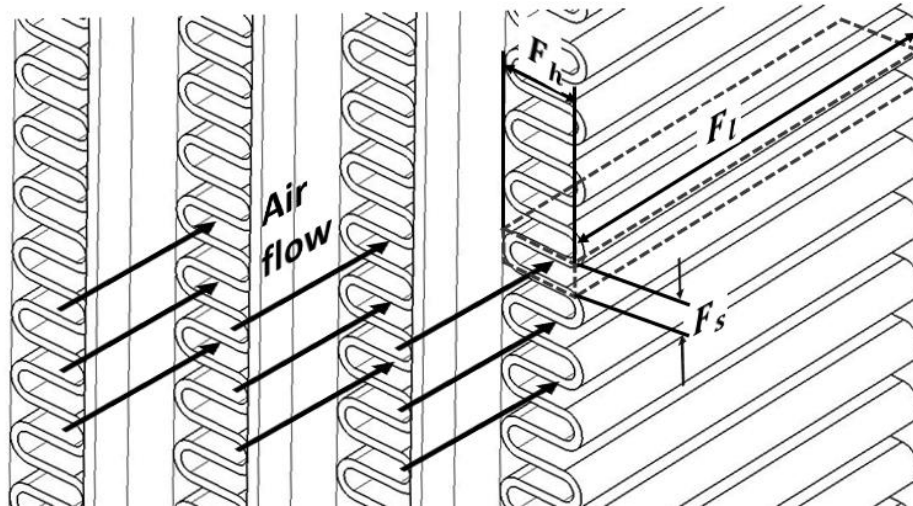


Figure 4.2. Approximation of air side flow channel

To account for blockage of air flow by the tubes and the corresponding increase in velocity through the channels, a contraction ratio (σ), which is the ratio of the minimum flow area to the maximum flow area for air as indicated in eq. (4-21), is used to estimate the flow velocity through the channels. The contraction ratio for the stock heat exchanger is 0.6, which results in a maximum flow velocity of 5.7 m/s for an air inlet velocity of 3.5 m/s.

$$\sigma = \frac{(F_s F_h) N_{fins} (N_{tubes} + 1)}{l_{tube} N_{tube} (F_h + h_{tube})} \quad (4-21)$$

$$V_{air} = \frac{V_{\infty}}{\sigma} \quad (4-22)$$

The Reynolds number calculated using eq. (4-20) is found to be in the laminar regime ($Re_{air, D_h} = 860$) based on the core air flow velocity ($V_{air} = 5.7 \text{ m/s}$) and the hydraulic diameter ($D_{h,air} = 0.0028 \text{ m}$).

The total pressure drop across the heat exchanger on the air side is expressed as a sum of three components viz., the entry pressure loss, the pressure loss due to flow through channel and the pressure rise at the exit of the channel [36]. The entry pressure loss is due to the increase in air velocity due to area contraction, the flow loss through channel is due to friction and the pressure rise at the exit is due to the reduction in air velocity due to flow area expansion.

$$\Delta p_{air, total} = \Delta p_{entry} + \Delta p_{air, channel} - \Delta p_{exit} \quad (4-23)$$

The pressure drop for developing flow through the approximated air flow channel is calculated using eq. (4-24).

$$\Delta p_{air,channel} = \frac{f_{air} l_{channel} V_{air}^2}{2D_{h,air}} \quad (4-24)$$

The friction factor for developing laminar flow through a non-circular duct is given by eq. (4-25) [37], where the Reynolds number is defined based on the modified length scale \mathcal{L} and the dimensionless duct length L^+ is used to account for this change of length scale. The correlation is valid for channels with aspect ratios (ϵ) ranging from 0.01 to 1. The aspect ratio for air flow channel is 0.21.

$$f_{air} = \frac{1}{Re_{air,\mathcal{L}}} \left[\left(\frac{3.44}{\sqrt{L_{air}^+}} \right)^2 + \left(\frac{12}{\sqrt{\epsilon}(1+\epsilon) \left[1 - \frac{192\epsilon}{\pi^5} \tanh\left(\frac{\pi}{2\epsilon}\right) \right]} \right)^2 \right]^{\frac{1}{2}} \quad (4-25)$$

$$Re_{air,\mathcal{L}} = \frac{V_{air} \mathcal{L}_{air}}{\nu_{air}} \quad (4-26)$$

$$L_{air}^+ = \frac{L/D_{h,air}}{Re_{air,\mathcal{L}}} \quad (4-27)$$

To evaluate the friction factor for non-circular ducts, the length scale (\mathcal{L}) chosen is the square root of the flow cross sectional area as defined in eq. (4-28) because it is found to be more appropriate than the hydraulic diameter [37].

$$\mathcal{L} = \sqrt{A_{cs,fc}} = \sqrt{(F_s \cdot F_h)} \quad (4-28)$$

The entrance pressure drop and exit pressure rise are given by eq. (4-29) and (4-30) respectively[36]. For the calculated values of σ and $Re_{D_{h,air}}$, the coefficients of entry and exit losses i.e., K_c and K_e are found to be 1.05 and 0.3 respectively[36].

$$\Delta p_{entry} = \rho_{air} \left[\frac{V_{air}^2}{2} (1 - \sigma^2) + \frac{K_c V_{air}^2}{2} \right] \quad (4-29)$$

$$\Delta p_{exit} = \rho_{air} \left[\frac{V_{air}^2}{2} (1 - \sigma^2) - \frac{K_e V_{air}^2}{2} \right] \quad (4-30)$$

To evaluate the heat transfer coefficient on for the oil, published correlations for offset strip fins are used[26]. The flow is found to be laminar ($Re_{oil,D_h} = 154$) using eq. (4-33) with a Prandtl number of 102. Implementation of enhancement techniques such as offset strip fins for laminar flows with high Prandtl numbers is a common practice in heat exchangers[26]. Consecutive rows of offset strip fins are generally offset by half-width of the fins. As a result, when the oil flows from one row of the offset strip fins to the next, oil with maximum flow velocity encounters an obstruction due to the next row of offset strip fins. This disrupts the boundary layer, and as the fluid flows through the next row of offset strip fins, the boundary layer redevelops until it is again disrupted by the following row of fins, resulting in substantial enhancement of the heat transfer on the oil side.

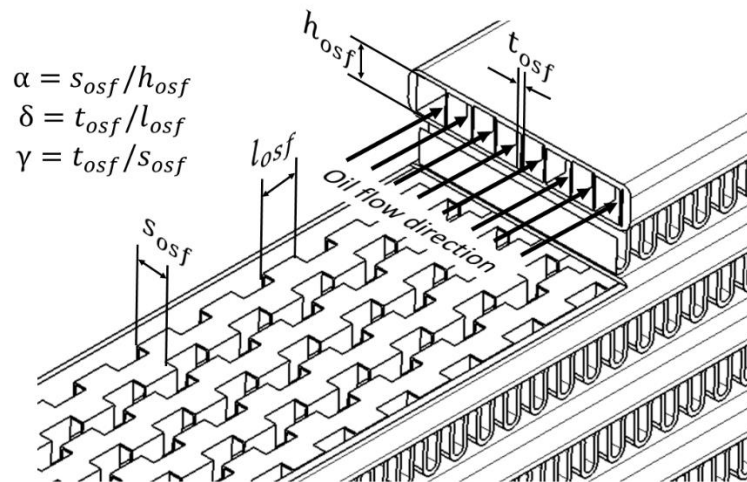


Figure 4.3. Offset strip fin layout for stock heat exchanger

The convective coefficient for oil is calculated from the j-factor using eqs. (4-31) [26] and (4-32). In this equation, α_{osf} accounts for the effect aspect ratio of the fin channel on friction factor and convective heat transfer coefficients (friction factor and convective heat transfer coefficients are higher for lower α_{osf}), δ_{osf} characterizes the effect of the

slenderness of the fin geometry on form drag and heat transfer (thicker and blunter fins have larger form drag and higher heat transfer coefficients as compared to slender and longer fins). γ_{osf} accounts for the reduction in free flow area due to the thickness of the fins[26]. The j-factor correlation is valid for Reynolds numbers ranging from 120 to 10^4 .

$$j_{oil} = 0.6522Re_{oil,D_h}^{-0.5403}\alpha^{-0.1541}\delta^{0.1499}\gamma^{-0.0678} \quad (4-31)$$

$$h_{oil} = \frac{j_{oil}Re_{oil,D_h}Pr_{oil}^{\frac{1}{3}}k_{oil}}{D_{h,oil}} \quad (4-32)$$

$$Re_{oil,D_h} = \frac{V_{oil}D_{h,oil}}{\nu_{oil}} \quad (4-33)$$

The hydraulic diameter for calculating the Reynolds number for oil flow is defined based on the dimensions of the offset strip fin channels and is calculated using eq. (4-34)[26] ($D_{h,oil} = 0.0023$ m) . The oil flow velocity is calculated from the specified oil flow rate of 65 lpm and flow cross sectional area ($V_{oil} = 0.507$ m/s).

$$D_{h,oil} = \frac{4s_{osf}h_{osf}l_{osf}}{2(s_{osf}l_{osf} + h_{osf}l_{osf} + t_{osf}h_{osf}) + t_{osf}s_{osf}} \quad (4-34)$$

The flow cross sectional area is defined as the product of the area of a single offset strip fin channel and the number of channels formed by the offset strip fins in one tube as given by eq. (4-35). The terminology used for offset strip fins is explained in Figure 4.3.

$$A_{cs,oil} = N_{osf}h_{osf}s_{osf} \quad (4-35)$$

A pressure drop increase accompanies the enhancement of heat transfer coefficient on oil side due to surface friction from the increased fin area and the form drag from the fins [26]. The pressure drop on oil side is calculated using eq. (4-36). The friction factor for flow through the offset strip fins is assumed to exist uniformly throughout the flow

length and is calculated using eq. (4-37)[26]. The friction factor correlation is valid for Reynolds numbers ranging from 120 to 10^4 .

$$\Delta p_{oil} = \frac{f_{oil} l_{tube} V_{oil}^2}{2D_{h,oil}} \quad (4-36)$$

$$f_{oil} = 9.6243 Re_{oil,D_h}^{-0.7422} \alpha_{osf}^{-0.1856} \delta_{osf}^{0.3053} \gamma_{osf}^{-0.2659} \quad (4-37)$$

4.1.2 Numerical method

A code is written using Matlab to implement the required iterative loop mentioned in section 4.1.1. Function m files are created to evaluate the pressure drop on the air side and thermo-physical properties in order to keep the code concise and simple. These function m files are then called multiple times in the main code as required. The inputs to the function m file of the pressure drop on air side are the flow channel length, width and height, air temperature and the air velocity while the output is the pressure drop, whereas the input to the function m file for thermo-physical properties is the mean temperature and the outputs are density, thermal conductivity, kinematic viscosity and specific heat. A flowchart of the solution approach is shown in Figure 4.4.

Outlet temperature is guessed for air and oil. Based on these guessed temperatures, a mean temperature is calculated for air and oil and heat transfer coefficients of both the fluids are evaluated using the function m files. The overall heat transfer coefficient is evaluated using these properties and is further used with eq. (4-6) and (4-4) to calculate the effectiveness of the heat exchanger. Once the effectiveness is evaluated, the heat transfer rate is calculated using eq. (4-8). To validate the guess, the outlet temperatures of air and oil are calculated using eq. (4-9) and eq. (4-10) and the values are compared with the guessed values. If the values do not match within 0.01%, the next loop is initiated using

these calculated values of outlet temperatures as the new guessed temperatures. This iterative procedure is continued until the solution is converged.

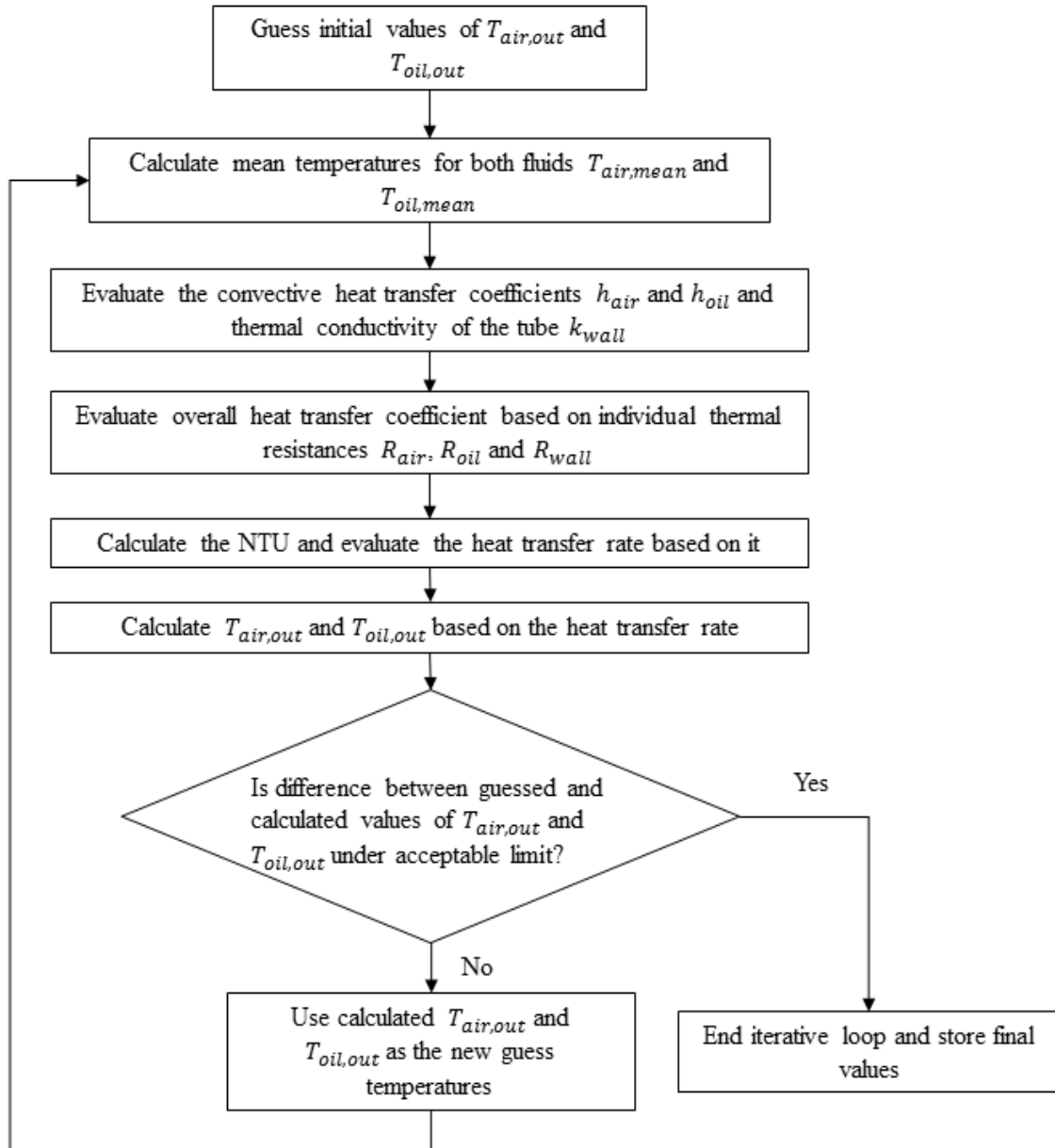


Figure 4.4. Flowchart of program implementation for stock heat exchanger

4.1.3 Mechanical analysis

The flat tube of the stock heat exchanger along with the offset strip fins is tested to check if it sustains the design pressure of 2 MPa. An FEA analysis of a quarter model of the tube with symmetry boundary conditions is done using SolidWorks. The geometry is shown in Figure 4.5. with the constrained faces marked with planar roller supports. A uniform internal pressure of 2 MPa is applied on all the inside surfaces of the flat tube.

Aluminum 6061 T6 is used for the analysis, which is a commonly used aluminum grade in heat exchangers. The yield strength and ultimate tensile strength for this grade of aluminum are 275 MPa and 310 MPa respectively. The maximum allowable hoop stress for process piping according to ASME B 31.3 is given by eq. (4-38) and results in a value of 103.3 MPa.

$$\sigma_{hoop,allowable} = \min\left(\frac{S_{UT}}{3}, \frac{2S_{YT}}{3}\right) \quad (4-38)$$

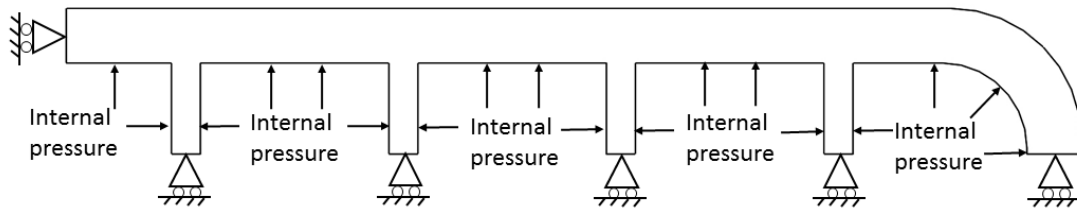


Figure 4.5. Tube geometry, loads and constraints used for mechanical analysis of flat tubes in stock heat exchanger

The circular header of the stock heat exchanger is analyzed with the same internal pressure of 2 MPa using the geometry shown in Figure 4.7. A quarter model is analyzed with symmetry boundary conditions. The constrained faces are modelled as roller supports

and an internal pressure of 2 MPa applied on the inside face. The outer diameter of the existing header is 50 mm and the wall thickness is 5 mm.

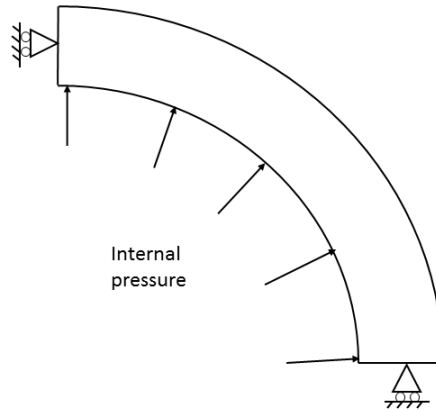


Figure 4.6. Geometry, loads and constraints used for analysis of the existing circular header of stock heat exchanger

4.2 Finned tube bank heat exchanger

This section presents the geometry and parametric analysis for the circular finned tube bank geometry, which is used as an approximation of the lenticular tube finned bank due to unavailability of heat transfer and pressure drop correlations for finned lenticular tube banks. The results from this analysis of finned circular tube banks are assumed to be equivalent to a finned lenticular tube bank (for the same diameter and pitch to diameter ratio) as long as the number of tubes in the defined space remain the same. The objective of the thermal analysis is to evaluate the heat transfer and pressure drop on the air and oil side for the circular tube finned banks. The mechanical analysis aims to design the heat exchanger to sustain a burst pressure of 2 MPa.

4.2.1 Geometry

The overall dimensions of the heat exchanger core are maintained same as that of the stock heat exchanger so that it can be a swap-in replacement. This restriction limits the cross section of to an area of 0.48 m (height) x 0.03 m (depth) and the length to 0.36 m.

The core of the heat exchanger consists of finned circular tube bank. A staggered tube staggered configuration is chosen over an inline configurations for the layout of tubes to enhance the heat transfer. The two options for the layout in the staggered configuration are the equal flow gap and the equilateral layout as shown in Figure 4.7 and Figure 4.8 respectively. In case of circular tubes, the equal flow gap configuration results in a lower longitudinal tube pitch, hence accommodating more tube rows in the confined space. A greater number of tube rows directly translates into more heat transfer due to increased heat transfer area. In case of lenticular tubes, the equal flow gap leads to a lower air pressure drop [38]. Hence, an equal flow gap configuration is selected for the analyzed designs.

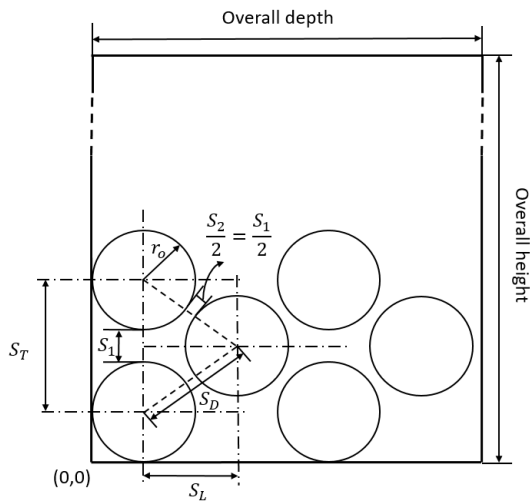


Figure 4.7. Equal flow gap layout for circular tubes

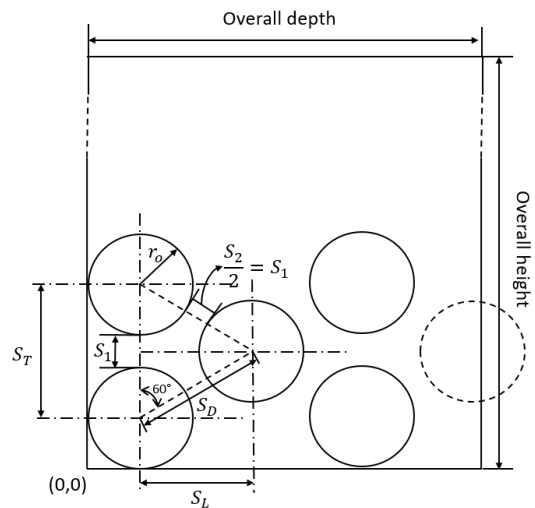


Figure 4.8. Equilateral layout for circular tubes

To define the geometry of the tube bank, two parameters i.e., a tube outer diameter

(D_o) and a transverse pitch to diameter ratio (S_T/D) are selected. Once these parameters are chosen, the flow gap S_1 is fixed. For an equal flow gap layout, the tubes are placed such that $S_2 = S_1$. For the parametric analysis, the tube outer diameter is varied from 5 mm to 10 mm while the S_T/D ratio is varied from 1.7 to 2.5. The tube thickness varies based on the hoop stress as explained in section 4.2.4. The calculated thickness is lesser than the minimum print resolution of the Concept Laser Xline 1000R, and hence a tube thickness of 1 mm is used for all calculations.

On the air side, the fin spacing is selected to optimize the total heat transfer rate from a finned tube bundle in a constrained volume based on the work by Matos et al.[39]. Fin density is the number of fins per unit length along the tube length and is given as

$$\Phi_f = \frac{t_f}{(t_f + \delta_f)} \quad (4-39)$$

The optimum fin density for a circular tube finned bank with a tube pitch to diameter ratio of 1.5 is 0.1 which results in an optimum fin spacing of 4.5 mm for a minimum fin thickness of 0.5 mm (based on Concept Laser Xline 1000R limitations). This fin spacing is considered for all the configurations due to unavailability of data at different tube pitch to diameter ratios.

On the oil side, for the entire range of diameters and S_T/D the oil flow remains in the laminar regime ($90 \leq Re_{oil} \leq 400$). Hence, to obtain convective coefficients similar to the stock heat exchanger, employment of enhancement methods is necessary. As the twisted ribbon is found to clog the tubes in the test prints (section 5.2), the offset strip fins are chosen with a fin length of 10 mm. This offset strip fin length is selected such that the minimum convective heat transfer coefficient obtained from these configurations over the

range of tube diameters and S_T/D ($\sim 1700 \text{ W/m}^2\text{-K}$) is higher than that obtained from the stock heat exchanger ($\sim 1500 \text{ W/m}^2\text{-K}$). The working principle of offset strip fins is explained in section 4.1.1. The minimum transverse spacing between these fins is limited to 1.4 mm based on manufacturing constraints inferred from the test prints for clearing residual powder.

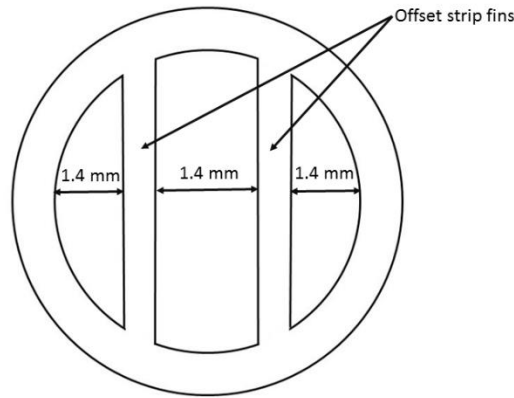


Figure 4.9. End view of circular tube with offset strip fins and the minimum spacing constraint based on test prints

4.2.2 Thermal analysis

To analyze the performance of the finned tube banks at the inlet conditions specified in Table 2.1., an approach suggested by standard texts employing log mean temperature difference (LMTD) based on the air side is used [13]. The heat transfer is evaluated using eq. (4-40) and eq. (4-41).

$$Q_{actual} = N_{tubes}(h_{air}A_{air}\Delta T_{lm,air}) \quad (4-40)$$

$$\Delta T_{lm,air} = \frac{(T_{wall,mean} - T_{air,in}) - (T_{wall,mean} - T_{air,out})}{\ln\left(\frac{T_{wall,mean} - T_{air,in}}{T_{wall,mean} - T_{air,out}}\right)} \quad (4-41)$$

The air outlet temperature can be calculated using eq. (4-42); however the evaluation of wall mean temperature for the tubes (using eq. (4-44)) requires the mean temperature of

oil to be known. The outlet temperature of oil is calculated using eq. (4-46).

$$T_{air,out} = T_{air,in} - \frac{Q_{actual}}{\dot{m}_{air}c_{p,air}} \quad (4-42)$$

$$\frac{T_{wall,mean} - T_{air,out}}{T_{wall,mean} - T_{air,in}} = \exp\left(-\frac{\pi D_o N_{tubes} h_{air}}{\rho_{air} V \omega N_{columns} S_T c_{p,air}}\right) \quad (4-43)$$

$$T_{wall,mean} = T_{oil,mean} - \frac{Q_{actual}}{h_{oil} A_{oil}} \quad (4-44)$$

$$T_{oil,mean} = \frac{T_{oil,in} + T_{oil,out}}{2} \quad (4-45)$$

$$T_{oil,out} = T_{oil,in} - \frac{Q_{actual}}{\dot{m}_{oil}c_{p,oil}} \quad (4-46)$$

Hence, for the evaluation of heat transfer we have a system of four equations (eq. (4-40), (4-42), (4-44) and (4-46)) [13] with four unknown variables viz., heat transfer, air outlet temperature, wall mean temperature and oil outlet temperature. To solve this system of equations, an iterative procedure is implemented as explained in section 4.2.3. Equation (4-43)[13] is used to get an initial guess of the wall mean temperature. The calculation of convective coefficients and heat transfer area for evaluating the heat transfer are calculated using published convective heat transfer correlations.

On the air side, the heat transfer coefficient is evaluated using correlation from the work of Wang et al.[40][41] for tube banks with circular tubes and plain fins for tube diameters greater between 6.35 mm and 12.7 mm with the transverse pitch varying from 17.7 mm to 31.75 mm and longitudinal pitch varying from 12.4 mm to 27.5 mm. Some diameters and tube pitches used in the analysis are outside the range of correlations, however these are the best available correlations in the range of parameters desired. The convective heat transfer coefficient for air is calculated using eq. (4-45). The Nusselt number is a function of the j-factor and is calculated using eq. (4-47). The j-factor is in turn

calculated using eq. (4-48) and is a function of fin pitch, transverse tube pitch, maximum flow velocity, fin collar outside diameter D_c and the hydraulic diameter. The various dimensionless numbers appearing in eq. (4-48) are defined in equations (4-49), (4-50), (4-51), and (4-52) and are used to account for the effects fin pitch, longitudinal tube pitch and number of tube rows. A finned circular tube bank is illustrated in Figure 4.10.

$$h_{air} = \frac{(Nu_{air}k_{air})}{D_{h,air}} \quad (4-45)$$

$$Nu_{air} = j_{air} Re_{air,D_c} Pr_{air}^{1/3} \quad (4-47)$$

$$j_{air} = 0.86 Re_{air,D_c} N_{rows}^{P4} \left(\frac{F_p}{D_c}\right)^{P5} \left(\frac{F_p}{D_{h,air}}\right)^{P6} \left(\frac{F_p}{S_T}\right)^{-0.93} \quad (4-48)$$

$$P3 = -0.361 - \frac{0.042 N_{rows}}{\log_e(Re_{D_c,air})} + 0.158 \log_e(N_{rows} \left(\frac{F_p}{D_c}\right)^{0.41}) \quad (4-49)$$

$$P4 = -1.224 - \frac{0.076 \left(\frac{S_L}{D_{h,air}}\right)^{1.42}}{\log_e(Re_{air,D_c})} \quad (4-50)$$

$$P5 = -0.083 + \frac{0.058 N_{rows}}{\log_e(Re_{air,D_c})} \quad (4-51)$$

$$P6 = -5.735 + 1.21 \log_e\left(\frac{Re_{air,D_c}}{N_{rows}}\right) \quad (4-52)$$

The hydraulic diameter on the air side for finned circular tube banks is defined based on the minimum flow area and the total heat transfer surface area to account for the effect of the fins and is given by eq. (4-53). The minimum flow area is calculated using eq. (4-54).

$$D_{h,air} = \frac{4A_c L_{airflow}}{A_{air}} \quad (4-53)$$

$$A_c = S_T F_S (N_{columns} - 1)(N_{fins} - 1) \quad (4-54)$$

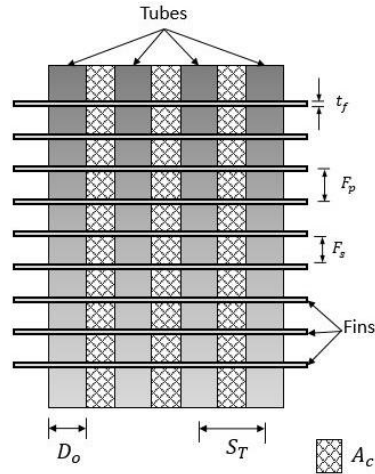


Figure 4.10. Illustration of circular finned tube bank with air flow going into the page

The air side Reynolds number is calculated using eq. (4-55) and is based on the fin collar outside diameter which is defined in equation (4-56).

$$Re_{air,D_c} = \frac{V_{air} D_c}{\nu_{air}} \quad (4-55)$$

$$D_c = D_o + 2t_f \quad (4-56)$$

The heat transfer area on the air side is calculated using eq. (4-57) by accounting for the temperature gradient along the fins by using the overall surface efficiency (eq. (4-58)). The overall surface efficiency ($\eta_{surface}$) is used to characterize the performance of a fin array and is based on the fin efficiency [13]. The efficiency for a single fin (η_{fin}) is calculated using eq. (4-59). The parameters m and Φ_m for evaluating the fin efficiency are calculated from eq. (4-60) and eq. (4-61) [42].

$$A_{air} = \eta_{surface} (N_{fins} A_{fin} + A_{tube,base}) \quad (4-57)$$

$$\eta_{surface} = 1 - \frac{N_{fins} A_{fins}}{A_{tube,base}} (1 - \eta_{fin}) \quad (4-58)$$

$$\eta_{fin} = \frac{\tanh(mr\Phi_m)}{mr\Phi_m} \quad (4-59)$$

$$m = \sqrt{\frac{2h_{air}}{k_{fin}\delta_{fin}}} \quad (4-60)$$

$$\Phi_m = \left(\frac{r_{f,eq}}{r} - 1\right) \left[1 + (0.3 + \left(\frac{m(r_{f,eq} - r)}{2.5}\right)^{1.5 - \frac{r_{f,eq}}{12r}}) (0.26 \left(\frac{r_{f,eq}}{r}\right) - 0.3)) \ln\left(\frac{r_{f,eq}}{r}\right)\right] \quad (4-61)$$

The temperature gradient along the fins is affected by the presence of multiple tubes in the cross section of a single fin. To account for this temperature gradient, the fin area is divided into hexagonal elements centered around individual tubes as shown in Figure 4.11. and an equivalent fin radius is calculated for the unit cell from eq. (4-62). This equivalent radius is used to calculate Φ_m [42].

$$r_{f,eq} = 1.27 S_T \sqrt{\frac{S_D}{S_T} - 0.3} \quad (4-62)$$

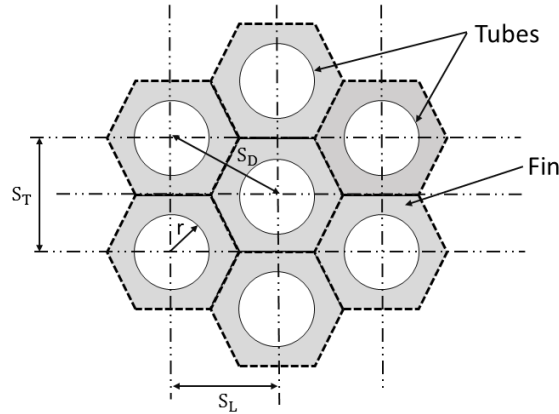


Figure 4.11. Division of fin area into hexagonal elements for evaluation of fin efficiency

The convective coefficient on the oil side is calculated from the Nusselt number using eq. (4-63). The Nusselt number for developing laminar flow for high Prandtl number fluids

(like oil) with a constant surface temperature boundary condition is given by eq. (4-64) [43][8] and depends on the length of the offset strip fin.

$$h_{oil} = \frac{Nu_{oil}k_{oil}}{D_{h,oil}} \quad (4-63)$$

$$Nu_{oil} = 3.66 + \frac{0.0668 \left(\frac{D_{h,oil}}{l_{osf}} \right) Re_{oil,D_h} Pr_{oil}}{1 + 0.04 \left[\left(\frac{D_{h,oil}}{l_{osf}} \right) Re_{oil,D_h} Pr_{oil} \right]^{2/3}} \quad (4-64)$$

$$Re_{oil,D_h} = \frac{V_{oil}D_{h,oil}}{\nu_{oil}} \quad (4-65)$$

The system of equations is solved using an iterative method detailed in section 4.2.3.

The air side pressure drop for a circular tube finned bank is the sum of the form and viscous drag and is given by eq. (4-66) [36]. The friction factor is given by eq. (4-67) and depends on the transverse and longitudinal tube pitches, and the fin pitch. The dimensionless numbers appearing in eq. (4-67) are given by eq. (4-68), (4-69) and (4-70) [41].

$$\Delta p_{air} = \left[f_{air} \frac{A_c}{A_{air}} \frac{\rho_{air,mean}}{\rho_{air,in}} + (1 + \sigma^2) \left(\frac{\rho_{air,in}}{\rho_{air,out}} - 1 \right) \right] \frac{G_c^2}{2\rho_{air,in}} \quad (4-66)$$

$$f_{air} = 0.0267 Re_{air,D_c}^{F1} \left(\frac{S_T}{S_L} \right)^{F2} \left(\frac{F_p}{D_c} \right)^{F3} \quad (4-67)$$

$$F1 = -0.764 + 0.739 \frac{S_T}{S_L} + 0.177 \frac{F_p}{D_c} - \frac{0.00758}{N_{rows}} \quad (4-68)$$

$$F2 = -15.689 + \frac{64.021}{\log_e(Re_{air,D_c})} \quad (4-69)$$

$$F3 = 1.696 - \frac{15.695}{\log_e(Re_{air,D_c})} \quad (4-70)$$

To calculate the pressure drop on the oil side, the friction factor for a laminar developing flow in non-circular ducts is used and is given by eq. (4-72) [37]. This friction

factor is then used in eq. (4-71) to calculate the pressure drop on oil side. The correlation for friction factor is valid for aspect ratios from 0.01 to 1. The aspect ratio for oil side flow channels varies between 0.25 and 0.41 for tube diameters under consideration assuming equal spacing between the offset strip fins.

$$\Delta p_{oil} = \frac{f_{oil} l_{tube} V_{oil}^2}{2D_{h,oil}} \quad (4-71)$$

$$f_{oil} = \frac{1}{Re_{oil,L}} \left[\left(\frac{3.44}{\sqrt{L_{oil}^+}} \right)^2 + \left(\frac{12}{\sqrt{\epsilon}(1+\epsilon) \left[1 - \frac{192\epsilon}{\pi^5} \tanh\left(\frac{\pi}{2\epsilon}\right) \right]} \right)^2 \right]^{\frac{1}{2}} \quad (4-72)$$

$$Re_{oil,L} = \frac{V_{oil} \mathcal{L}_{oil}}{\nu_{oil}} \quad (4-73)$$

$$\mathcal{L}_{oil} = \sqrt{A_{cs,fc,oil}} \quad (4-74)$$

$$L_{oil}^+ = \frac{L_{tube}/D_{h,oil}}{Re_{oil}} \quad (4-75)$$

4.2.3 Numerical method

The solution approach is shown in the flowchart in Figure 4.12. It is implemented identically to the code for the stock heat exchanger. A computer program is written using Matlab to implement the iterative procedure. Function m files are created for repetitive portions of the calculations such as evaluating the thermo-physical properties of fluids, evaluating friction factors on oil side etc. These function m files are called by a main program in every iterative loop.

In this main program, the geometry is defined by defining the tube diameter and pitch to diameter ratio. Geometrical parameters including minimum longitudinal tube pitch, minimum flow gap and contraction ratio are calculated for equal flow gap configuration. After this, an outlet temperature of air is guessed. A mean temperature is calculated as the

arithmetic mean of inlet temperature and the guessed outlet temperature of air, and the thermo-physical properties and convective heat transfer coefficient is evaluated.

For the first iterative loop, the wall mean temperature is calculated using eq. (4-43) and for the subsequent iterations, the wall temperature was calculated using eq. (4-44). The use of eq. (4-43) helps in getting a good initial guess which helps in convergence of the solution. A randomly guessed wall temperature can also be used for the first loop, but it would lead to a slower convergence to a solution or no convergence at all. Based on the air inlet, air outlet and wall mean temperatures, the logarithmic mean temperature difference is calculated for the air side using eq. (4-41) and the heat transfer rate is then calculated using eq. (4-40). From this heat transfer rate, the actual outlet temperature of air and mean temperature of tube is calculated using eq. (4-42) and eq. (4-44).

If the sum of difference between the calculated and guessed outlet temperatures of air and mean temperatures of tube wall from successive iterations is greater than 0.01%, the calculated temperatures are used as the guessed temperatures for the next iteration. The thermo-physical properties and heat transfer coefficients are evaluated at this calculated temperature in the next loop and then the heat transfer is re-evaluated. This iterative procedure is continued until the solution is converged.

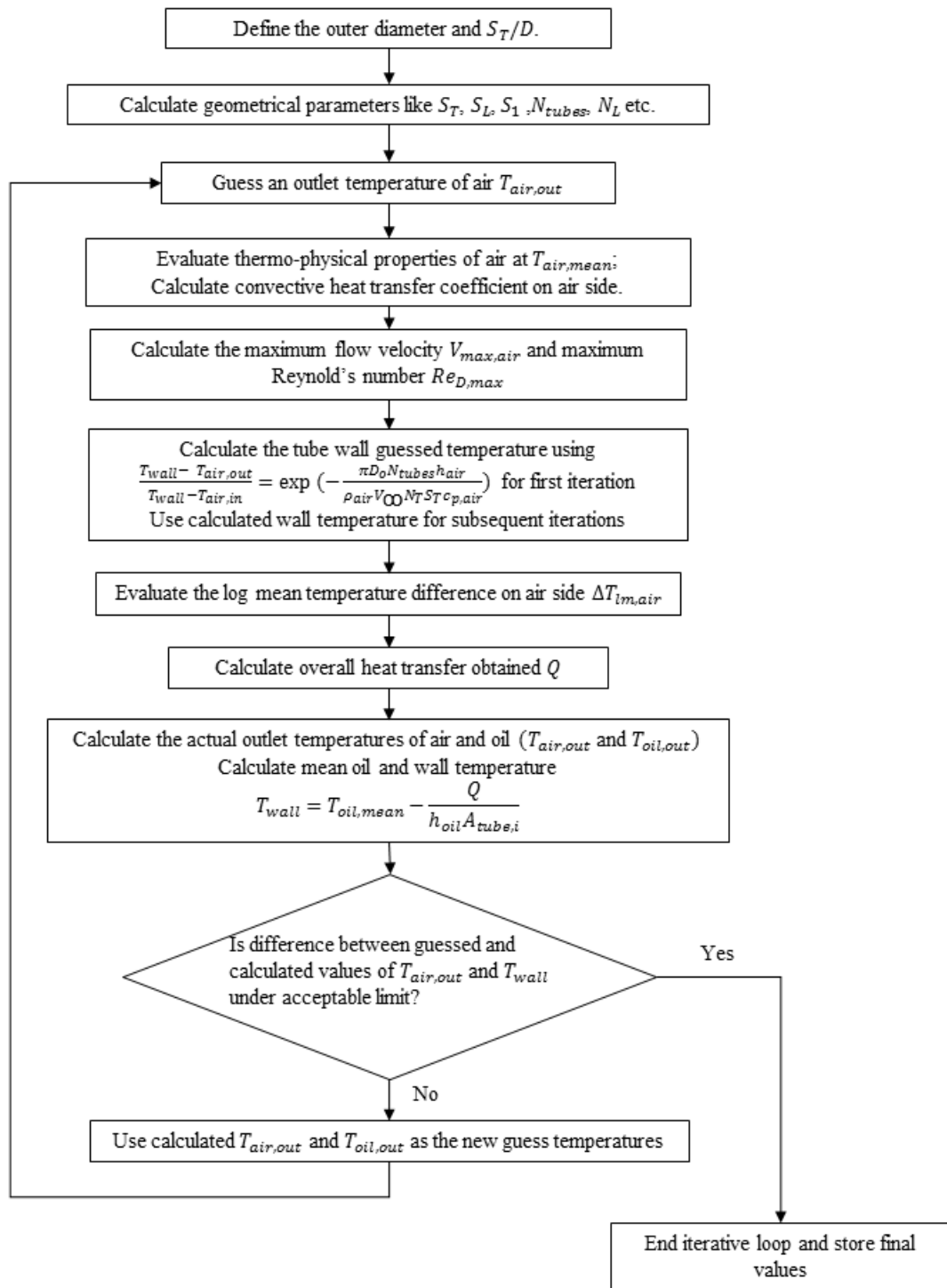


Figure 4.12. Flowchart of program implementation for circular finned tube banks

4.2.4 Mechanical analysis

For defining a tube thickness that can sustain a burst pressure of 2 MPa, a simplified hoop stress calculation is done. The physical properties of the AlSi10Mg powder are used for this calculation. The yield strength and the ultimate tensile strength are 170 MPa and 265 MPa respectively. The maximum allowable stress according to ASME B31.3 for pipes is given by eq. (4-38) and is 86.67 MPa. The hoop stress produced in a thin walled tube subjected to an internal pressure ($P_{internal}$) is given using eq. (4-76).

$$\sigma_{Hoop} = \frac{P_{internal} D_o}{2t_{tube}} \quad (4-76)$$

For fatigue cycle testing, the mean and alternating pressures are equal and have a value of 62500 Pa. The fatigue failure limit is evaluated for the final design using a Goodman fatigue criteria. To analyze the rotated square header for the new design, an FEA analysis is done in SolidWorks. The geometry used for the analysis is shown in Figure 4.13. and accounts for the holes in the header at the tube attachment points. The diagonal of the header is selected to be 50 mm to satisfy the volume constraints. One end face of the tube is constrained using a fixed support while the other end face is constrained as a planar roller joint. An internal pressure of 2 MPa is applied on the inside faces.

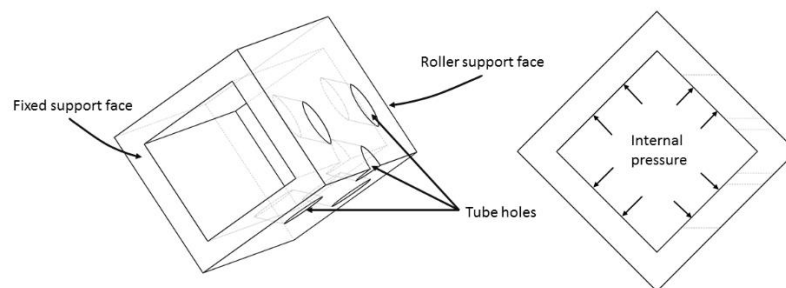


Figure 4.13. Geometry, loads and constraints used for the analysis of the rotated square header

4.3 Lenticular design selection

The lenticular tube shape offers more space for internal features and is hence favorable from a manufacturing perspective. The lenticular shape is characterized by a slenderness ratio (λ) which is the ratio of the semi minor axis to the semi major axis as shown in Figure 4.14 and is given by eq. [27]. $\lambda = 0$ is an infinitely elongated tube while $\lambda = 1$ is a circular tube. The variation of tube shape with slenderness ratio is shown in Figure 4.15.

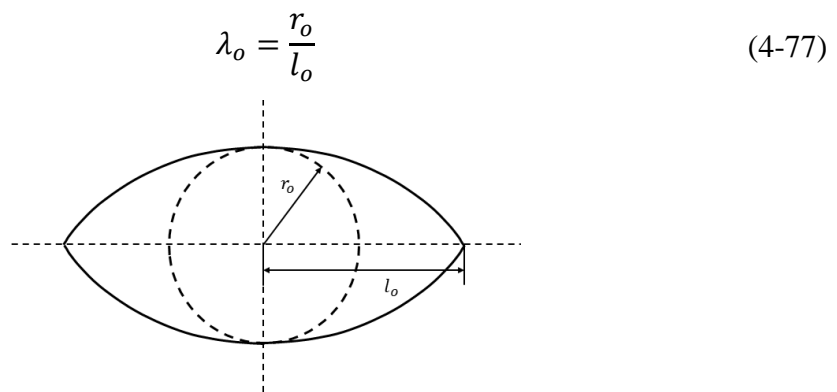


Figure 4.14. Definition of slenderness ratio for lenticular tube shape

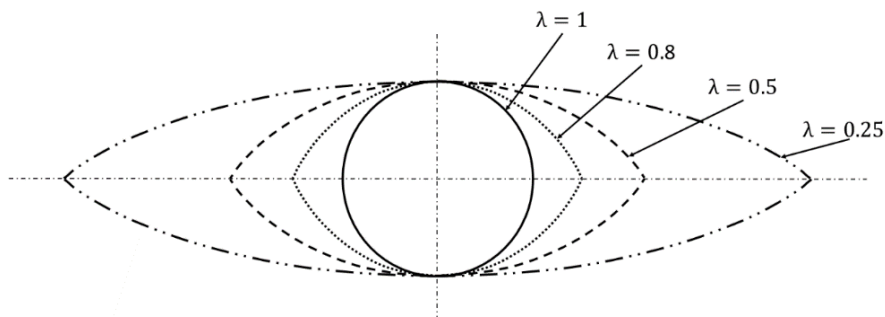


Figure 4.15. Effect of varying slenderness ratio on lenticular tube shape

The shape of the interior of the tubes is also lenticular with the same slenderness ratio i.e. $\lambda_i = \lambda_o$. The same slenderness ratio option results in a greater thickness at the stress concentration points for the same tube diameter and minimum tube thickness (Figure 4.16)

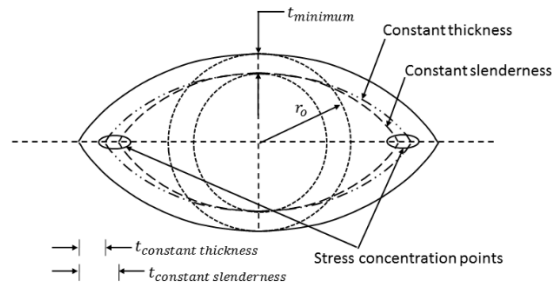


Figure 4.16. Tube thickness comparison for constant thickness and constant slenderness options for same tube diameter and minimum thickness

For a required thickness at the stress concentration points (based on burst pressure), the constant slenderness results in lower minimum tube thickness as shown in Figure 4.17, hence offering more internal space.

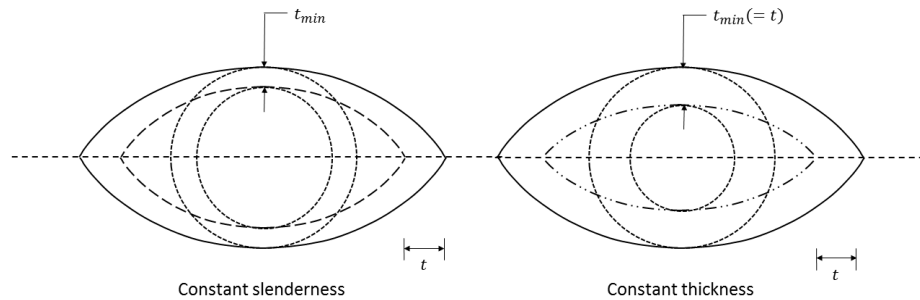


Figure 4.17. Minimum tube thickness for constant slenderness and constant thickness options for lenticular tubes

The circular tube banks are transformed into lenticular tube banks by varying the slenderness ratio while maintaining the same tube outer diameter and S_T/D ratio in the equal flow gap configuration. This variation changes the longitudinal tube pitch (S_L) and the variation in configuration with slenderness ratio is shown in Figure 4.18. As the tube diameter and transverse pitch are kept constant, there is no loss of tubes in the transverse direction. Decreasing the slenderness ratio increases the longitudinal pitch, leading to a loss of tube rows in the longitudinal direction after a threshold value of slenderness ratio

(which is dependent on the tube diameter and transverse pitch).

To utilize the advantages of the lenticular shape (greater internal space and lower air side pressure drop) without adversely affecting the heat transfer, the slenderness of the circular tube banks is decreased until a point where there is no loss of tube rows so that there is not decrease in the heat transfer area on air and oil side. The advantage of greater internal space has been explained in Figure 3.4.

At an 8 mm tube diameter and S_T/D of 1.8, decreasing the slenderness ratio from 1 (circular tubes) to 0.8 (lenticular tubes) reduces the pressure drop contribution from bare tubes from 56 Pa to 28 Pa. The contribution from bare tubes is significant compared to the total pressure drop on 92 Pa. The pressure drop on the air side is dependent on the maximum velocity due to flow obstruction. Maintaining the equal flow gap configuration ensures that the maximum air velocity remains the same for configurations with same tube diameters and transverse pitch. Hence the transition from circular to lenticular tubes does not affect pressure drop on the air side adversely.

On the oil side the heat transfer area increases with decreasing slenderness ratio, as long as the number of tubes remain the same for similar tube diameters. For an inside tube diameter of 6 mm and slenderness ratio of 0.8, the heat transfer area (excluding the offset strip fins) increases from 0.66 m² for circular tubes to 0.73 m² for lenticular tubes.

The results from the analysis of the circular tube banks are then combined with the manufacturing constraints based on the test prints (section 5.2) to select a final tube diameter and S_T/D . To finalize the lenticular finned tube bank, a slenderness ratio λ is selected following the thought process mentioned above.

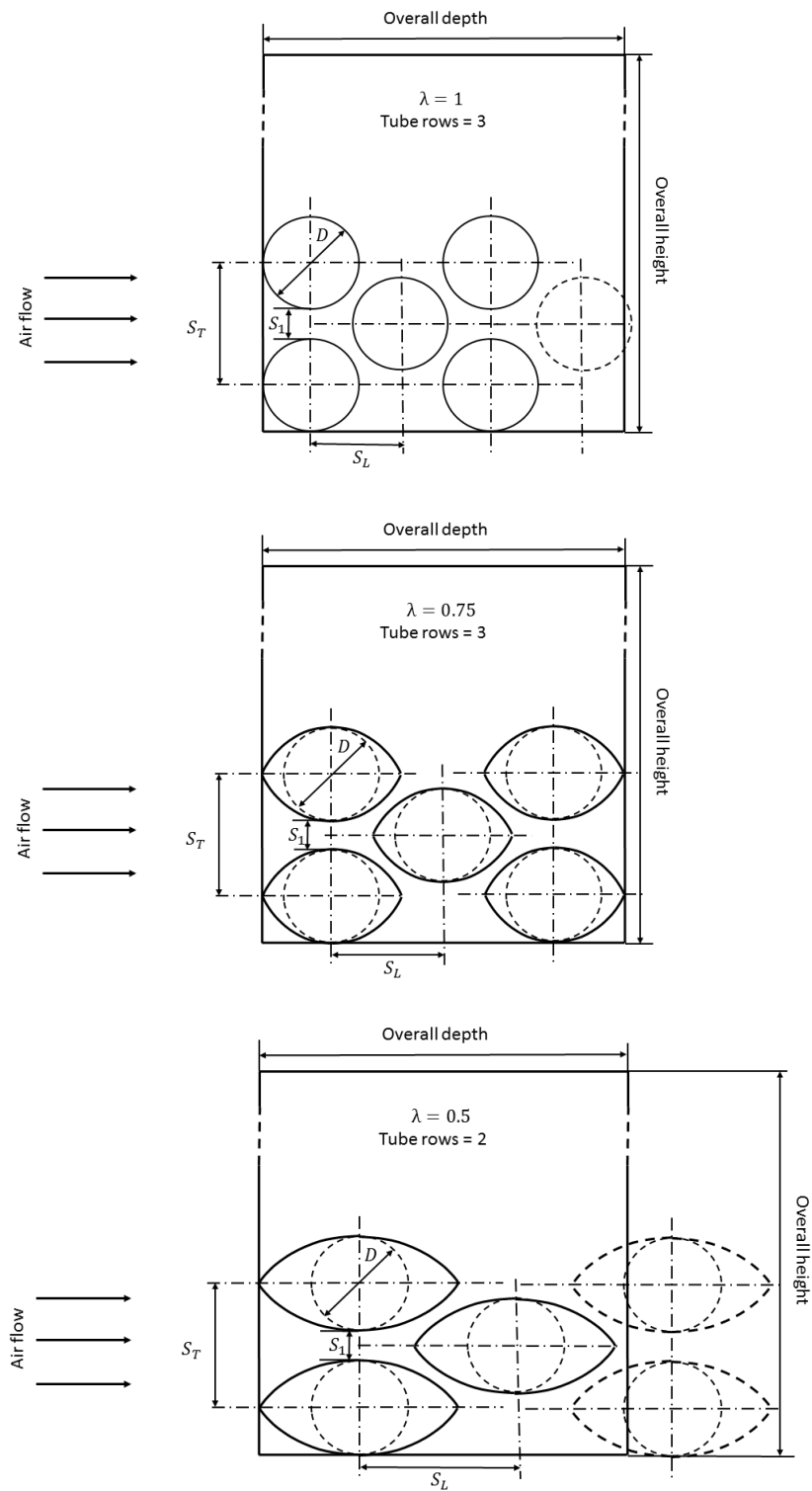


Figure 4.18. Transformation of circular tube bank into lenticular tube bank in equal flow gap configuration

Chapter 5. Results

This chapter summarizes the results of the thermal and mechanical analysis of the stock and finned tube bank heat exchanger. The results from the finned tube bank analysis are interpreted to select the potential combinations of tube and fin geometry for the AM heat exchanger. These potential geometries are evaluated for manufacturability in two trial test prints described in section 5.2. The results of the test prints are used to evaluate the printability of various feature combinations and dimensions. The observations from the test prints are then combined with the results of the thermal and mechanical analysis to arrive at a final design.

5.1 Modelling results

Sections 5.1.1 and 5.1.2 describe the predicted thermal and mechanical performance of the stock heat exchanger and compare the results to the desired baseline performance, while section 5.1.3 and 5.1.4 present the results for the thermal and mechanical analysis of the tube bank heat exchanger.

5.1.1 Thermal analysis of stock heat exchanger

The stock heat exchanger is analyzed at the design conditions specified in Table 2.1. using the method detailed in section 4.1. The results are summarized in Table 5.1. The predicted heat transfer rate is ~7 kW lower than the desired value of 15 kW. The convective resistances on the air and oil side are $5.2e-3$ K/W and $5.5e-4$ K/W respectively. The conductive resistance across the tube wall is $3.8e-6$ K/W.

The Reynolds number for air flow is 860 with an entrance length of 120 mm. As the channel length is 27 mm, the flow is in the developing regime with a convective heat transfer coefficient of $76 \text{ W/m}^2\text{-K}$. The area contribution by bare tubes is 0.8 m^2 while that from the fins is 1.75 m^2 . After calculating a surface efficiency ($\eta_{surface}$) of 0.98, the total effective heat transfer area on the air side is 2.5 m^2 . The pressure drop on the air side is 40 Pa, which is within the threshold of 343 Pa. The outlet temperature of air is 330 K.

The Reynolds number on the oil side is 153 with a thermal entrance length of 1.7 m. An offset strip fin length (l_{osf}) of 3 mm ensures that the flow remains in the developing regime with a convective coefficient of $1467 \text{ W/m}^2\text{-K}$. The heat transfer area on the oil side after considering the area contribution from 100 % efficient offset strip fins is 1.23 m^2 . The oil side pressure drop is 13.5 kPa which is significantly lower than the maximum acceptable pressure drop of 170 kPa. The oil outlet temperature is 368.8 K. Overall, the heat exchanger underperforms in terms of heat transfer while the pressure drops are acceptable.

The heat transfer increases to 10.1 kW for the maximum measured flow velocity of 7 m/s with the convective heat transfer coefficient increasing from $76 \text{ W/m}^2\text{-K}$ to $99 \text{ W/m}^2\text{-K}$. With the existing geometry of the heat exchanger, the convective coefficient on the air side would have to be $155 \text{ W/m}^2\text{-K}$ to produce the desired heat transfer rate of 15 kW. Due to the approximation of the wavy channel to a straight channel on the air side, the convective coefficients could be under predicted. With the existing prediction of convective coefficient of $76 \text{ W/m}^2\text{-K}$, the air side area would have to be $\sim 5.2 \text{ m}^2$, which is twice the area offered by the existing geometry. Hence, with all the operating conditions

kept the same, the heat exchanger would have to be almost twice its current size to produce the required heat duty.

Table 5.1. Performance estimate of the stock heat exchanger

	Heat transfer rate (kW)	7.9
Air side	Air side pressure drop (Pa)	40
	Air side convective heat transfer coefficient (W/m ² -K)	76
	Air outlet temperature (K)	330
	Air side heat transfer area (m ²)	2.5
	Air side convective resistance (K/W)	5.2e-3
Oil side	Oil side pressure drop (kPa)	13.5
	Oil side convective heat transfer coefficient (W/m ² -K)	1467
	Oil outlet temperature (K)	368.8
	Oil side heat transfer area (m ²)	1.2
	Oil side convective resistance (K/W)	5.5e-4

5.1.2 Mechanical analysis of stock heat exchanger

The stress plot from the mechanical analysis is presented in Figure 5.1. The maximum von Mises stress in the flat tubes is 31.7 MPa and is located at the attachment point of the offset strip fins to the tube. As the induced stress is less than the allowable stress of 101.3 Pa, the flat tube geometry with the offset strip fins is sufficiently strong to withstand the design burst pressure. The stress plot for the existing circular header is shown in Figure 5.2. The maximum induced stress (10.27 MPa) is less than the allowable stress and hence the header is also safe for the design burst pressure.

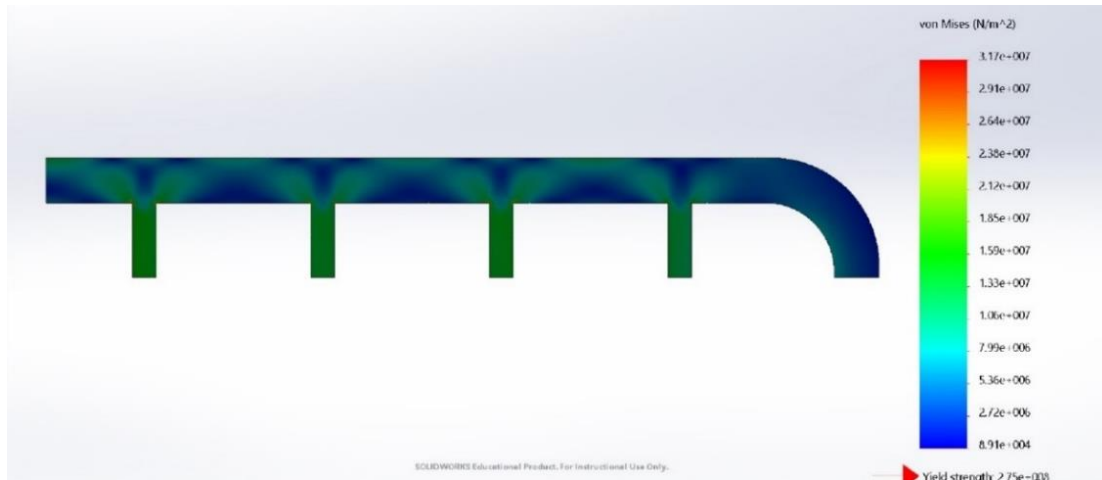


Figure 5.1. von Mises stress plot for the flat tube with offset strip fins with a 2 MPa internal pressure load

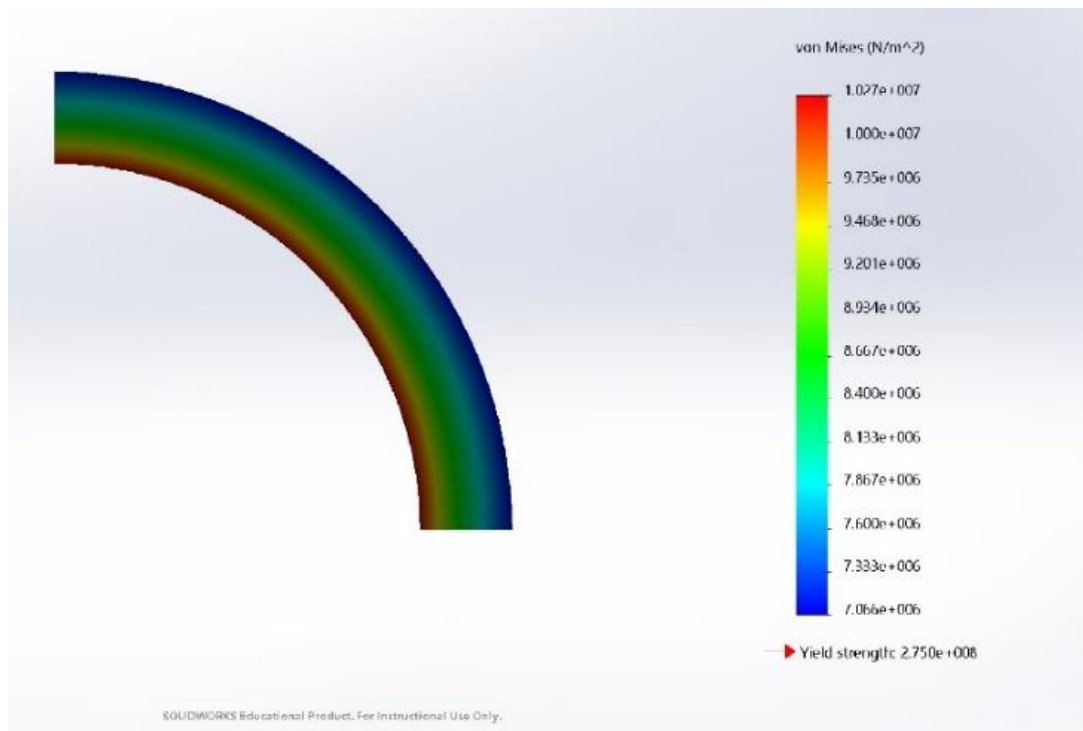


Figure 5.2. von Mises stress plot for the existing circular header with a 2 MPa internal pressure load

5.1.3 Thermal analysis of finned tube bank heat exchanger

As mentioned in section 4.2.1, the lenticular finned tube banks are approximated and analyzed as circular tube finned banks. The analysis is conducted for the design conditions mentioned in the product design specifications mentioned in Table 2.1. The air side flow rate is $0.6 \text{ m}^3/\text{s}$ while the oil side flow rate is 65 lpm. For both the fluids, the flow rate is kept constant but the flow velocities depend on the configuration (specifically the tube diameter and S_T/D) under consideration. The fin spacing is 4.5 mm for all cases considered. Figure 5.3. presents a contour plot of the heat transfer for various pitch to diameter ratios S_T/D on the x-axis and tube diameters on the y-axis.

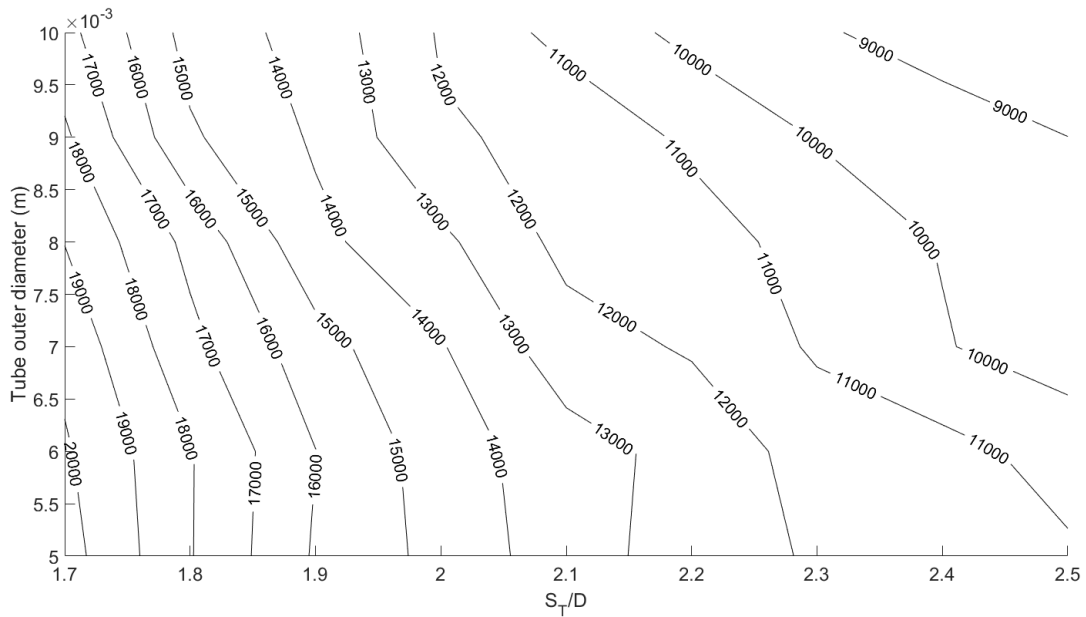


Figure 5.3. Contour plot of heat transfer rate (W) for finned tube bank heat exchanger assuming circular tubes

$$T_{\text{air,in}} = 318\text{K}, \dot{V}_{\text{air}} = 0.6 \text{ m}^3/\text{s}, T_{\text{oil,in}} = 373\text{K}, \dot{V}_{\text{oil}} = 65 \text{ lpm}, F_s = 4.5 \text{ mm}$$

For tube diameters between 5 mm and 10 mm and S_T/D from 1.7 to 2.5, the heat transfer rate varies between ~9 kW and ~20 kW. Heat transfer increases as the tube diameter and S_T/D are decreased. This result is due to the corresponding increase in the number of tubes that can be accommodated in the constrained volume. Smaller tube diameters (at constant pitch to diameter ratio) and lower pitch to diameter ratios (at a constant diameter) result in larger convective heat transfer coefficients on the oil and air side. The convective coefficients are shown in Figure 5.4. Hence, to obtain a higher heat transfer rate, smaller tube diameters with lower S_T/D are preferred.

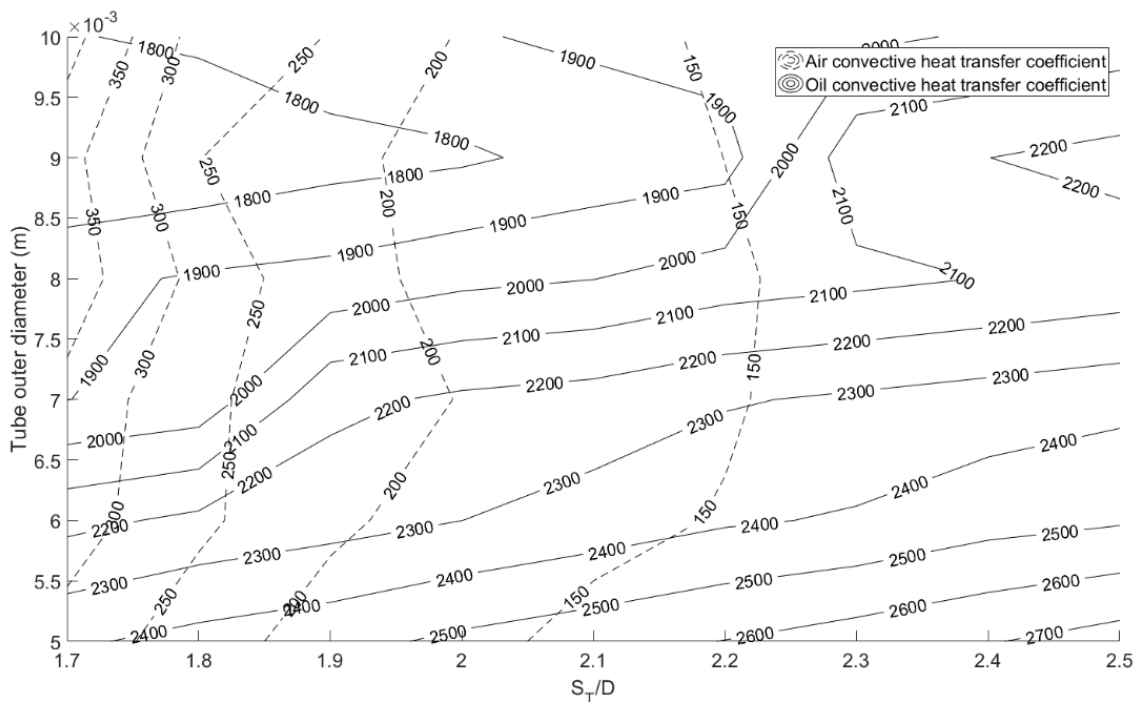


Figure 5.4. Contour plot of air and oil side convective heat transfer coefficients for finned tube banks heat exchanger assuming circular tubes

$$T_{\text{air,in}} = 318\text{K}, \dot{V}_{\text{air}} = 0.6 \text{ m}^3/\text{s}, T_{\text{oil,in}} = 373\text{K}, \dot{V}_{\text{oil}} = 65 \text{ lpm}, F_s = 4.5 \text{ mm}$$

The contour plot for pressure drop on the air side is shown in Figure 5.5. For tube diameters from 5 mm to 10 mm and S_T/D from 1.7 to 2.5, the pressure drop varies from ~60 Pa to ~170 Pa. At a constant tube diameter, the pressure drop increases as the pitch to diameter ratio is decreased. Similarly, at a constant pitch to diameter ratio, the pressure drop increases as the tube diameter is increased. These trends are due to increased air velocities accompanying both scenarios mentioned above.

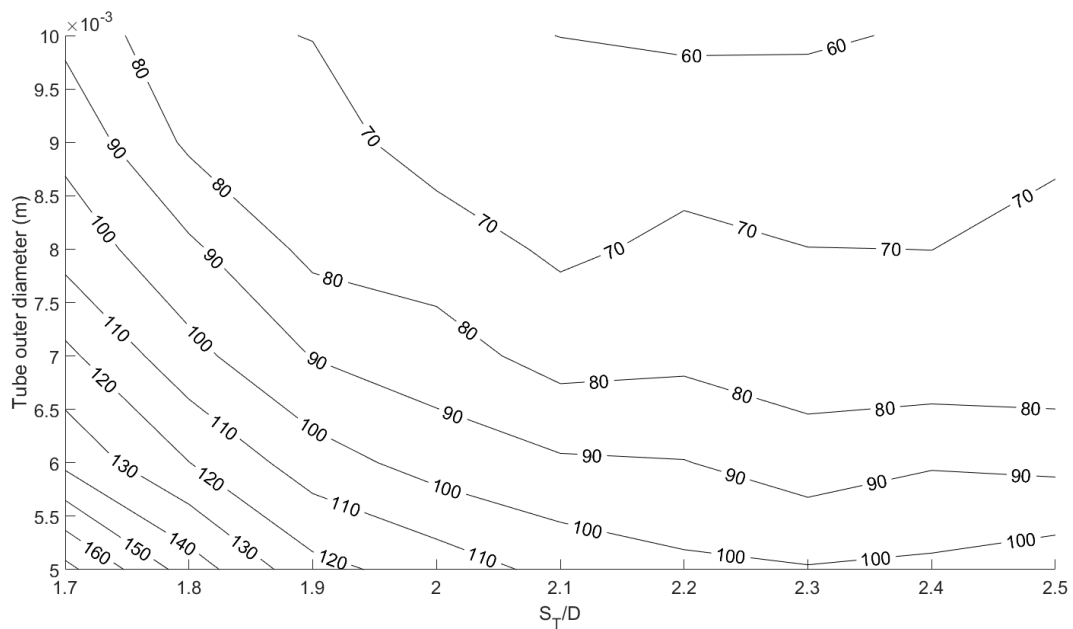


Figure 5.5. Contour plot for air side pressure drop (Pa) for finned tube bank heat exchanger assuming circular tubes

$$T_{\text{air,in}} = 318\text{K}, \dot{V}_{\text{air}} = 0.6 \text{ m}^3/\text{s}, T_{\text{oil,in}} = 373\text{K}, \dot{V}_{\text{oil}} = 65 \text{ lpm}, F_s = 4.5 \text{ mm}$$

The contour plot for oil side pressure drop is shown in Figure 5.6. The pressure drop increases as the tube diameter is decreased (at constant S_T/D) and the S_T/D is increased (at constant tube diameter). For tube diameters between 5 mm and 10 mm and S_T/D from 1.7 to 2.5, the oil side pressure drop increases from ~20 kPa to ~110 kPa.

This increase in pressure drop is due to the increase in oil flow velocity because of the reduction in flow area on the oil side accompanying the aforementioned scenarios. Although the pressure drop is higher than the stock heat exchanger, it is less than the threshold of 170 kPa.

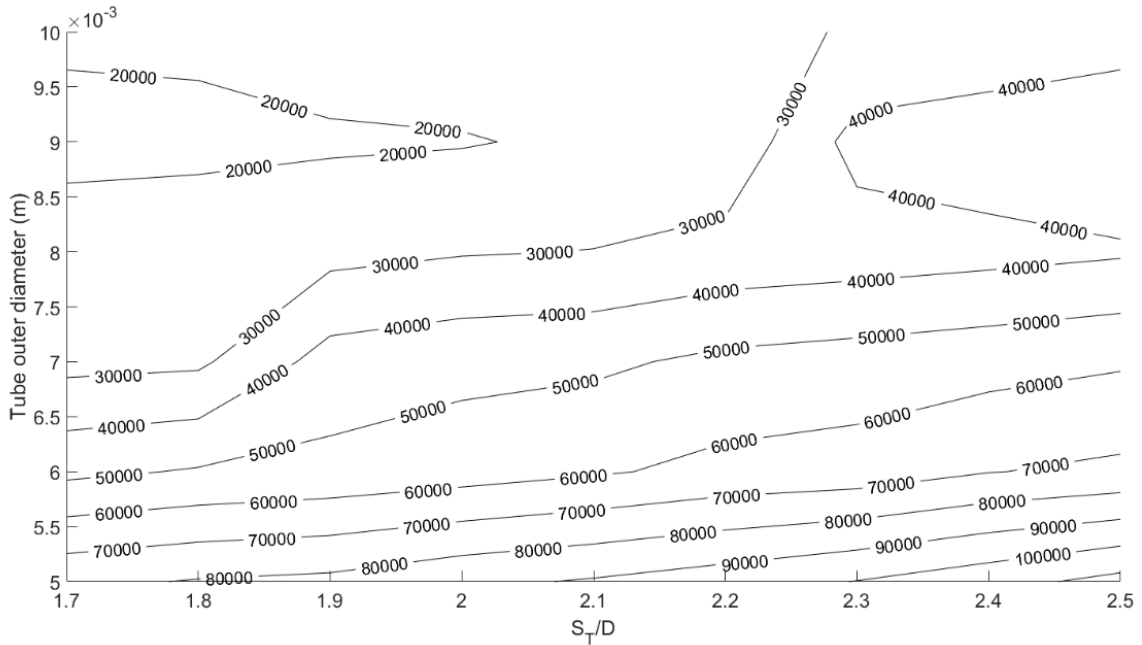


Figure 5.6. Contour plot for oil side pressure drop (Pa) for finned tube bank heat exchanger assuming circular tubes

$$T_{\text{air,in}} = 318\text{K}, \dot{V}_{\text{air}} = 0.6 \text{ m}^3/\text{s}, T_{\text{oil,in}} = 373\text{K}, \dot{V}_{\text{oil}} = 65 \text{ lpm}, F_s = 4.5 \text{ mm}$$

All the analyzed configurations have acceptable pressure drops on the air and oil side, but the number of configurations that satisfy the heat transfer requirements are limited. As the pressure drops are not a concern, obtaining the maximum heat transfer rate is prioritized. Prioritizing the maximum heat transfer also introduces a safety factor for the heat duty which is calculated based on approximations mentioned in previous sections.

Hence, smaller tube diameters with lower S_T/D are preferred to ensure adequate heat

transfer is obtained. This arrangement can also reduce the volume required for the heat exchanger. A maximum heat transfer of 20 kW can be obtained from the smallest tube diameter of 5 mm and S_T/D of 1.7. This tube diameter however does not provide sufficient internal space for fabrication of enhancement features. Hence, the lowest tube diameter is restricted to 6 mm for the test prints detailed in section 5.2. Examples of configurations that meet the heat transfer requirements are tube diameters of 6 mm, 8 mm and 10 mm with pitch to diameter ratios less than ~ 1.9 , ~ 1.8 and ~ 1.7 respectively.

Smaller diameter tubes can be made more slender (while keeping the same number of tubes within the constrained volume) as compared to larger diameter tubes (shown in Figure 5.7). Decreasing the slenderness ratio of the tubes also decreases the air side pressure drop contribution from bare tubes. For a finned circular tube bank configuration with a tube diameter of 8 mm and S_T/D of 1.8, bare tubes contribute 56 Pa of the total pressure drop of 92 Pa. Decreasing the slenderness ratio to 0.8 reduces the pressure drop contributed by bare tubes to 28 Pa. As the contribution to pressure drop by the tubes is significant, decreasing the slenderness ratio can reduce the air side pressure drop considerably.

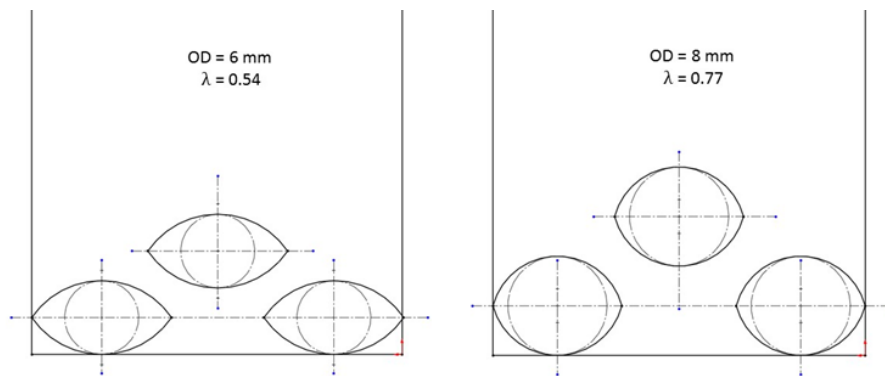


Figure 5.7. Decrease in slenderness ratio made possible by decreasing tube diameter

5.1.4 Mechanical analysis of finned tube banks

A tube thickness based on the tube outer diameter is given by eq. (4-78) using the burst pressure of 2 MPa. This equation results in tube thicknesses varying between 0.06 mm and 0.12 mm, which are smaller than the minimum resolution of the Concept Laser Xline 1000R. Hence, a minimum tube thickness of 1 mm is adopted for the thermal analysis based on manufacturing constraints.

$$t_{tube} = 0.012 D_o \quad (4-78)$$

The stress plot from the analysis of the header is shown in Figure 5.8. The maximum stress induced in the header is 59.8 MPa while the maximum allowable hoop stress is 86.67 MPa. Hence, a thickness of 5 mm is sufficient for the burst pressure requirements.

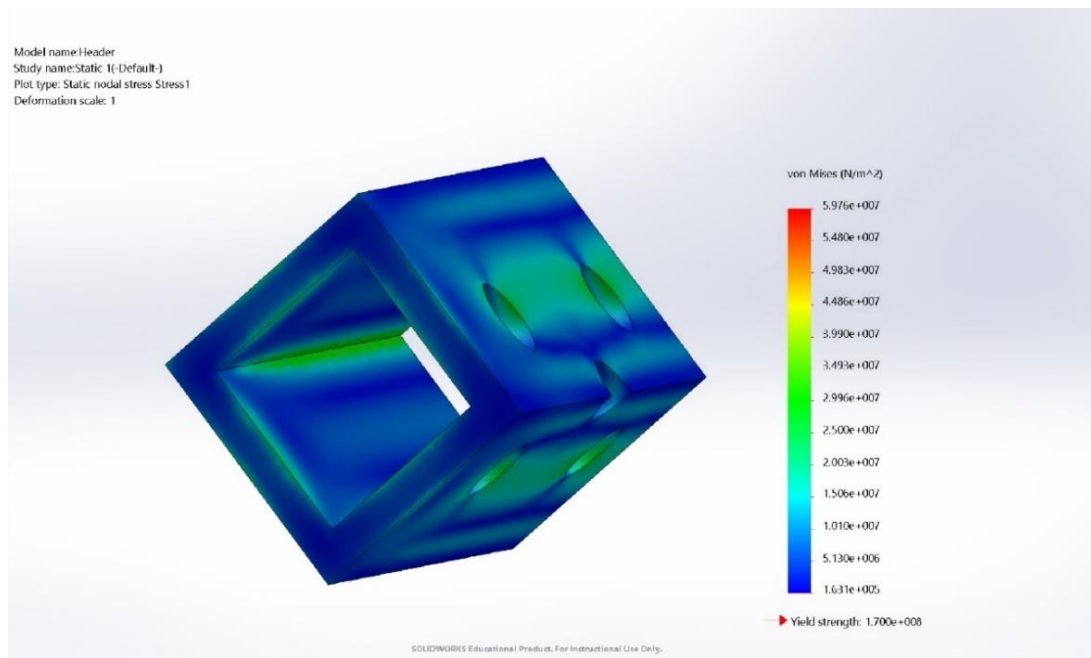


Figure 5.8. von Mises stress plot for rotated square header for AM heat exchanger for a 2MPa internal pressure load

5.2 Test prints

To evaluate the design options of circular versus lenticular tube shapes, tube diameter and strip fins versus twisted ribbon internal features, two test prints with multiple parts were fabricated. These test prints would then assist in finalizing the parameters for the final heat exchanger design by accounting for manufacturing limitations.

The aim of the first print, based on the results of thermal analysis, is to evaluate the smallest printable tube diameter with internal features. Hence, for this print a tube diameter of 6 mm and 8 mm are selected. Circular and lenticular tubes with these diameters are printed with offset strip fins and twisted ribbons. A slenderness ratio of 0.5 is selected for the lenticular tubes. A tube thickness of 1.2 mm and 1.6 mm is used with the 6 mm and 8 mm tubes respectively. The pitch for the internal features is 10 mm in the oil flow direction based on the developing oil flow length used in the thermal analysis. With the lenticular tubes, an offset arrangement of twisted ribbons is tested. All the tubes are printed with the print direction perpendicular to the tube axis. For compatibility with this print direction, the offset strip fins are oriented at an angle of 45 degrees with the print direction.

The prints are inspected visually by holding the tube axis against a light source. If light can be seen through the passageways formed in the tubes, the tubes are said to be okay. If no light passes through the passageways, a flow test is done by blowing air manually from one end of the tubes to check if it comes out of the other end. If air passes through the tubes, the tubes are said to be acceptable in terms of fluid flow. The tubes are also visually inspected for checking any deformities in shapes of the tubes or the internal features.

The details of the parts printed in the first print are mentioned in Table 5.2. The fabricated parts from the first print are displayed in Figure 5.9.

Table 5.2. Details of parts printed in first test print

Part 8	Circular	8	Offset strip fin	1.6	Okay	Okay
Part 7	Circular	8	Twisted ribbon	1.6	Not okay	Okay
Part 6	Circular	6	Offset strip fin	1.2	Not okay	Not okay
Part 5	Circular	6	Twisted ribbon	1.2	Not okay	Not okay
Part 4	Lenticular	8	Angled offset strip fin	1.6	Okay	Okay
Part 3	Lenticular	8	Offset twisted ribbon	1.6	Okay	Okay
Part 2	Lenticular	6	Angled offset strip fin	1.2	Okay	Okay
Part 1	Lenticular	6	Offset twisted ribbon	1.2	Not okay	Okay
	Tube type					
	Tube dia. (mm)					
	Internal feature					
	Tube thickness (mm)					
	Visual inspection					
	Flow test					

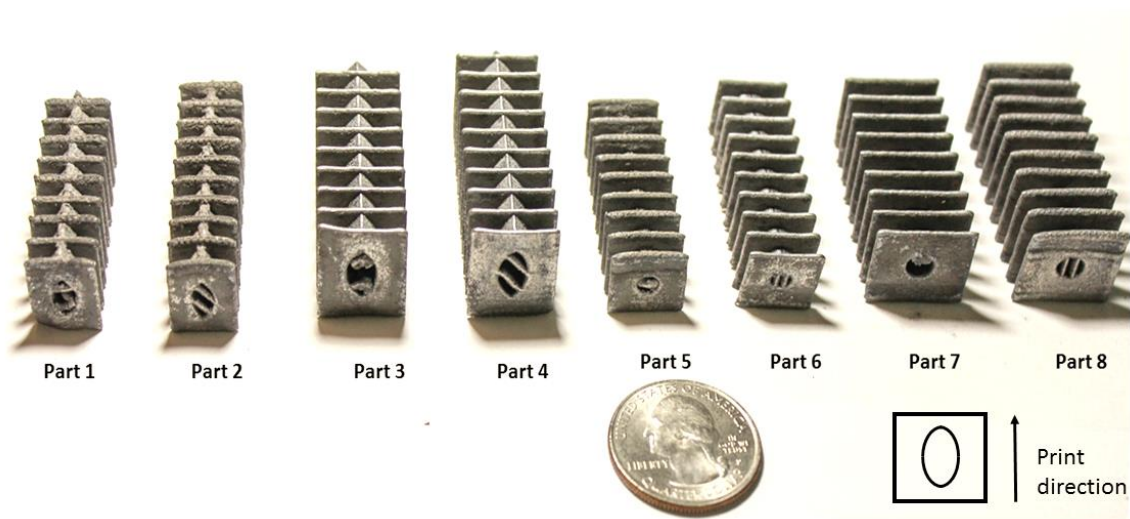


Figure 5.9. Parts fabricated in the first test print

Although the print direction of this print is different than the one chosen for the final print, a few observations can be made which are independent of the print direction. By visual inspection of both tube shapes, light is observed to pass through the 8 mm tubes better than the 6 mm tubes suggesting better clearance of residual un-melted powder. More flow resistance can be felt for the 6 mm tubes as compared to the 8 mm tubes.

The offset strip fins print well with both the 8 mm diameter tubes. The twisted ribbons result in blunter edges as compared to the offset strip fins. The printed geometry of the offset strip fins is in good agreement with the computer aided design (CAD) model on which it is based, while the twisted ribbon geometry is not. Although the twisted ribbons pass the flow test in most cases, a higher resistance to air flow is observed while blowing air through it, suggesting more clogging of passageways as compared to offset strip fins. Both the tube thicknesses print well without any deformities and are hence larger than the minimum printable tube thickness.

Based on these observations from the first test print, a tube diameter of 8 mm is selected for all the tubes in the second print. A tube thicknesses of 0.8 mm is printed along with 1.6 mm to test the minimum printable thickness. Circular and lenticular tubes are printed with offset strip fins (OSF) and twisted ribbon (TR) inserts. The slenderness ratio for the lenticular tubes is 0.5. Different pitches of internal features are tested in these prints. The print direction for this print is along the tube axis, which is the same as that of the final print. For compatibility with this print orientation, the external fins are oriented at an angle greater than 45 degrees with the horizontal (see Figure 3.6) and the internal features are modified to have a 45 degree starting angle (see Figure 3.7). Three different external fin angles (45°, 50°, and 55°) are tried in these prints. Fin thicknesses of 0.5 mm and 0.3 mm are tried to evaluate the minimum printable thickness of the fins.

At a tube diameter of 8 mm, a maximum S_T/D ratio of 1.8 is tried based on the criteria of meeting the heat transfer requirements, while a minimum ratio of 1.4 is tried to test the limit for clearance of air side flow passages. A total of six parts are printed, three without headers and three with headers. The parts with headers are printed to test the strength of the joint at which the tubes attach to the header.

The details of the parts printed in the second print are given in Table 5.3. A photograph of the printed parts is shown in Figure 5.5. Similar to the first test print, visual and flow inspection is done for the parts printed without headers. Inspection of the parts with headers is not possible due to the presence of the headers. The results of these tests are summarized in Table 5.4.

Table 5.3. Details of parts printed in the second test print

Header	Part 1		Part 2		Part 3		Part 4		Part 5		Part 6	
	No	Circ. (1)	Lent. (5)	Circ. (1)	Lent. (4)	Circ. (2)	Lent. (4)	Circ. (2)	Lent. (4)	Circ. (2)	Lent. (4)	Circ. (2)
Lambda	0.5	1	0.5	1	0.5	1	0.5	1	0.5	1	0.5	1
Tube diameter (mm)	8	8	8	8	8	8	8	8	8	8	8	8
Tube thickness (mm)	1.6	1.6	1.6	1.6	1.6	1.6	1.6	1.6	0.8	0.8	0.8	0.8
Internal feature	OSF, TR	TR	OSF, TR	TR	OSF, TR	OSF, TR	OSF, TR	OSF, TR	OSF, TR	OSF, TR	OSF, TR	OSF, TR
OSF pitch (mm)	10	-	10	-	6	6	6	6	3	3	3	3
TR pitch (mm)	33	33	33	33	25	25	25	25	18	18	18	18
S_T/D	1.4	1.4	1.4	1.4	1.4	1.4	1.4	1.4	1.8	1.8	1.8	1.8
Fin angle (degrees)	45	45	45	45	50	50	50	50	55	55	55	55
Fin thickness (mm)	0.5	0.5	0.5	0.5	0.3	0.3	0.3	0.3	0.5	0.5	0.5	0.5

Table 5.4. Results of visual and flow tests for second test print

Test	Part 1				Part 3				Part 5			
	Lenticular		Circular		Lenticular		Circular		Lenticular		Circular	
	OSF	TR	OSF	TR	OSF	TR	OSF	TR	OSF	TR	OSF	TR
Visual	OK	Not okay	-	Not OK	OK	Not OK	Not OK	Not OK	OK	Not OK	OK	Not OK
Flow	OK	Not okay	-	Not OK	OK	Not OK	Not OK	OK	OK	Not OK	OK	Not OK

From the second test print, it is observed that only a combination of lenticular shaped tubes with offset strip fins clears powder consistently in all the parts. Lenticular tubes with twisted ribbon internal features never pass the flow test suggesting internal clogging for this combination. Circular tubes with offset strip fins clear only with the reduced tube thickness (which allows for greater internal space), while results from printing of circular tubes with twisted ribbon inserts are not consistent to lead to an inference.

On visual inspection of the test parts, it is observed that even though the lenticular tubes with offset strip fins passes the flow test, some of the passages in these parts are clogged. Based on the measurements of the gaps between the features for the printed parts, it is inferred that a gap of 1.41 mm is required between the features for the internal residual powder to be cleared out completely.

Both the tube thicknesses printed well without any deformations. The tubes also appear non-porous on visual inspection, however small scale porosity could only be tested by pressure testing, which was not done due to unavailability of testing equipment and time constraints. Based on feedback from experts at ORNL, the minimum tube thickness is selected to be 1 mm.

The 50° fins with a thickness of 0.3 mm (in the xy plane) could not be printed, while the fin angles of 45° and 55° print well with a thickness of 0.5 mm. Hence, the minimum fin thickness is selected to be 0.5 mm. A fin angle of 45° is chosen for the final design to keep the fins as close to perpendicular (with the tubes) as possible, which is the case for which all the analysis is done. Both the S_T/D ratios print well and can be cleared of residual powder with compressed air. The headers in parts 2, 4, and 6 print well with the tubes without any concerns at the attachment points.

The overall inferences from the two test prints are as follows:

- 8 mm tube outer diameter is the smallest tested tube diameter that prints well with internal features,
- Residual powder is cleared better from the lenticular tubes as compared to circular tubes as they have more internal space,
- Offset strip fins are more suitable as internal features due to better clearance of residual powder,
- Minimum tested spacing between features for clearing internal residual powder is 1.41 mm,
- Minimum recommended tube wall thickness is 1 mm
- Minimum tested external fin angle which prints successfully is 45°, and
- Attachment of tubes to the header is sufficiently strong

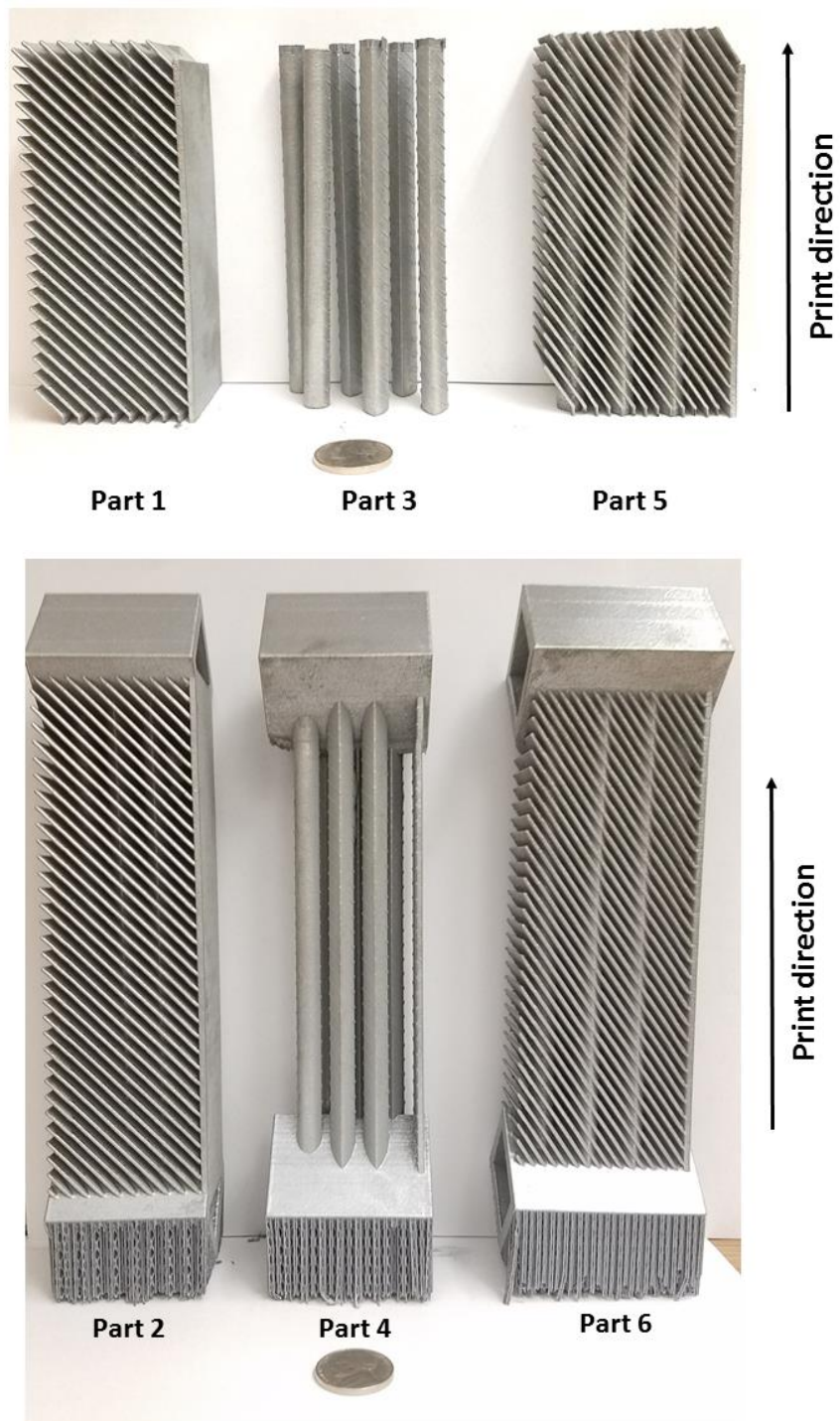


Figure 5.10. Parts fabricated in the second test print

5.3 Final design selection

Based on the inferences from the test prints, a tube diameter of 8 mm is selected with offset strip fins for the final design. For this tube diameter, the maximum pitch to diameter ratio that results in a configuration with specified heat transfer is 1.8 with a total of 98 tubes arranged in three tube rows. Following the thought process explained in section 4.3, the slenderness of the tubes is decreased (maintaining S_T/D at 1.8) while keeping the equal flow gap configuration. For maintaining the same number of tubes in the constrained volume during this transition, the smallest slenderness ratio that can be achieved is 0.77. This configuration is depicted in Figure 5.11 which shows the cross section of the tubes placed within the boundary defined in the product design specifications.

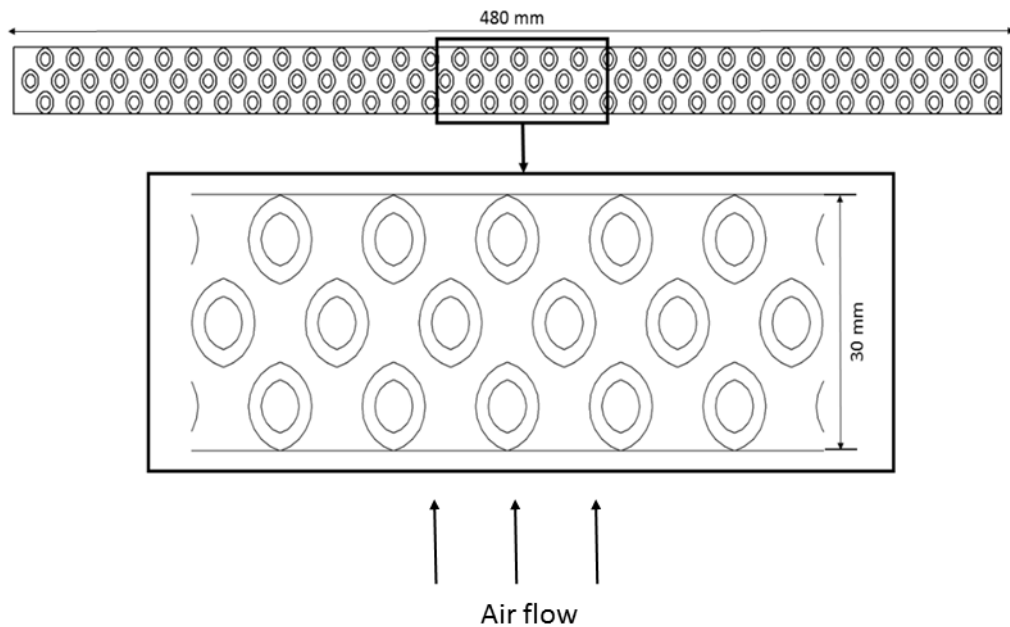


Figure 5.11. Depiction of final configuration with a slenderness ratio of 0.77

$$OD = 8\text{mm}, S_T/D = 1.8, \lambda = 0.77$$

Once the slenderness of the tube is finalized, it is critical to determine if the von Mises stress induced in the tube for a thickness of 1mm is within the allowable limit. An FEA analysis is performed for the tubes with the material properties for the AlSi10Mg alloy and an internal design pressure of 2 MPa. A quarter model of the tube cross section with symmetry boundary conditions is analyzed for 1 mm tube wall thicknesses. The allowable stress is calculated using (4-38). This results in maximum von Mises stress of 54 MPa which is less than the allowable value of 86.67 MPa. The stress plot of this analysis is shown in Figure 5.8.

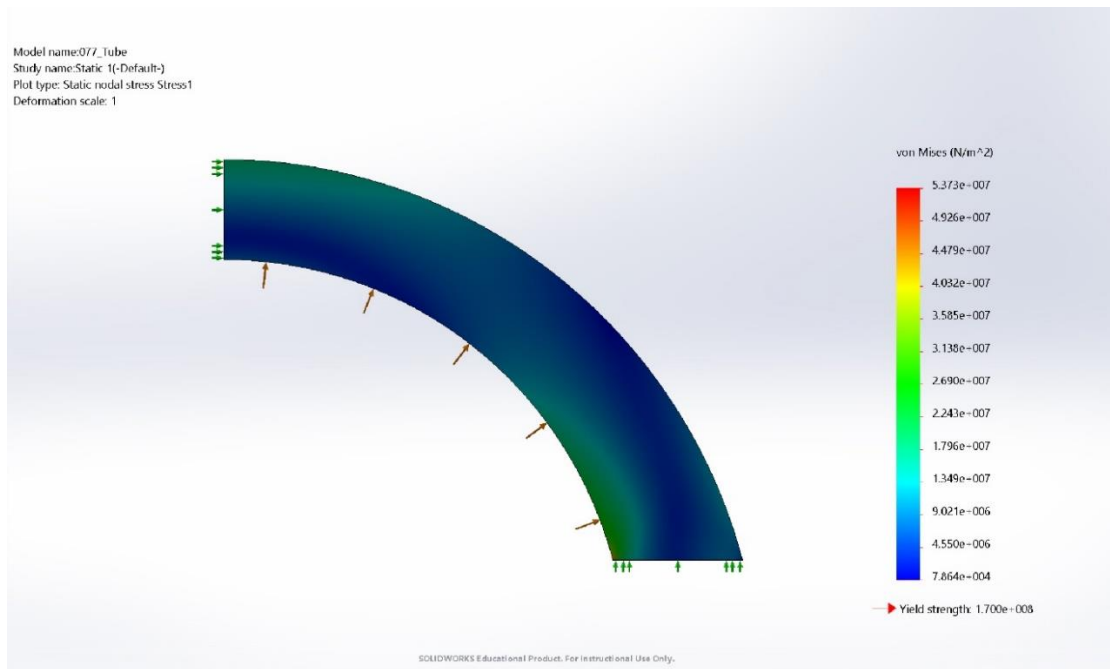


Figure 5.12. Von Mises stress plot for tube with slenderness ratio of 0.77 and tube wall thickness of 1 mm with a 2 MPa internal pressure load

For the fatigue analysis, the von Mises stress for the fatigue cycle loading (internal pressure cycling between 0 Pa and 125000 Pa) is compared to the Goodman fatigue limit. In this case, the mean and alternating von Mises stresses corresponding to a pressure load

of 62500 Pa are equal and have a value of 1.688 MPa. The Goodman limit is evaluated by constructing a line (assuming a $5e8$ cycles for aluminum) with a completely reversed stress limit of 86.67 MPa and the ultimate strength of 265 MPa. For a load case where the mean and alternating stresses are equal, the fatigue stress limit is 65.3 MPa. Hence, the proposed design will satisfy the fatigue loading requirements.

The analysis concluded with a final design of the heat exchanger with parameters listed in Table 5.5. The engineering drawings for this selected design are presented in Figures 5.13 to 5.16. The final printed heat exchanger is shown in Figure 5.17.

Table 5.5. Dimensions of the final printed heat exchanger design

Feature (unit)	Value
Tube diameter (mm)	8
Transverse tube pitch (mm)	14.4
Slenderness ratio	0.77
Number of tubes	98
Tube wall thickness (mm)	1
Offset strip fin length (mm)	10
Offset strip fin thickness (mm)	0.5
Offset strip fin spacing (mm)	1.41
Fin thickness (mm)	0.5
Fin spacing (mm)	4.5
Fin angle (degrees)	45
Number of fins	72
Header thickness (mm)	5

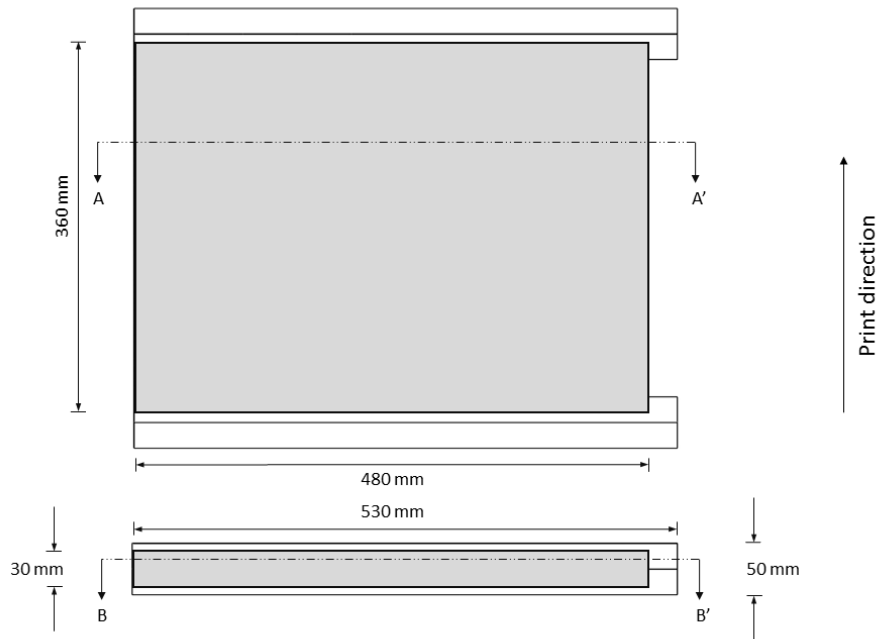


Figure 5.13. Overall dimensions of the heat exchanger core and header

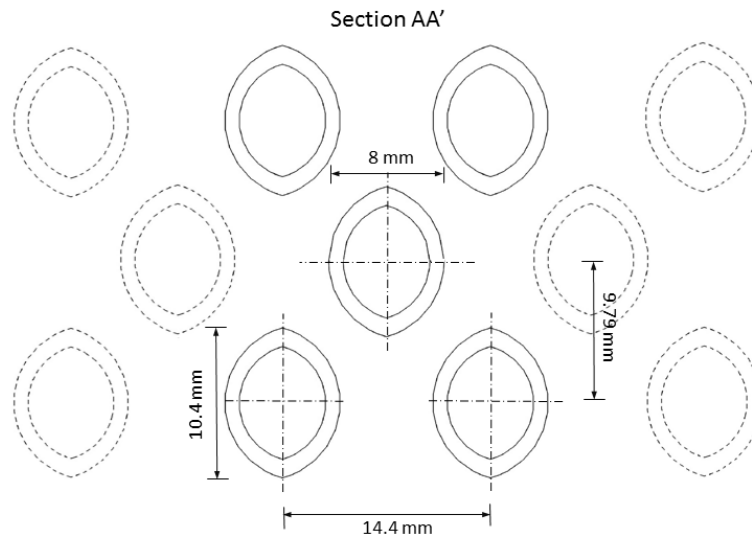


Figure 5.14. Dimensions of lenticular tubes with corresponding tube pitches

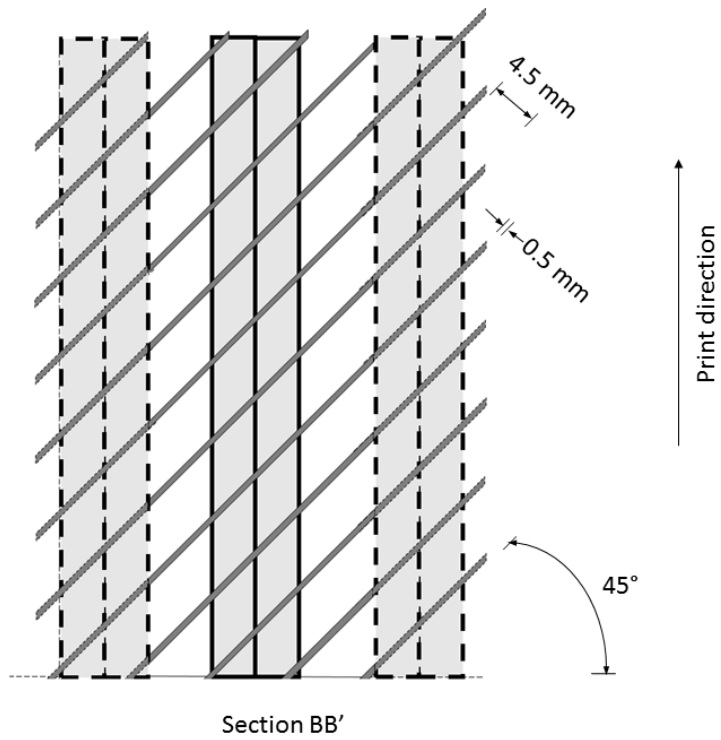


Figure 5.15. Dimension of external plain fins

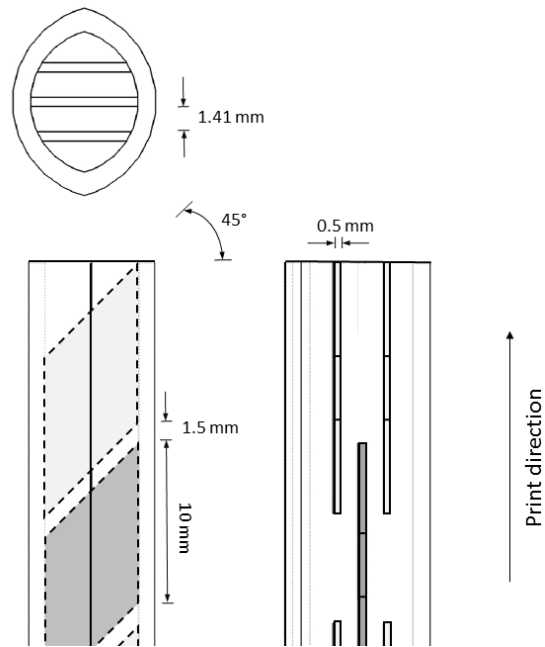


Figure 5.16. Dimensions of internal offset strip fins

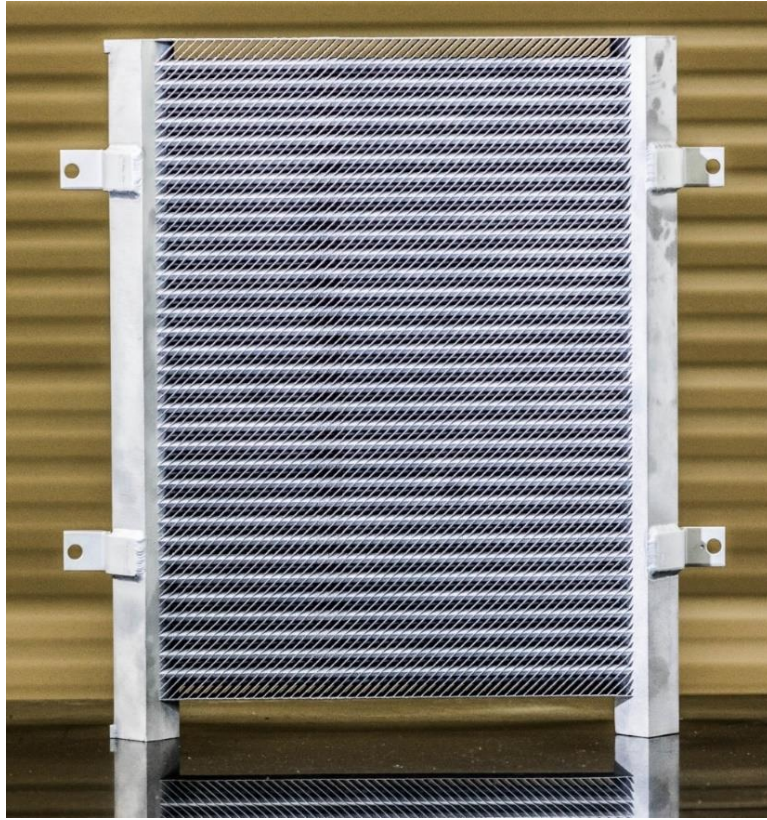


Figure 5.17. Final printed heat exchanger

The heat exchanger meets the heat duty and pressure drop requirements. The air side convective resistance is reduced to a third of the stock heat exchanger while the oil side resistance is almost the same, hence leading to an increased heat transfer from the same volume as compared to the stock heat exchanger. This change is due to the drastic increase in the air side convective coefficient while the oil side convective coefficient is increased by a relatively smaller amount as compared to the stock heat exchanger. The pressure drop on air side is 92 Pa which is less than the allowable pressure drop of 343 Pa while that on the oil side is 26.6 kPa which is also within the limit of 170 kPa. The predicted thermal performance for this design is summarized in Table 5.6.

Table 5.6. Thermal performance estimate for the final heat exchanger

	Heat transfer rate (kW)	16.9
Air side	Air side pressure drop (Pa)	92
	Air side convective heat transfer coefficient (W/m ² -K)	287
	Air outlet temperature (K)	343.3
	Air side heat transfer area (m ²)	2.15
	Air side convective resistance (K/W)	1.6e-3
Oil side	Oil side pressure drop (kPa)	26.6
	Oil side convective heat transfer coefficient (W/m ² -K)	1911
	Oil outlet temperature (K)	364.1
	Oil side heat transfer area (m ²)	1.1
	Oil side convective resistance (K/W)	4.9e-4

The heat exchanger is successfully printed using the Concept Laser Xline 1000R machine available at ORNL, hence satisfying all the constraints related to compatibility with additive manufacturing. The overall dimensions of the heat exchanger are the same as the stock heat exchanger hence complying with the volume restrictions.

After fabrication, SAE O Ring -12 threads are tapped onto the inlet and outlet ports which can be adapted to the existing hydraulic hoses. Attachment tabs are welded onto the printed heat exchanger such that they use the existing mounting points on the excavator. These post fabrications operations make the printed heat exchanger a swap-in replacement for the stock heat exchanger. The heat exchanger is also designed to handle a burst pressure of 2 MPa.

The printed design satisfies all the requirements mentioned in the product design specifications other than compliance with the standard test requirements could not be testing within the time constraints of the project. The specifications of this design are summarized in Table 5.7.

Table 5.7. Product specification of printed heat exchanger

Specification	Value
AM equipment	Concept Laser Xline 1000R
Material used	AlSi10Mg
Minimum feature size (mm)	0.5
Minimum overhang angle (degrees)	45
Minimum internal passageway dimension (mm)	6
Showcase additive manufacturing	Yes
Maximum height (mm)	430
Maximum width (mm)	530
Maximum depth (mm)	50
Threaded connections	SAE O Ring -12
Uses existing mounting points	Yes
Air side pressure drop (Pa)	92
Oil side pressure drop (kPa)	26.6
Heat transfer (kW)	16.9
Burst pressure (MPa)	2
Fatigue loading from 0 Pa to 125000 Pa at 30 cycles/min for 50,000 cycles	Pass

Chapter 6. Conclusion

A functional additively manufactured oil cooler for the Case New Holland model CX55B excavator was designed and fabricated using selective laser melting (SLM). Based on an engineering analysis, the heat exchanger design is projected to transfer heat at 15 kW at the design conditions with acceptable pressure drops of 92 Pa and 26.6 kPa on the air and oil side respectively. The heat exchanger is fabricated using AlSi10Mg alloy powder as a single part and requires minimal post processing.

The heat exchanger consists of a finned lenticular tube bank with internal offset strip fins, having a tube diameter of 8 mm and a slenderness of 0.77. The transverse pitch to diameter ratio is 1.8 based on heat transfer predictions. The slender lenticular tubes offer more internal space for fabricating the offset strip fins and offer lower air side pressure drops in unfinned configurations. A fin spacing of 4.5 mm is implemented based on previous work for optimization of fin spacing for heat transfer obtained from a constrained volume [39]. The external fins and internal offset strip fins are oriented at an angle of 45 degrees for printability in the orientation required based on build volume.

In this work, finned lenticular tube banks are analyzed as finned circular tube banks. Two test prints are fabricated to evaluate the manufacturability of small diameter shaped tubes with internal features such as offset strip fins and twisted ribbon inserts and external plain fins. The analysis of the circular finned tube banks is then combined with observations from these two test prints to select a final design.

The lenticular tube shape enables manufacturing of tubes in multiple orientations as opposed to circular tubes which can be printed only when the tube axis is aligned with

the print direction. From the test prints, the twisted ribbon inserts are found to be incompatible with small diameter tubes.

For future work, a computerized tomography (CT) scan can be done for the test prints as well as the final printed heat exchanger to study the surface roughness on the exterior as well as interior of the tubes. Images from a CT scan can help in estimating the amount of clogging of internal passageways which cannot be inspected visually. The findings from these images can then be incorporated into the thermal analysis to estimate the performance variation due to surface roughness.

Functional testing of the heat exchanger should be done to evaluate the actual thermal performance obtained from the heat exchanger under the specified design conditions. The predicted and measured performance can then be compared and if any differences are observed, they can be attributed to possible causes. The final design can be analyzed using computational fluid dynamics which would help understand the effects of the slenderness of the tubes and external fin angles on the flow field around the heat exchanger. Results from this analysis can also be utilized to optimize the design in future iterations.

The successful printing of the heat exchanger bolsters the applicability of metal AM processes heat exchangers, however extensive testing and analysis is necessary to put these to practical use in construction equipment.

References

- [1] “World’s First 3D Printed Car.” [Online]. Available: <http://web.ornl.gov/sci/manufacturing/media/news/3d-car/>. [Accessed: 02-Dec-2016].
- [2] “ORNL revealed the 3D printed Shelby Cobra.” [Online]. Available: <http://web.ornl.gov/sci/manufacturing/media/news/detroit-show/>. [Accessed: 12-Dec-2016].
- [3] D. J. Saltzman, M. Bichnevicius, S. P. Lynch, T. Simpson, E. W. Reutzler, C. Dickman, and R. Martukanitz, “Experimental comparison of a traditionally built versus additively manufactured aircraft heat exchanger,” *55th AIAA Aerosp. Sci. Meet.*, no. January, pp. 1–11, 2017.
- [4] K. L. Kirsch and K. A. Thole, “Heat Transfer and Pressure Loss Measurements in Additively Manufactured Wavy Microchannels,” *J. Turbomach.*, vol. 139, no. 1, p. 11007, 2017.
- [5] “Miniaturized air to refrigerant heat exchangers.” [Online]. Available: <http://energy.gov/eere/buildings/downloads/miniaturized-air-refrigerant-heat-exchangers>. [Accessed: 01-Dec-2016].
- [6] M. Norfolk and H. Johnson, “Solid-State Additive Manufacturing for Heat Exchangers,” vol. 67, no. 3, pp. 655–659, 2015.
- [7] “Additive world awards designed and 3D printed by Addlab.” [Online]. Available: <http://addlab.com/News/Additive-world-awards-designed-and-3d-printed-by-addlab>. [Accessed: 12-Dec-2016].
- [8] J. Assaad, A. Corbeil, P. F. Richer, and B. Jodoin, “Novel Stacked Wire Mesh Compact Heat Exchangers Produced Using Cold Spray,” vol. 20, no. December, pp. 1192–1200, 2011.
- [9] P. Dupuis, Y. Cormier, M. Fenech, and B. Jodoin, “Heat transfer and flow structure characterization for pin fins produced by cold spray additive manufacturing,” *Int. J. Heat Mass Transf.*, vol. 98, pp. 650–661, 2016.
- [10] “Reference*,” 2016. [Online]. Available: <https://www.reference.com/home-garden/iso-vg-46-hydraulic-oil-da644ead8618622f>. [Accessed: 01-Jan-2016].
- [11] A. J. Caines, R. F. Haycock, and J. E. Hillier, *Automotive Lubricants Reference Book*, 2nd ed. Society of Automotive Engineers, Inc.; Professional Engineering Publishing, 2004.
- [12] T.RAD, “Heat Exchanger for Construction Machine.” [Online]. Available: <http://www.trad.co.jp/english/products/kikai.html>. [Accessed: 01-Jan-2016].
- [13] F. P. Incropera, D. P. DeWitt, T. L. Bergman, and A. S. Lavine, *Fundamentals of Heat and Mass Transfer*, vol. 6th. John Wiley & Sons, 2007.
- [14] J. Zimmerman, “Personal Communication (10/21/2016).” Project Engineer, CNH Industrial, Burr Ridge, IL. Contact: +1 630 887 3795.
- [15] Concept Laser, “X Line 1000R Metal laser melting system.” [Online]. Available: https://platforms.monash.edu/mcam/images/stories/Concept/xline_1000.pdf. [Accessed: 01-Jan-2016].
- [16] Oak Ridge National Laboratory, “Capabilities - Oak Ridge National Laboratory.” [Online]. Available:

- <http://web.ornl.gov/sci/manufacturing/research/additive/equipment/>. [Accessed: 01-Jan-2017].
- [17] “Material Specification Aluminum AlSi10Mg.” [Online]. Available: <https://www.3trpd.co.uk/wp-content/uploads/2013/03/aluminium-alsi10mg-2012.pdf>. [Accessed: 04-Jun-2017].
- [18] “Inconel alloy 718 - Heat Resisting Alloy (Ni53/Fe19/Cr19/Nb/Mo/Ti) Material Information.” [Online]. Available: <http://www.goodfellow.com/E/Inconel-alloy-718-Heat-Resisting-Alloy.html>. [Accessed: 04-Jun-2017].
- [19] Zapp, “Specialty Materials TiAl6V4.” [Online]. Available: http://www.rsalloys.eu/cmsMateriali/produzioni/47/TiAl6V4_e_02.12.pdf. [Accessed: 04-Jun-2017].
- [20] J. F. Jones, “Personal conversation.” Oak Ridge National Lab, TN, email: jonesjf@ornl.gov, 2016.
- [21] Uli Melchinger, “Personal conversation.” CNH Industrial Ag&CE Hydr. Components, Adv. Systems & Hydrostatic Drives; email: uli.melchinger@cnhind.com, 2017.
- [22] CNH, “Fan curve for ECS part number 422753,” 2006.
- [23] Mike Gust, “Personal conversation.” Center for Compact and Efficient Fluid Power, University of Minnesota - Twin Cities; email: mjgust@umn.edu, 2017.
- [24] D. Calamas and J. Baker, “Experimental Performance of a Solid Heat Exchanger with Tree-Like Flow Passages,” *Exp. Heat Transf.*, vol. 28, no. 3, pp. 205–221, 2014.
- [25] A. A. Gholami, M. A. Wahid, and H. A. Mohammed, “Heat transfer enhancement and pressure drop for fin-and-tube compact heat exchangers with wavy rectangular winglet-type vortex generators,” *Int. Commun. Heat Mass Transf.*, vol. 54, pp. 132–140, 2014.
- [26] A. E. Bergles, “Heat Transfer and Pressure Drop Correlations for the Rectangular Offset Strip Fin Compact Heat Exchanger,” *Exp. Therm. Fluid Sci.*, vol. 1777, no. 94, pp. 171–180, 1995.
- [27] Z. Li, “Heat Transfer Enhancement Using Streamlined Tubes in Polymer Heat Exchangers,” University of Minnesota, 2005.
- [28] W. M. Kays and A. L. London, *Compact Heat Exchangers*, 2nd ed. New York: McGraw-Hill, 1984.
- [29] J. R. Davis, *Aluminum and aluminum alloys ASM specialty handbook*. Materials Park, Ohio: ASM International. Handbook Committee., 1993.
- [30] “MatWeb Material Property Data.” [Online]. Available: <http://www.matweb.com/search/datasheet.aspx?matguid=b96cfe7b0eb14997b3ff2c70c2ca0bea&ckck=1>. [Accessed: 01-Jan-2016].
- [31] The Engineering Toolbox, “Dry Air Properties.” [Online]. Available: http://www.engineeringtoolbox.com/dry-air-properties-d_973.html. [Accessed: 01-Jan-2016].
- [32] Y. A. Cengel, *Heat transfer: A Practical Approach*, 2nd ed. New York: McGraw-Hill.
- [33] H. L. Langhaar, “Steady flow in the transition length of a straight tube,” *J. Appl.*

- Mech.*, vol. 64, p. A-55, 1942.
- [34] W. M. Kays and M. E. Crawford, *Convective heat and mass transfer*, 2nd ed. New York: McGraw-Hill, 1980.
- [35] H. D. Baehr and K. Stephan, *Heat and mass transfer*, Second., vol. 32. Berlin, 2006.
- [36] W. M. Kays and A. L. London, *Compact Heat Exchangers*, 2nd ed. United States of America, 1964.
- [37] Y. S. Muzychka and M. M. Yovanovich, "Pressure Drop in Laminar Developing Flow in Noncircular Ducts: A Scaling and Modeling Approach," *J. Fluids Eng.*, vol. 131, no. 11, p. 111105, 2009.
- [38] Z. Li, "Heat Transfer Enhancement Using Streamlined Tubes in Polymer Heat Exchangers," 2005.
- [39] R. S. Matos, T. A. Laursen, J. V. C. Vargas, and A. Bejan, "Three-dimensional optimization of staggered finned circular and elliptic tubes in forced convection," *Int. J. Therm. Sci.*, vol. 43, 2003.
- [40] C. Wang and K. Chi, "Heat transfer and friction characteristics of plain fin-and-tube heat exchangers , part I : new experimental data," *Int. J. Heat Mass Transf.*, vol. 43, 2000.
- [41] C. Wang, K. Chi, and C. Chang, "Heat transfer and friction characteristics of plain fin-and- tube heat exchangers , part II : Correlation," *Int. J. Heat Mass Transf.*, vol. 43, pp. 0–7, 2000.
- [42] T. Perrotin and D. Clodic, "Fin Efficiency Calculation In Enhanced Fin-and-tube Heat Exchangers In Dry Conditions," in *International Congress of Refrigeration*, 2003, pp. 1–8.
- [43] H. Hausen, "Darstellung des warmueberganges in Rohrendurch Verallgemeinerte Potenziehungen," *Z. VDI Beih. Verfahrenstech.*, vol. 4, p. 91, 1943.
- [44] Y. He, P. Chu, W. Tao, Y. Zhang, and T. Xie, "Analysis of heat transfer and pressure drop for fin-and-tube heat exchangers with rectangular winglet-type vortex generators," *Appl. Therm. Eng.*, vol. 61, 2012.
- [45] D. A. Ramirez, L. E. Murr, S. J. Li, Y. X. Tian, E. Martinez, J. L. Martinez, B. I. Machado, S. M. Gaytan, F. Medina, and R. B. Wicker, "Open-cellular copper structures fabricated by additive manufacturing using electron beam melting," *Mater. Sci. Eng. A*, vol. 528, pp. 5379–5386, 2011.
- [46] E. M. Dede, S. N. Joshi, and F. Zhou, "Topology Optimization, Additive Layer Manufacturing, and Experimental Testing of an Air-Cooled Heat Sink," *J. Mech. Des.*, vol. 137, no. November, pp. 1–9, 2015.
- [47] M. Sheikholeslami, M. Gorji-Bandpy, and D. D. Ganji, "Review of heat transfer enhancement methods: Focus on passive methods using swirl flow devices," *Renew. Sustain. Energy Rev.*, vol. 49, pp. 444–469, 2015.
- [48] L. C. Montemayor and J. R. Greer, "Mechanical Response of Hollow Metallic Nanolattices: Combining Structural and Material Size Effects," *J. Appl. Mech.*, vol. 82, no. July, pp. 1–10, 2015.

Appendix A: Air flow measurement

Air flow data for the design of the heat exchanger was not provided. Hence, to establish a baseline for design, air flow measurements were done on a running excavator. The excavator was a model similar to the one considered for this design process. The excavator was operated at a fixed engine speed of 2400 rpm with the air conditioning circuit turned off. A hot wire anemometer (TSI Model 8330 VelociCheck) was used for measuring air flow velocity at various points under the hood of the excavator. A log of these measurements is included in this appendix with recorded values reported against the measurement locations. Figure A.1 explains the symbols used in the log entries.

Flow measurements are taken with the hood open as well as closed. As the excavator was operating in an open environment, considerable wind velocities were observed. The position of measurement is either described verbally or indicated by small line diagrams that represent the air intake slots present on the excavator body. Air flow velocities ranged from 3.5 m/s to 7 m/s. A conservative value of 3.5 m/s was hence assumed for all the thermal design calculations.

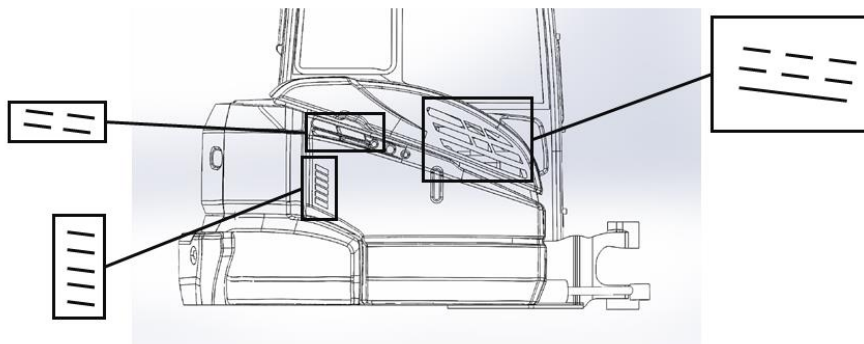


Figure A.1. Symbols used for locations of air velocity measurements in the excavator

constant, 2400 rpm

Serial No.	Position	Engine Setting	(ft/min) Air Velocity	Comments
1	top left			
2	in front of device background just wind		~ 500 / 200-800	
3	#5		1650/2300	± 50
4	#2		1900/2300	1900-2000
5	top left right		2100/2300-2600	another reading - less wind 1800
6			1700/2400	
7			1400/1500	gusty
8			1400/1500	
9			1000/1100	
10	side panel in front of filter		700 700/800	low value - wind missing w/ other values
11	inside through right bottom hole		730/700-800	close to horizontal
12	inside thru hole of 8 under the panel for air snorkel		730 740/700	similar to above right in front of filter
13	#3		1200/1000-2000	at angle
14				
15				
16				
17				
18				
19				
20				

top left holes { 1, 2, 3, 4, 5, 6, 7, 8, 9

top right holes { 10, 11, 12

varies depending on how you turn probe
 engine running constant 2400 rpm
 doing no work

open hood - not ~~are~~ operating velocities

Serial No.	Position	Engine Setting	Air Velocity	Comments
21	vertical - see comments		1000/1050	vertical in front of filter (pointing down)
22			700-1100	vertical in front of filter - far left
23				
24				
25				
26		CLOSED TOP AGAIN!		
27	inside		700 1200	below slits ~ 700 anywhere where slits present 1100 1100
28				
29	"	" below snorkel	1200	end of snorkel for air
30	"		700	near filter
31				
32			2200	in air snorkel high here - low as gets to filter
33	inside, on right side of filter		~ 750	consistent with open results higher on right than on left } at an angle
34	inside, middle front of filter		~ 700	
35	inside left side of filter in front		~ 620	
36				
37				
38				
39				
40				

observation: can feel suction on left slits
don't feel much suction (if any) on right slits

OPEN TOP temp + vel

Serial No.	Position	temp (°F) Engine Setting	(ft/min) Air Velocity	more position/comments Comments
41	between AC/oil cooler	100	900-1000/1000	open top } constant across from left to right
42	between oil cooler/radiator	118	~400/550	
43		83		in front of filter below snorkel
44		90		behind reservoir
45		88		in front of reservoir
46	near engine after the fan	131		
47	between filter + AC		1150/1050	
48			1150/1100	air bypasses the AC and goes directly thru oil cooler
49				
50				
51				
52				
53				
54				
55				
56				
57				
58				
59				
60				

Appendix B: Ideas from brainstorming



Figure B.1. Teardrop shaped fins[5]

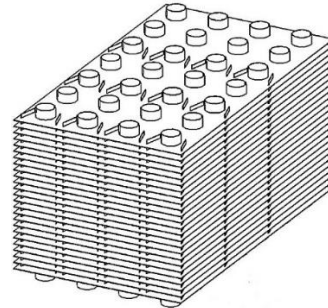


Figure B.2. Vortex generators[44]

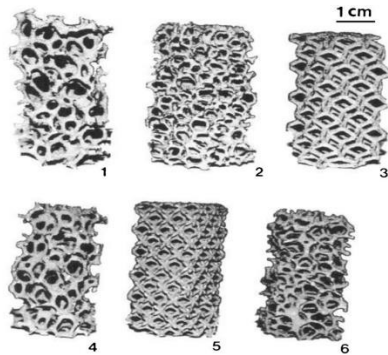


Figure B.3. Metal foams[45]

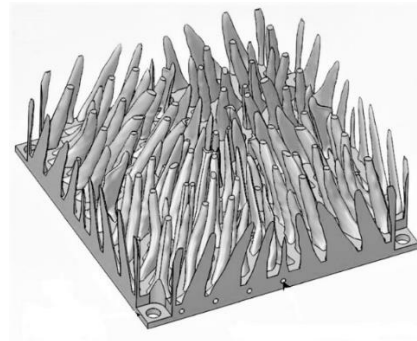


Figure B.4. Optimized pin fins[46]

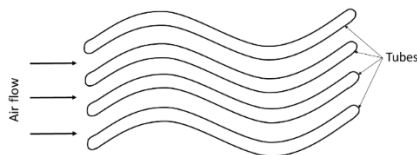


Figure B.5. Sinusoidal cross section tubes

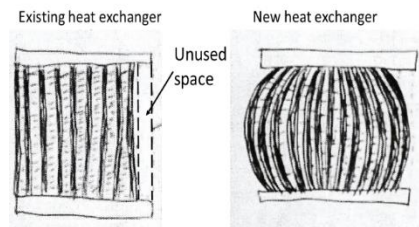


Figure B.6. Modification to used bypassed cooler air

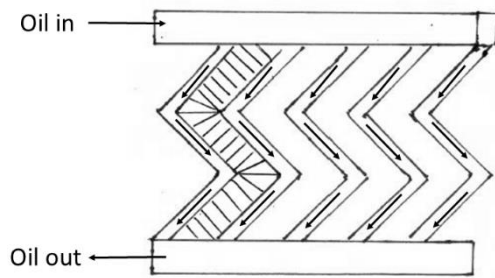


Figure B.7. Zig zag oil tubes

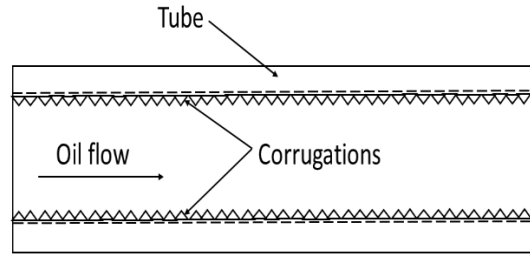


Figure B.8. Tube with corrugations

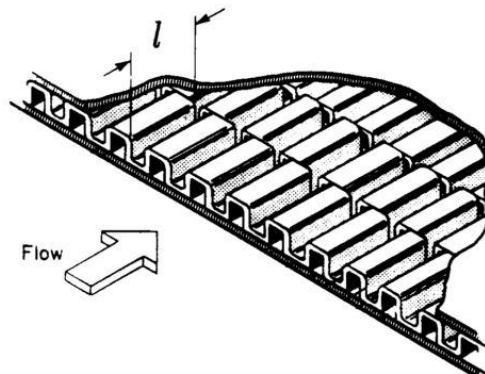


Figure B.9. Offset strip fins[26]

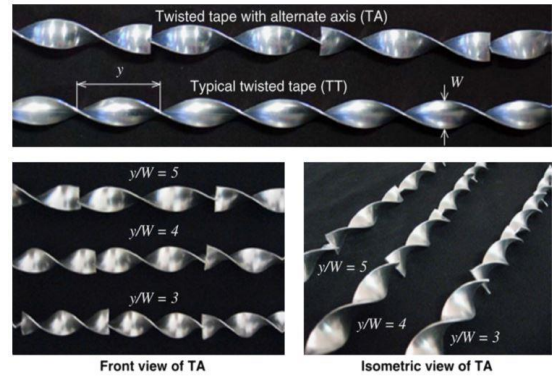


Figure B.10. Twisted ribbon insert[47]

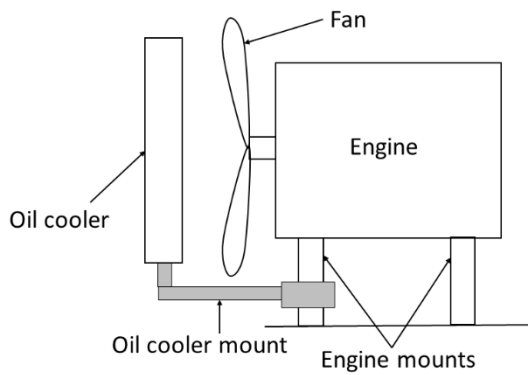


Figure B.11. Utilizing engine vibrations

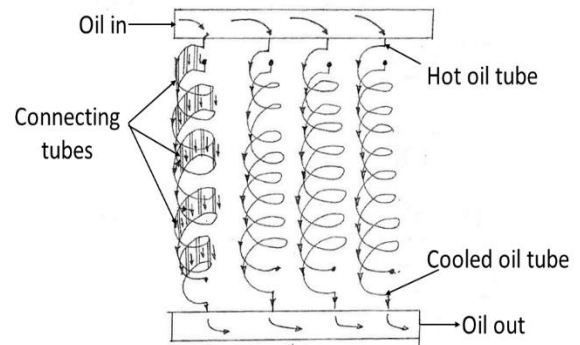


Figure B.12. Connected double spiral tubes

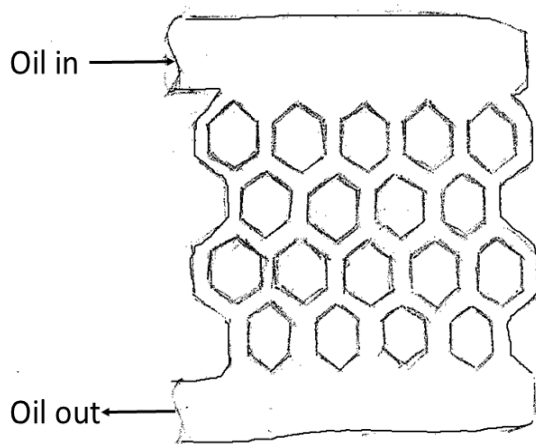


Figure B.13. Honeycomb tubes

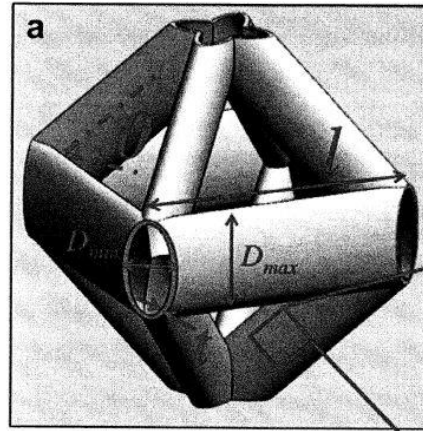


Figure B.14. Hollow strut metal foams[48]

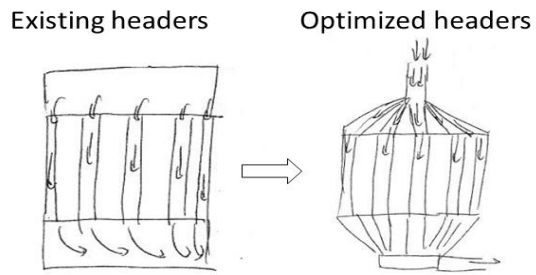


Figure B.15. Header redesign

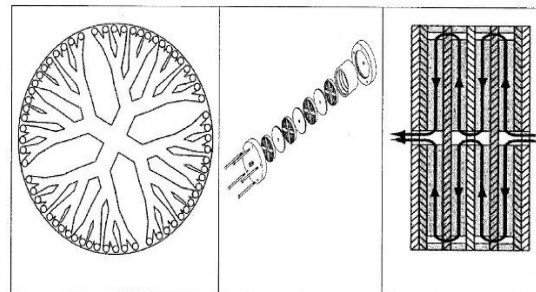


Figure B.16. Tree like oil passages[24]